UNIVERSITY OF LONDON THESIS

Degree PhD Year 2008 Name of Author BROWN, MARTIN.

Monte Carlo simulations of cold atom ratchets

Martin Brown

Summer 2008

Department of Physics and Astronomy
University College London

A thesis submitted in fulfilment of the requirements
for the degree of Doctor of Philosophy
of the University of London.

ProQuest LLC
789 East Eisenhower Parkway
P.O. Box 1346
Ann Arbor, MI 48106-1346

Monte Carlo simulations of cold atom ratchets

Martin Brown

I, Martin Brown, confirm that the work presented in this thesis is my own. Where information has been derived from other sources, I confirm that this has been indicated in the thesis.

Signature: ___ Date: 28/8/08

(Martin Brown)

Signature: ___ Date: 28·08·2008

(Dr. Ferruccio Renzoni)

Abstract

This thesis reports the theoretical study of several cold atom ratchet systems. In particular the focus of the work is the determination of the ratchet current as a function of the ratchet parameters through analysis of the system symmetries and through numerical simulation.

Ratchets are devices that exhibit directed motion in the absence of net forces. It is necessary to drive them away from thermal equilibrium so as to not violate the second law of thermodynamics. Currents are generated when the symmetries of the ratchet do not forbid it, a consequence of Curie's principle. An analysis of the symmetries will help determine for what parameters currents will be generated; we perform such analyses in our investigations.

The ratchets studied are modelled on the experimentally realised implementation of cold atoms in a driven optical lattice. Through the parameters of the driving and the optical lattice itself, we control the breaking of the symmetries and thus the generation of atomic currents. The precise relationship between current and ratchet parameters is explored by numerical simulation.

In experiments the driving is achieved through a phase-modulation of the optical lattice beams. In numerical simulations we include the driving force directly in the equations of motion. We verify theoretically and numerically that the two approaches are equivalent.

We have modelled the dynamics of atoms in light-fields through semiclassical and quantum treatments. The semiclassical treatment results in stochastic differential equations for the external degrees of freedom. These are simulated using the Monte-Carlo technique. For the fully quantum treatment we apply a stochastic trajectory method to simulate the master equation. We perform a comparison between different treatments for an over-damped ratchet.

Acknowledgements

I am indebted to Dr Ferruccio Renzoni, my PhD supervisor, for the time and energy he has devoted to me these last few years. His ideas and his enthusiasm have been invaluable in getting me to this point.

I would like to thank the present, and recent-past, members of the experimental team of the laser cooling group at UCL and wish them all the best in their future endeavours.

I am grateful for the use of UCLs C^3 computing facilities.

Contents

List of Figures

Chapter 1

Introduction

The radiation pressure of light had been observed in the early 1900s but it wasn't until the 1970s that the field of laser cooling was born. In 1975 Hänsch and Schawlow [45] and Wineland and Dehmelt [85] proposed to cool an atomic vapour using the radiation pressure from a laser beam. More proposals and experimental demonstrations soon followed and laser cooling developed into an important field of research. More information on laser cooling can be found in Refs. [17, 43, 62].

The laser cooling field has matured to the extent that cold atoms are frequently employed as a tool for other research e.g. atomic clocks [46], Bose Einstein Condensates [2], atom lithography [60], atomic interferometry [6], and quantum information processing [28]. My research has focused on the theoretical study of ratchets realised with cold atoms.

1.1 Ratchets

For the purposes of this document the working definition of a ratchet will be:

> a device, operating away from equilibrium, producing directed motion in the absence of net forces.

It's worth spending a bit of time to explain exactly what this means.

The clause 'operating away from equilibrium' is a fundamental requirement of a ratchet and is perhaps best illustrated by the following discussion of Brownian motors. Brownian motors are ratchets that rectify the unbiased random motion of Brownian particles [12]. The most celebrated theoretical treatments of Brownian motors are by Smoluchowski [82] and Feynman [30]. They addressed the question of whether useful work can be extracted from thermal fluctuations. I précis their work and indicate the pertinent conclusions. [A recent exposition on the Brownian motor can be found in Ref. [44].]

Consider the following microscopic device of Feynman's *gedanken* experiment. A paddle wheel immersed in a thermal bath of temperature T_2 is connected via an axle to a cogwheel and pawl, immersed in a separate heat bath at temperature T_1; see Fig. 1.1. The pawl prevents rotation of the axle in one direction. Collisions between the particles in the heat bath and the paddles translate into a rotational force on the axle.

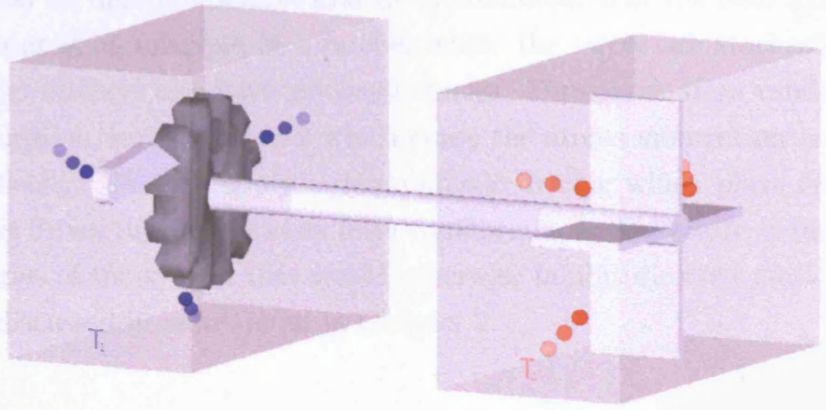

Figure 1.1: Microscopic Brownian motor. Attached to an axle at one end is a paddle wheel (right of picture) and at the other a cogwheel and pawl (left of picture). The paddle wheel is immersed in a heat bath at temperature T_2 and the cogwheel and pawl in a different heat bath at temperature T_1. With the pawl removed collisions with the paddles result in unbiased rotatory Brownian motion. The question is whether the pawl can rectify these rotations. One finds this occurs only for $T_2 > T_1$.

With the pawl removed the device would exhibit unbiased random rotations in both directions. With the pawl in place it would seem entirely plausible that the axle rotates in one direction only. It was shown, however, that at thermal equilibrium i.e. for $T_1 = T_2$ no net rotation occurs. This would otherwise represent a "perpetual motion machine" in contradiction of the laws of thermodynamics. The reason no net rotation occurs is because the pawl, also subject to random collisions, will at times lift and allow rotation of the axle in the other direction. The probabilities of these events at thermal equilibrium is exactly such that no net rotation results. Useful work can be extracted away from equilibrium and specifically for $T_2 > T_1$ but in this case the device is acting as a microscopic heat engine. A recent investigation into the exact workings for this configuration can be found in Ref. [55].

The next part of the definition of a ratchet says that a ratchet produces directed motion. In the case of the Brownian motor described above this is in the form of rotations of the axle, paddlewheel and cog assembly. For the cold atom ratchets studied later directed motion is exhibited through the centre-of-mass of the cloud of atoms acquiring a non-zero average velocity. This can be measured in laboratory experiments by imaging the atoms over the course of the experiment.

Lastly, the directed motion is produced in the absence of net forces. These forces may be deterministic, stochastic or combination of the two. The Brownian motor is an example of a ratchet where the forces are stochastic. Our cold atom ratchets also have stochastic forces. These arise from random photon absorption/emission events which cause the atoms momentum to change stochastically. We also apply a deterministic driving which plays two roles. Firstly, it drives the system away from equilibrium, and secondly, it breaks the symmetries of the system that would otherwise inhibit directed motion. This will be discussed in more detail in Chapter 2.

1.2 Motivation

Interest in ratchets has been renewed in recent years partly sparked by novel applications of the ratchet effect. The fields of interest are markedly varied. For example, it was suggested that the ratchet effect could be used in particle separation [78] and may represent a simple model of molecular motors [4, 48, 54]. Ratchets have been realised with quantum dots [50–52], Josephson junctions [7, 63] and other superconductor devices [69, 87]. Accompanying the experimental work has been a considerable amount of theoretical research. There are too many papers to mention individually; a good review of the historical developments made in the field can be found in Ref. [75]. Some formative papers worth particular mention are Refs. [1, 5, 29, 32, 53, 57, 86].

Ratchets realised with cold atoms represent an interesting alternative to more typical realisations. The laser parameters can be precisely controlled allowing for detailed and involved investigations. It is hoped our findings will offer insights into other branches of ratchet research.

1.3 Outline of thesis

The work this thesis documents is the detailed theoretical analysis, and numerical simulation of, several interesting cold atom ratchets. Before presenting these studies, in Chapter 2 I discuss ratchets in more detail, explain how sym-

metries determine generation of currents, and describe how cold atom ratchets are realised. In Chapter 3 I present the treatments and methods that have been applied in the numerical simulations of this work.

Two chapters of detailed analysis follow the introductory chapters. In Chapter 4 I look at three ratchets based on the same optical lattice configuration; they are differentiated by the driving that is applied. To realise the first two we apply temporal-asymmetric drivings that uniquely determine current generation; the third is realised through the combination of a temporal-symmetric driving and a modulation of the optical potential amplitude.

The ratchet discussed in Chapter 5 is based on a different lattice configuration to that of Chapter 4. The study of this particular system has proved quite problematic and substantial effort has been expended to resolve the issues that have arisen.

We conclude this document in Chapter 6 summarising the main findings of the work presented here, indicating any issues that remain to be addressed and areas for possible further investigation.

Chapter 2

Ratchets

2.1 What is a ratchet

Ratchets have attracted much attention since the early days of Smoluchowski [82]. Though many different types of ratchet have been explored they all perform one necessary function - they produce, in the absence of net forces, directed transport, the *ratchet effect*.

Directed transport is not possible in a symmetric system at equilibrium in the presence of a single source of unbiased fluctuations. This would otherwise be in violation of the second law of thermodynamics. Therefore, to generate a current such a system has to be driven out of equilibrium. This perturbative *driving* can be deterministic or stochastic. An interesting class of drivings which exhibit a rich and diverse set of behaviour are themselves unbiased, deterministic and periodic. The drivings that I study later are of this type.

Even being out of equilibrium, a symmetric periodic system will not generate a current. Conversely, if the symmetry is broken we can expect a current to be generated. This is a consequence of Curie's principle [20], that is, if an effect is not ruled out by the symmetries of a system, then in general it can be expected to occur.

A further and necessary requirement for a ratchet then is to break one or more symmetries of the system. This may be through the periodic system itself being asymmetric; for example the archetypal asymmetric sawtooth or 'ratchet' potential. Alternatively this asymmetry can come about through the non-equilibrium perturbation.

In summary, there are two fundamental requirements for the ratchet effect to take place. Firstly, the system has to be driven out of equilibrium as otherwise the second law of thermodynamics forbids currents to be generated. Secondly, the symmetries of the system that would otherwise prevent a current

need to be broken.

2.2 A simple dynamical model

The starting point for a simple dynamical model of a ratchet is that of a Brownian particle. This was considered by Einstein, Smoluchowski and later by Langevin. Indeed the model of the dynamics that we obtain is called a Langevin equation. Here I'll restrict myself to motion in one dimension for the sake of simplicity. Consider a Brownian particle with spatial coordinate $x(t)$ and mass m at equilibrium with a dissipative environment. The environment damps the particles motion and also introduces random fluctuations to it.

We follow the common assumptions in these matters [75], specifically that the damping is linear with velocity and that the environment is Markovian i.e. memory effects can be neglected. This last assumption is fulfilled when the state variable $x(t)$ is relatively 'slow' compared to the large environment.

Under these assumptions the particle's dynamics can be modelled by a Newtonian equation of motion

$$m\ddot{x} = -\gamma\dot{x} + \xi(t) \ . \tag{2.1}$$

where γ is a friction coefficient representing the damping of the particles motion, $\xi(t)$ models the random fluctuations and $\dot{x}$ denotes the derivative of x wrt t.

The terms γ and $\xi(t)$ are related as they both originate from the particles interaction with its environment. One finds that $\xi(t)$ is a Gaussian white noise with the statistical properties restricted to

$$\langle \xi(t) \rangle = 0 \tag{2.2}$$

and

$$\langle \xi(t)\xi(t') \rangle = 2\gamma k_B T \delta(t - t') \ . \tag{2.3}$$

The first condition states that the noise is unbiased and the second that it satisfies Einstein's *fluctuation-dissipation relation*. In the second condition k_B is Boltzmann's constant and T is the temperature of the system.

The remaining elements commonly found in a ratchet are the potential and the perturbative driving; these are introduced now. The potential gives rise to a force through the usual spatial derivative and together with the driving, can be added directly to the equation of motion. We denote the potential by

V and the driving by F and so obtain the Langevin equation

$$m\ddot{x} = -V'(x,t) + F(x,t) - \gamma\dot{x} + \xi(t) \tag{2.4}$$

where $V'(x,t)$ is the derivative of $V(x,t)$ wrt x. Such equations will be derived in Chapter 4 and used in the numerical simulation of the first ratchets that we study.

Three labels in common use to describe the dynamics of a ratchet system are *Hamiltonian*, *underdamped* and *overdamped*. These terms have the following significance:

- *overdamped* - a heavily damped system. That is, referring to the Langevin equation Eq. 2.4, the damping term '$-\gamma\dot{x}$' is large and dominates the inertial term '$m\ddot{x}$'. As an approximation we may take $m = 0$ to, in effect, exclude inertial effects from the dynamics.

- *underdamped* - a system where the damping term is small, but not negligible, compared to the inertial term.

- *Hamiltonian* - a system in the vanishing limit of dissipation and noise. This may be represented in our model by setting $\gamma = 0$ and $\xi(t) = 0$.

2.3 Main ratchet types

Many different types of ratchets have been proposed and studied. Two main types of ratchet that have attracted extensive attention are the *flashing* ratchet and the *rocking* ratchet. I describe these below, following the classification in Ref. [75].

2.3.1 Flashing ratchet

The *flashing* or *pulsating* ratchets are those that have a time-dependent potential and no additional driving. In terms of the simple one dimensional model Eq. 2.4 we have $V \equiv V(x,t)$ and $F(x,t) \equiv 0$. Necessarily then, the potential $V(x,t)$ is either spatially or temporally asymmetric. One sub-type of the *flashing* ratchet are the *fluctuating potential ratchets*. These have a potential of the form

$$V(x,t) \equiv V(x)f(t) \tag{2.5}$$

for some function $f(t)$.

It should be noted that if the potential $V(x)$ is symmetric no current can be generated whatever the function $f(t)$. Only by including a driving can a current be generated in this case.

The archetypal example of the *fluctuating potential ratchet* is the 'on/off' ratchet where $f(t)$ evaluates to two values only:

$$f(t) = \begin{cases} 0 & \text{meaning the potential is off} \\ 1 & \text{(by convention) meaning the potential is on .} \end{cases} \tag{2.6}$$

The principle of the 'on/off' ratchet is illustrated in Fig. 2.1.

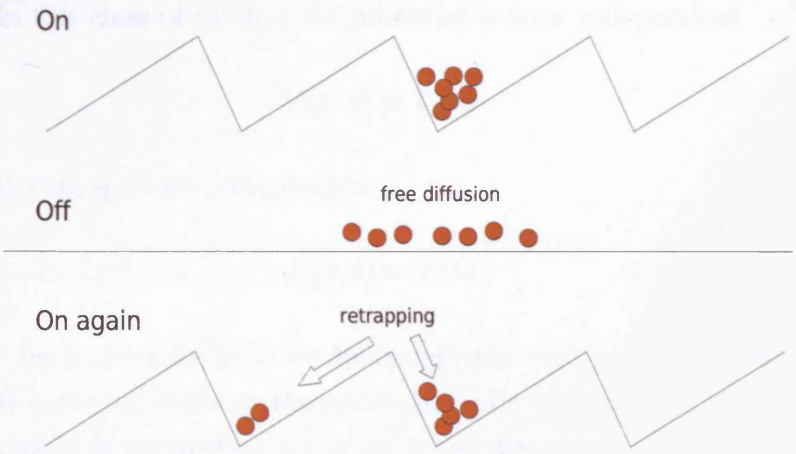

Figure 2.1: Illustration of a flashing ratchet, an 'on-off' ratchet. The particles are initially trapped in the potential wells. With the potential off, the particles undergo free diffusion through Brownian motion. Switching the potential back on causes the retrapping of the particles whence more are localised to one side than the other due to the spatial asymmetry of the potential.

We start with the potential 'on' and the particles localised in the wells (local minima) of the potential (top figure). The potential is then switched off (middle figure); without a confining potential the particles undergo Brownian motion and diffuse freely and symmetrically in both directions. With the potential back on (bottom figure), the particles are retrapped in the potential wells. If the duration of the 'off' phase is sufficiently long, particles will be trapped in wells neighbouring that of the original. More particles will be trapped to one side than the other for an asymmetric potential. In the example illustrated there will be more particles trapped to the left than to the right, compared to the starting configuration. The net effect of repeated 'on/off'

cycles is a particle current to the left.

It should be noted that the generation of a current here is not in violation of the second law of thermodynamics as it may at first appear. Indeed, in the process of switching on the potential work is performed in moving the particles such that they are trapped in the potential wells. Thus it is this additional work in combination with the spatial asymmetry that generates a current in this ratchet.

2.3.2 Rocking ratchet

The next important type of ratchet is the *rocking* ratchet, also known as *tilting* or *forcing* ratchet. In these ratchets the potential is 'rocked' by an unbiased driving. In this class of ratchet the potential is time independent

$$V(x,t) \equiv V(x) \ . \tag{2.7}$$

and the driving spatially independent

$$F(x,t) \equiv F(t) \ . \tag{2.8}$$

As will be discussed in detail in the following, when the potential is asymmetric, a symmetric driving leads to the generation of a current. On the other hand if the potential is symmetric, we require the driving to be asymmetric for a current to be generated. An example of this latter type is illustrated in Fig. 2.2.

In this figure a symmetric potential, middle drawing, is rocked by a zero-mean biharmonic driving (defined later in Eq. 4.59). The driving rocks the potential between two extremes, up and down, represented by the upper and lower drawings in Fig. 2.2. The asymmetry in the driving leads to an asymmetry in these extreme tilts. But in order to be unbiased, the driving tilts the potential for longer one way more than the other and overall the average tilt is zero.

The driving is just strong enough to cause some particles to occasionally move from well to well whilst not too strong so that the potential still presents local minima. The asymmetry in the driving combined with a non-linear response of the medium results in more particles moving in one direction than the other. In all but the simplest of cases the direction and amplitude of the current exhibit complex behaviour. Indeed currents can change sign (current reversal [75]) when parameters of the ratchet are changed. Examples of current reversals will be studied later.

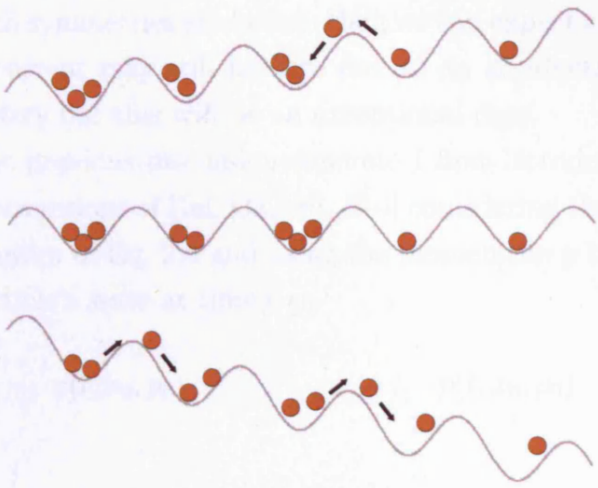

Figure 2.2: Illustration of a rocking ratchet. A symmetric potential (middle figure) is rocked by a zero-mean time-asymmetric biharmonic driving. The driving oscillates between two asymmetric extreme values, rocking the potential between two extreme tilts (upper and lower figures). The potential spends more time tilted one way than the other such that overall the average tilt is zero.

Of course there are many other types of ratchet besides the two described here; further examples can be found in Ref. [75].

2.4 Role of symmetries

Earlier I explained that one can expect a ratchet to generate a current when the symmetries do not prevent it from occurring. This is a consequence of Curie's principle [20]. Thus, symmetries have an important role in determining when currents occur. Before I describe the types of symmetries that play a role it is important to understand how symmetries inhibit currents.

Suppose we have a number of identical particles following the stochastic dynamics of our Langevin equation Eq. 2.4. Each particle evolves in time producing a trajectory in x and $\dot{x}$ space. The trajectories are unique due to independent sequences of realisations of the random process $\xi(t)$. The initial state of each particle is sampled so as to not introduce a bias that way. We define the current to be the ensemble-averaged particle velocity. Now, if the system possesses a symmetry that maps one trajectory onto another with the opposite velocity, averaging over a large ensemble will yield a zero current. Thus symmetries inhibit the generation of currents.

In an analysis of a system's symmetries we are looking for symmetries

that invert a trajectories velocity. This will indicate when a zero current is expected. If such symmetries are broken then we can expect a non-zero current. Of course the current may still be zero due to an accidental combination of ratchet parameters but this will be an exceptional case.

To make the previous discussion concrete I first introduce some notation following the conventions of Ref. [32, 86]. Still considering the one dimensional stochastic dynamics of Eq. 2.4 and using the momentum p instead of velocity $\dot{x}$, denote a particle's state at time t as

$$x(t; x_0, p_0) \qquad\qquad p(t; x_0, p_0) \tag{2.9}$$

where

$$x(t_0; x_0, p_0) = x_0 \qquad\qquad p(t_0; x_0, p_0) = p_0 \ . \tag{2.10}$$

The symmetries, $\hat{S}$, of Eq. 2.4 which lead to a change in sign of p are based on transformations in x and t . Clearly the transformations can only be an inversion of one variable with a shift in the other:

- $x \to -x + x', \quad t \to t + t'$
- $x \to x + x', \quad t \to -t + t'$

where x' and t' are constants.

Whether a particular transformation leads to a symmetry and invariance of Eq. 2.4 depends on the particular forms of the potential $V(x,t)$ and the driving $F(x,t)$. [The term $\xi(t)$ can be ignored in the symmetry analysis as it is assumed to be unbiased.] In characterising the symmetries of V and F we use the terminology and notation of Ref. [32] which is summarised here. A periodic function $g(y)$ of period L is said to be

- *symmetric* and labelled as g_s if $g(y + y') = g(-y + y')$
- *antisymmetric* and labelled as g_a if $g(y + y') = -g(-y + y')$
- *shift-symmetric* and labelled as g_{sh} if $g(y + L/2) = -g(y)$

for some constant y'.

Simplifying matters by taking V and F to be functions of one parameter only, that is to say, $V(x,t) \equiv V(x)$ and $F(x,t) \equiv F(t)$ and assuming V is periodic in x with period X and F is periodic in t with period T, we note the

following transformations lead to an invariance of Eq. 2.4

$$\hat{S}_a : x \to -x + 2x', \quad t \to t + T/2 \qquad \text{given } f_a,\ F_{sh} \tag{2.11a}$$

$$\hat{S}_b : x \to x, \quad t \to -t + 2t' \qquad \text{given } F_s, \gamma = 0 \tag{2.11b}$$

$$\hat{S}_c : x \to x + X/2, \quad t \to -t \qquad \text{given } f_{sh},\ F_a, m = 0 \tag{2.11c}$$

where $f(x) \equiv V'(x)$. Thus if any of these conditions apply current generation is forbidden.

For symmetry $\hat{S}_b$, the condition $\gamma = 0$ signifies zero damping. This is appropriate in the lower limit of underdamped ratchets and for Hamiltonian ratchets when noise is absent.

Symmetry $\hat{S}_c$ may be present in overdamped ratchets where the condition $m = 0$ is appropriate. This symmetry was found theoretically in overdamped rocking ratchets in Ref. [74] and coined 'supersymmetry'.

An analysis of the symmetries of a system through the specific forms of V and F is a very useful component of a theoretical study of a ratchet. I will present several such analyses later.

2.5 Cold atom ratchets

Ratchets using cold atoms are realised with an optical lattice. An optical lattice is a periodic structure produced by the interference of two or more laser beams. The interference produces a spatial modulation of light-field intensity and/or polarisation. The light-field interacts with the atom and shifts the energy (*light-shift*) of the various atomic states. To simplify calculations the number of atomic states is often limited to two.

The spatial modulation of the light-field, and so the light-shifts, results in periodic potentials (*optical potential*) for the atom. The depth of these potentials can be varied by changing the laser parameters, typically the intensity and the frequency detuning from atomic transition.

The optical lattice can also cool atoms which will then become trapped in the wells of the potentials. Several cooling schemes exist[1] which precisely depend on the light-field configuration and the atomic transition being considered. The generic aim is to reduce the kinetic energy of the atoms.

In the low intensity Sisyphus cooling scheme of Chapter 4 it is the combination of the modulated light shifts together with *optical pumping* that cools the atoms. Optical pumping transfers an atom between ground state sublevels

[1]For a review see Ref. [16]

through photon absorption/emission cycles. Sequences of such cycles result in a loss of atomic kinetic energy which is carried away by the emitted photons. This energy dissipation damps the atomic motion.

Optical pumping also introduces fluctuations in the atomic motion. This is due to the natural statistical uncertainty in the photon absorption and emission events The fluctuations in momentum that result from these events are unbiased and can be considered as a stochastic noise. The magnitude of this noise varies with the optical pumping rate which in turn depends on the laser parameters.

Optical lattices are naturally symmetric; some asymmetry needs to be introduced into the system in order to generate a current. One method of doing this is by applying an asymmetric driving. This is the method adopted by our group [47]. In experiments this can be achieved by phase-modulating one of the laser beams. This modulation results in an instantaneous force on the atoms [80]. Studies of ratchets with such drivings are presented in detail in Chapters 4 and 5.

An alternative method is to introduce an asymmetry directly into the lattice. One means of doing this is through the use of an external magnetic field as proposed in Ref. [42] and implemented in Ref. [59]. This system has received some attention but will not be reported upon here.

In conclusion a cold atom ratchet represents a highly tunable system. Damping and noise levels can be varied by changing laser parameters. An asymmetric driving can be applied in a relatively simple manner. Lastly, an optical lattice has a predictable potential and is defect free which gives them a certain advantage compared to other realisations of ratchets.

2.5.1 Experimental setup

Much of my work has been done in parallel with experiments performed by other members of the group. Here I briefly describe a typical rocking ratchet experiment; more details can be found in Refs. [34, 36, 47].

A typical experimental run consists of a few distinct stages, each of a duration of a few milli-seconds up to a few seconds. The first stage is to prepare a cloud of cold, trapped atoms for the optical lattice. This is done using a magneto-optical trap (MOT). A glass cell at near vacuum is filled with atoms from a source of rubidium or caesium. A MOT is produced in the cell by three pairs of counter-propagating laser beams that cool the atoms and by two magnetic coils forming a quadrupole field that trap the atoms. Running the MOT for a few seconds produces a cloud of approximately 10^8 atoms at a

temperature of approximately $100\mu K$.

The atoms are further cooled using optical molasses [61] before an optical lattice is formed from additional laser beams. The atoms are allowed to thermalise in the lattice before the driving is applied. This is done by phase-modulating one of the lattice laser beams through the use of acousto-optical modulators (AOMs). Images of the cloud of atoms, captured with CCD cameras, are taken before and after the driving stage. From these images we can determine the distance travelled by the centre-of-mass, and hence the atomic current given a driving of known duration.

The sequencing and timing of the distinct phases (MOT, optical molasses, driving, etc) is precisely controlled via computer meaning experimental reproducibility is greatly enhanced. The form of the driving is also controlled by a computer providing great flexibility in the forms that can be studied with the same experimental setup.

Chapter 3

Simulations

In this chapter I present some details on the main approaches used in the numerical simulation of atomic motion in a light-field. There are two aspects to each approach: what treatment is applied to the modelling of the state and dynamics of the system, and secondly, what numerical methods can be applied in order to simulate the system.

The system we're modelling consists of atoms with two or more internal states, a light field and the vacuum modes that absorb the spontaneously emitted photons. We ignore atomic collisional and collective effects and treat atoms individually. This is consistent with our experimentally realised optical lattices where lattice site occupation is of the order of one percent.

3.1 The three main treatments

There are three main treatments in common use. These are

- *quantum* - the atomic internal and external degrees of freedom are treated as quantum mechanical variables. The dynamics are governed by a master equation.
- *semiclassical* - the external degrees of freedom are treated as classical variables whilst retaining the true internal state,
- *classical* - the internal state is eliminated with the external degrees of freedom treated as classical variables.

These main treatments will be summarised below; more details may be found in Refs. [22, 83].

3.1.1 Quantum

The coupling between the atom and light-field is relatively strong in comparison to the coupling to the vacuum modes. We assume that the vacuum is therefore unaltered by its interaction with our system and also that it has no 'memory'. In the usual way then, we may consider the atom plus light-field as a small system S weakly coupled to a large reservoir R, the vacuum. The state of the complete system may be described by a density operator ρ_{SR} whose dynamics are governed by the von-Neumann equation

$$\dot{\rho}_{SR} = -\frac{i}{\hbar}\Big[H, \rho_{SR}\Big] \ . \tag{3.1}$$

Here H is the total system Hamiltonian consisting of the sum of the individual Hamiltonian's for S, R and the interaction between them

$$H = H_S + H_R + H_{SR} \ . \tag{3.2}$$

We're generally only interested in the state of the small system S. We obtain a reduced density operator for S by tracing over the degrees of freedom for R

$$\rho_S = \mathrm{Tr}_R\, \rho_{SR} \ . \tag{3.3}$$

The dynamics of ρ_S are governed by the so-called quantum master equation

$$\dot{\rho}_S = \frac{i}{\hbar}\left[\rho_S, H_S\right] + \mathcal{L}_{relax}(\rho_S) \tag{3.4}$$

where $\mathcal{L}_{relax}$ represents the dissipative couplings to the reservoir. In many cases it can be written in the following form

$$\mathcal{L}_{relax}(\rho_S) = -\frac{1}{2}\sum_m (C_m^\dagger C_m \rho_S + \rho_S C_m^\dagger C_m) + 2\sum_m C_m \rho_S C_m^\dagger \ . \tag{3.5}$$

This form of the master equation was derived mathematically by Lindblad and is called the Lindblad form[81]. The operators C_m represent the effect of the reservoir on the system. Their particular form depends on the problem being investigated; several examples common in quantum optics can be found in Ref. [67].

State representation

The atomic state is represented as a wave-function on a Hilbert space. This Hilbert space is the tensor product of two orthogonal spaces, the space for the centre-of-mass wave-packet and the space for the internal state.

In a simulation scheme the representation of the Hilbert space is necessarily discrete and finite. We follow the 'Fourier Method orthogonal collocation representation' of Ref. [49] and as exemplified in Ref. [58]. We form discrete grids for the atoms spatial coordinate x and momentum p, of size n, so that x extends over the range $[0, x_{max}]$ and p over the range $[-p_{max}, p_{max}]$.

Working in the spatial representation we represent the atomic wave-function as

$$|\psi(x)\rangle = \sum_{j=1}^{n} \alpha_{x_j}|a_1; x_j\rangle + \beta_{x_j}|a_2; x_j\rangle + \cdots \tag{3.6}$$

where the a_i represent the i^{th} internal state and $|a_1; x_j\rangle$ denotes the product state $|a_1\rangle \otimes |x_j\rangle$ and where $x_j = j\,\Delta x$ with $\Delta x = x_{max}/n$. The $\alpha_{x_j}, \beta_{x_j}, \cdots$ are c-number amplitudes for each of the internal states a_i. The number of internal states is generally much smaller than the size of the external basis n.

In the momentum representation we have

$$|\psi(p)\rangle = \sum_{j=1}^{n} \alpha_{p_j}|a_1; p_j\rangle + \beta_{p_j}|a_2; p_j\rangle + \cdots \tag{3.7}$$

where $p_j = -p_{max} + j\,\Delta p$ with $\Delta p = 2p_{max}/n$. The two representations are connected by discrete Fourier transform.

In the scheme of Ref. [49] x_{max} and p_{max} aren't independent. The minimum volume of phase-space a 1D quantum-mechanical system can be localised in is h, Planck's constant. The volume of phase-space covered by our discrete representation is

$$2\,p_{max}\,x_{max} \equiv n\,h \tag{3.8}$$

from which we find

$$p_{max}/\hbar = n\pi/x_{max} \tag{3.9}$$

and

$$\Delta x\,\Delta p/\hbar = 2\pi/n\ . \tag{3.10}$$

The range $[0, x_{max}]$ should be set to a whole number of spatial periods. At the same time we must choose p_{max} sufficiently large so to accommodate the expected momentum distribution of the atoms. We should also make Δx small enough to sample several times over the spatial period of the light field as the spatial variation of the field intensity and/or polarisation is the essence of the laser cooling schemes studied here. This requirement for Δx should be balanced against any restrictions on Δp. For example in sub-recoil cooling schemes we necessarily require $\Delta p \ll \hbar k$.

Dynamics

The dynamics of the atomic system are governed by a master equation like Eq. 3.4 with the Hamiltonian acting on the atomic Hilbert space. The master equation could be inverted to give the steady state value of the density operator ρ. However, with the discretisation of the external degrees of freedom, and noting that ρ scales with n^2, this would involve inverting a very large matrix for even modest values of n. This would prove problematic in it's requirements on computer memory, but can also be very time consuming. An alternative approach is to perform a time integration of the equation starting from some suitable initial form of the density matrix, continuing until a steady state is reached.

Rather than solving the master equation directly we use a trajectory method to 'unravel' the master equation. Several trajectory methods were developed in the late 1980s; for a review refer to Ref. [71]. The main advantage of these methods is that the calculations scale with n compared to n^2 in the density matrix based methods.

The method I chose to use is the Monte Carlo Wave Function (MCWF) method [25, 67]. We start by initialising each atom to a well defined state e.g. the ground state of a localised harmonic oscillator. The method then proceeds by repeatedly performing two steps.

The first step is to evolve the wave-function over a timestep Δt with a non-Hermitian Hamiltonian. This effective Hamiltonian is formed from the system Hamiltonian by the addition of the dissipative terms resulting from the coupling to the environment

$$H = H_S - \frac{i\hbar}{2}\sum_m C_m^\dagger C_m \ . \tag{3.11}$$

For the case of spontaneous emission from a two-level system we have [67]

$$\sum_m C_m^\dagger C_m = \Gamma P_e \tag{3.12}$$

with P_e the projection operator onto the excited state subspace and Γ being the excited state linewidth. The effective Hamiltonian is then

$$H = H_S - \frac{i\hbar}{2}\Gamma P_e \tag{3.13}$$

The time evolution of the system state can be performed in several ways.

One way is to expand Schrödinger 's equation for a small timestep to obtain

$$|\psi(t+\Delta t)\rangle = \left(1 - \frac{i}{\hbar} H \Delta t\right)|\psi(t)\rangle \tag{3.14}$$

where $|\psi(t)\rangle$ is the normalised wave-function at time t.

Another way to evolve the wave-function is to use the Split Operator Fourier Transform (SOFT) method [49]. This relies on the Hamiltonian being formed of terms which aren't functions of both x and p. This is the usual case for the systems I study where we have separate kinetic and potential terms

$$H \equiv \frac{p^2}{2m} + V(x) \ . \tag{3.15}$$

To second order in the timestep this method evolves the wave-function as

$$|\psi(t+\Delta t)\rangle = U_K\left(\frac{\Delta t}{2}\right) U_V(\Delta t) U_K\left(\frac{\Delta t}{2}\right)|\psi(t)\rangle \tag{3.16}$$

or equivalently

$$|\psi(t+\Delta t)\rangle = U_V\left(\frac{\Delta t}{2}\right) U_K(\Delta t) U_V\left(\frac{\Delta t}{2}\right)|\psi(t)\rangle \ . \tag{3.17}$$

The terms U_V and U_K are the time evolution operators for the potential and kinetic terms respectively

$$U_V(\Delta t) = \exp\left(-\frac{i}{\hbar} V \Delta t\right) \tag{3.18}$$

$$U_K(\Delta t) = \exp\left(-\frac{i}{\hbar}\frac{p^2}{2m}\Delta t\right) \ . \tag{3.19}$$

It should be noted that in calculating $|\psi(t+\Delta t)\rangle$ according to Eq. 3.16 or Eq. 3.17, before the action of the operators U_V and U_K the wavefunction must be in the appropriate representation. That is to say U_V may only operate on the spatial representation of $|\psi\rangle$ and U_K only on the momentum representation. To minimise unnecessary Fourier Transforms between representations, Eq. 3.16 would be used when working in the momentum representation and Eq. 3.17 with the spatial representation.

The second step in the MCWF method is determining the occurrence of a quantum jump; this models the detection of a decay from our system. The jump probability is calculated using the new wave-function obtained in the first step. We note that in using the either of the two time integration methods described in the first step, the norm of the wave-function is not conserved.

The jump probability is given as

$$dp = 1 - \langle\psi(t + \Delta t)|\psi(t + \Delta t)\rangle \tag{3.20}$$

as $\langle\psi(t + \Delta t)|\psi(t + \Delta t)\rangle$ is the probability that no decay occurs in the time interval $[t, t + \Delta t]$.

We compare the jump probability to a random number η sampled from a uniform distribution on the interval $[0, 1]$. The case $\eta < dp$ corresponds to detection of a photon and $\eta > dp$ to a non-detection. If there is a detection we deem a quantum jump has occurred and 'collapse' the wave function to the decayed state. If more than one decay channel exists then another uniformly-distributed random number is compared to the relevant branching probabilities and the decayed state selected accordingly. If a jump does not occur the new wave-function obtained from the first step is normalised and taken as the new starting state. By repeating this two-step process we obtain a unique trajectory for each atom.

Measurements of 'observables' are obtained by averaging over an ensemble of individual realisations of the system. For large sample sizes, the measurements closely approximate those obtained by simulating the master equation directly [67].

The obvious advantage of the quantum treatment compared to the others is the fewer approximations made. However this comes at a cost in terms of the sheer number of calculations. The computer implementation is not so straightforward and numerical computation is relatively slow.

3.1.2 Semiclassical

In a semiclassical treatment the width of the momentum distribution is assumed to be large compared to $\hbar k$. The atoms position and momentum which are operators in the fully quantum treatment are replaced by their average values. The internal state dependent force and momentum diffusion experienced by the atoms determine the dynamics of the position and momentum. One way to determine these kinetic coefficients is to derive a Fokker-Planck equation for the Wigner distribution.

The derivation starts by applying the Wigner transform [84] of the density matrix to the master equation. In one dimension the Wigner transform is

$$W(x, p, t) = \int dx' \, \langle x + \frac{x'}{2}| \, \rho(t) \, |x - \frac{x'}{2}\rangle e^{-ip \cdot x'/\hbar} \, . \tag{3.21}$$

Making an expansion to second order in $\hbar k/\bar{p}$ with $\bar{p}$ the r.m.s. momentum one obtains [22] a Fokker-Planck equation with identifiable force (F), and diffusion (D) coefficients

$$\frac{d}{dt}W(x,p,t) = -\frac{\partial}{\partial p}\Big(F(x,p)W(x,p,t)\Big) + D(x,p)\frac{\partial^2}{\partial p^2}\Big(W(x,p,t)\Big) \ . \quad (3.22)$$

In the internal state basis the Wigner distribution is often diagonal so that these diagonal elements can be identified as semiclassical state populations. This treatment is applied to the cooling scheme studied in Chapter 4.

The Fokker-Planck equation describes the dynamics of the probability density W of the stochastic variable p at a fixed point in space x. Corresponding to this Fokker-Planck equation is the stochastic differential equation of the stochastic variable p itself [10, 77]. For example the stochastic differential equation equivalent to the Fokker-Planck equation above is

$$p(t+dt) = p(t) + F(x,p)dt + \sqrt{2D(x,p)}\ dW \ . \quad (3.23)$$

In the last term dW represents a Wiener process, that is a process having a Gaussian distribution with zero mean and variance dt.

These stochastic differential equations are generally intuitive and reflect the underlying physical processes well. We can perform a Monte-Carlo analysis of these stochastic equations by evolving a set of atoms. Each atom is initialised to a random internal state, with position and momentum sampled from some Gaussian distribution to represent a localised thermal atomic cloud. The momentum is evolved according to the Langevin equation and the position updated accordingly. Various algorithms exist for this time integration; see for example Refs. [33, 73, 77]. Internal state changes are modelled as random quantum jumps. Computer implementation is straightforward and numerical simulations fast in comparison to the quantum approach.

As the semiclassical treatment introduces approximations, some of the finer details of the physical processes are not reproducible. It also goes without saying that this approach is not appropriate for sub-recoil cooling schemes where the approximations employed are invalid or where purely quantum effects (e.g. tunnelling) are prevalent; in such cases a quantum treatment is required.

3.1.3 Classical

In the classical treatment, as in the semiclassical treatment, the atoms momentum and position are treated as classical variables assuming a very small wave-packet. The classical treatment extends the semiclassical treatment by

eliminating the internal state from the equations of motion. The aim of the classical treatment then is to derive an equation of motion with force and diffusion coefficients that depend solely on the atoms momentum and/or position.

We start with the force expressed in the semiclassical treatment as the spatial gradient of the atom light-field coupling. This coupling, in the usual rotating wave and dipole approximations, is written in terms of the various atom internal states and coherences. For some cooling schemes and under some conditions, some of these states can be expressed in terms of other states and then eliminated from the expression for the force (adiabatic elimination). The stationary values of the remaining internal states may be determined resulting in the force being expressed in terms of the atoms momentum and/or position only.

The momentum diffusion coefficient is generally computed from the correlation function of the force operator. It may also be determined for some cooling schemes following heuristic arguments. For further details pertaining to the cooling schemes I study later see Refs. [23], [21], and [72].

The force and diffusion coefficients may be used as-is to form a Fokker-Planck equation for the Wigner representation of the external variables. This can be simulated directly using appropriate methods.

Alternatively, the equivalent Langevin equations can be integrated e.g. [33, 56, 73, 77]. Due to the stochastic nature of the Langevin equation a Monte-Carlo simulation method is generally required.

The computer implementation is relatively straightforward and numerical computation relatively fast. However, due to the approximations introduced through the inherent nature of the classical approach not all physical behaviour can be reproduced.

3.2 Stages of numerical simulation

A typical numerical simulation of a cold atom ratchet has three distinct stages in the time evolution. In the first stage the atoms are allowed to thermalise in the optical lattice in the absence of driving. The length of this stage is determined apriori such that a steady temperature is achieved and this typically varies with laser parameters. Note that for laser cooling the temperature T of the system is generally defined by [61]

$$\frac{1}{2}k_B T = \langle \frac{p^2}{2m} \rangle \equiv \langle \left(\frac{p}{p_r}\right)^2 \rangle E_r \tag{3.24}$$

where k_B is Boltzmann's constant, $p_r = \hbar k, E_r = \hbar^2 k^2/2m$ are the recoil momentum and energy respectively. In the simulations I generally use $\langle p^2/p_r^2 \rangle$ as a proxy for the temperature.

In the second stage of our simulations the driving is switched on adiabatically. This is so as to reduce the shock to the system from the application of the driving. The typical length of this stage is 100 periods of the driving force.

In the final stage of the simulation the full driving is applied, typically for 1000+ driving periods. Any transient effects should have died out by that time. To reduce possible timing effects the ratchet current I is determined as a temporal average of the atomic current $\langle v \rangle$ over the final few (10 to 50) driving periods

$$I = \frac{1}{t_2 - t_1} \sum_i \langle v \rangle (t_1 + i\Delta t) \tag{3.25}$$

where the sum is over the number of timesteps Δt in the interval $t_2 - t_1$.

Chapter 4

Red-Sisyphus ratchets

In this chapter I present detailed numerical studies of three ratchets based on the same 1D red-Sisyphus cold atom system. This work was performed largely in parallel to experiments conducted by the group. The first two of the three ratchets are of the 'rocking' type. The breaking of the symmetries, and hence the generation of current, is controlled by certain parameters of the driving. The last of the three ratchets, the gating ratchet, is a hybrid of the 'flashing' and 'rocking' types. The potential fluctuates and at the same time a driving is applied. The main findings of these studies, together with corresponding experimental work, have been published [11, 38, 39]:

- M. Brown and F. Renzoni. Ratchet effect in an optical lattice with biharmonic driving: A numerical analysis. *Physical Review A*, 77(3): 033405, March 2008.
- R. Gommers, M. Brown, and F. Renzoni. Symmetry and transport in a cold atom ratchet with multifrequency driving. *Physical Review A*, 75 (5):053406, May 2007.
- R. Gommers, V. Lebedev, M. Brown, and F. Renzoni. Gating ratchet for cold atoms. *Physical Review Letters*, 100(4):040603, February 2008.

Modelling of these ratchet systems is based on the simplest 1D system that gives rise to Sisyphus cooling. The optical lattice is formed by two counter-propagating light beams linearly polarised and orthogonal to each other, a configuration called lin⊥lin. This light-field is combined with a $J_g = 1/2$ to $J_e = 3/2$ atomic transition. At low saturation where cooling is effective, the excited states can be adiabatically eliminated [19] from the dynamics which then reduces to that of a simple two state system. Associated with each of the two atomic ground state Zeeman sublevels $|g, m = \pm\frac{1}{2}\rangle$ is a potential $U_{\pm}(x)$. Atoms jump between these potentials through optical pumping, the transition

of the atom from one ground state sublevel to another through absorption-spontaneous emission cycles. The random nature of these events introduces fluctuations in the atomic motion. For a red laser detuning, the jumps lead to a loss in atomic energy.

For our numerical calculations of this system a semiclassical approach was taken. The dynamics are modelled with stochastic differential equations derived from the Fokker-Planck equation. This in turn is derived from the Wigner transform of the Optical Bloch Equations. Drivings are applied by adding terms directly to these differential equations - this is equivalent to phase-modulating the light-field as is done in experiments. Numerical results were obtained through Monte Carlo simulations.

We point out that the configuration we study here numerically does not correspond exactly to the experimental one [35, 36, 47] which involves atomic transitions with larger angular momentum and three dimensional optical lattices. However our configuration has the benefit of being much simpler to treat numerically whilst still exhibiting all the essential features required.

4.1 System overview

4.1.1 Light-field

The lin⊥lin light-field consists of two counter-propagating linearly and orthogonally polarised laser beams. Denoting the frequency of the beams as ω_L and considering propagation aligned along the z axis the resultant light-field is given by

$$E(z,t) = \frac{E_0}{2}\Big(\hat{e}_x\big(e^{i(kz-\omega_L t)} + \text{c.c.}\big) + \hat{e}_y\big(e^{i(kz+\omega_L t+\phi)} + \text{c.c.}\big)\Big) \tag{4.1}$$

$$\equiv E^+(z)e^{-i\omega_L t} + \text{c.c.} \tag{4.2}$$

with

$$E^+(z) = \frac{E_0}{\sqrt{2}}\Big(\hat{e}_- \cos kz - i\hat{e}_+ \sin kz\Big) \tag{4.3}$$

for an appropriate choice of the phase ϕ and where E_0 is the amplitude of each travelling wave beam, $\hat{e}_\pm$ are the circular basis vectors and $k = 2\pi/\lambda$ is the wave number.

This field configuration does not produce a spatial intensity modulation but does produce a polarisation modulation. The field polarisation

$$\hat{e}(z) = \hat{e}_- \cos kz - i\hat{e}_+ \sin kz \tag{4.4}$$

has an elliptical spatial gradient changing from σ^- at $z = 0$, linear at $z = \lambda/8$, σ^+ at $z = \lambda/4$, linear at $z = 3\lambda/8$ and orthogonal to that at $z = \lambda/8$, σ^- at $z = \lambda/2$, etc (see Fig. 4.1). This polarisation gradient induces position dependent light-shifts for the ground state sublevels as we shall see.

4.1.2 Atomic transition

The atomic transition $J_g = 1/2$ to $J_e = 3/2$ is the simplest one that gives rise to Sisyphus cooling. Before the elimination of the excited states there are 6 atomic states for consideration, depicted below, with the associated Clebsch-Gordan coefficients for the various transitions labelled.

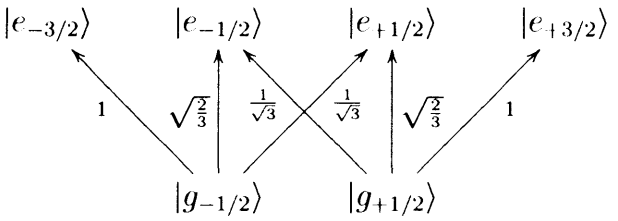

We've denoted the state $|e, m = +3/2\rangle$ as $|e_{+3/2}\rangle$ and the other states similarly.

4.1.3 Optical pumping

Absorption-spontaneous emission cycles transfer atoms from one ground state sublevel to another. At sites where the light-field polarisation is σ^+ the probability to transition from $|g_{+1/2}\rangle$ to $|e_{+3/2}\rangle$ is three times larger than that for $|g_{-1/2}\rangle$ to $|e_{+1/2}\rangle$. This is due to the relative magnitudes of the Clebsch-Gordan coefficients. The light-shift of $|g_{+1/2}\rangle$ is also three times larger than that of $|g_{-1/2}\rangle$ at these sites. After a few cycles atoms in the $|g_{-1/2}\rangle$ state are optically pumped to the $|g_{+1/2}\rangle$ state. This is assuming a red laser detuning ($\delta := \omega_L - \omega_A < 0$) so that the light-shifts are negative.

Similarly at sites of σ^- polarisation the atoms are optically pumped to the $|g_{-1/2}\rangle$ state. At sites of linear polarisation the transitions from the two ground state sublevels have equal probability and the light-shifts are also equal. The two ground state sublevels are then equally populated at sites of linear polarisation.

Optical pumping introduces random fluctuations in the motion of the atoms. The transitions occur at a well defined rate but at random times and the atoms receive the random momentum recoils from the spontaneous emission events.

4.1.4 Bipotential

The spatially modulated light-shifts form the spatially symmetric and periodic bipotential $U_{\pm}(z)$. That is, the ground state $|g_{+1/2}\rangle$ (resp. $|g_{-1/2}\rangle$) experiences the potential $U_{+}(z)$ (resp. $U_{-}(z)$). The maxima of U_{+} coincide with the minima of U_{-} and vice-versa. These extrema occur at sites where the field is purely circularly polarised (see Fig. 4.1).

The bipotentials can be expressed as

$$U_{\pm}(z) = \frac{U_0}{2}(-2 \pm \cos 2kz) \tag{4.5}$$

with U_0 representing the potential depth.

The light-shifts and the transition probabilities of optical pumping, are modulated in the exact same way so that the probability to transition from $|g_{+1/2}\rangle$ (resp. $|g_{-1/2}\rangle$) is maximal where the potential U_{+} (resp. U_{-}) is maximal.

4.1.5 Sisyphus cooling

The spatial modulation of the light-shifts and the transition probabilities leads to an appealing explanation of the Sisyphus cooling mechanism in the semi-classical picture.

Consider an atom in the $|g_{+1/2}\rangle$ state moving along the potential $U_{+}(z)$ (see Fig. 4.1). The atom will jump preferentially near the crests of $U_{+}(z)$ ($z = 0, \lambda/2, \cdots$) where the probability is greatest. If the transition is back to $|g_{+1/2}\rangle$ (and hence $U_{+}(z)$) through the emission of a π-polarised photon, the atoms total energy (kinetic + potential) does not change. However if the transition is to $|g_{-1/2}\rangle$ (and hence $U_{-}(z)$), an inter-state transition, through the emission of a σ^{+}-polarised photon, the atom is deposited in the well of $U_{-}(z)$. Assuming a red laser detuning so that U_0 is positive, the atom loses potential energy of the order of U_0 because of this jump. This energy is carried away by the emitted photon.

Similarly, the atom now moving in $U_{-}(z)$ potential will preferentially jump near the crests of U_{-}. A transition to $|g_{+1/2}\rangle$ will put the atom in a well of the $U_{+}(z)$ potential. Through repeated transitions the atom on average climbs uphill more than downhill and hence the name 'Sisyphus'. The total energy reduces until the atom can no longer climb the potential hills when it effectively becomes trapped. The final temperatures scale with U_0.

Trapped atoms still undergo transitions as the transition probabilities in the wells although small are non-zero and these transitions introduce random

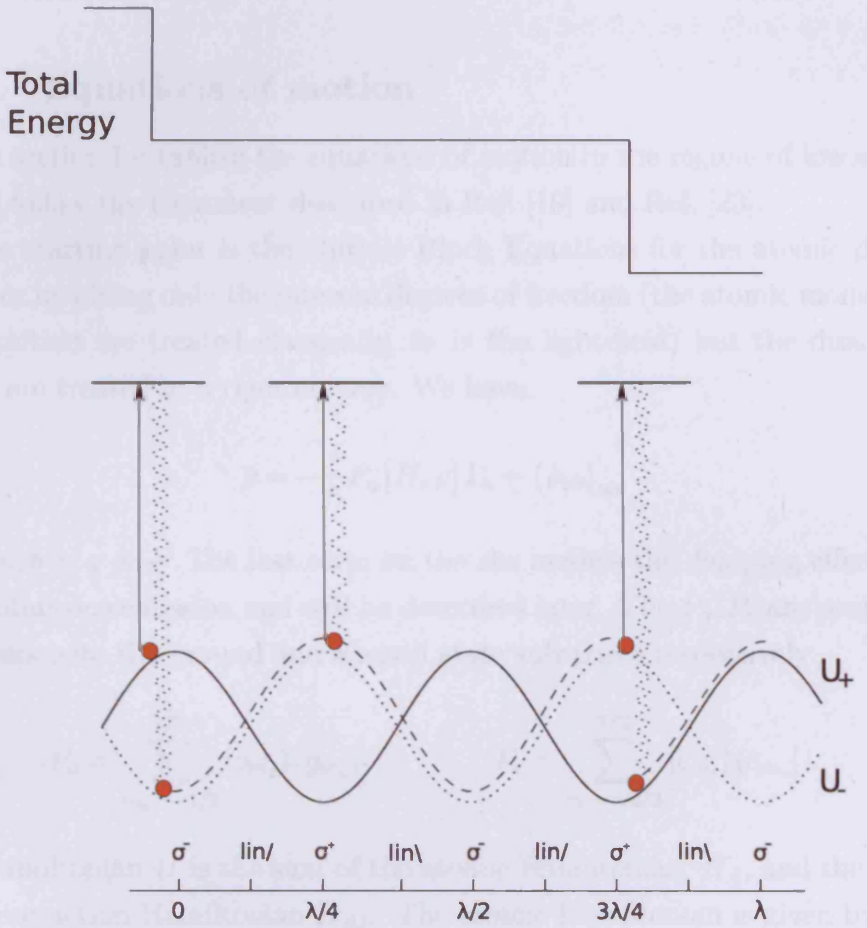

Figure 4.1: Bipotential for $|g_{\pm 1/2}\rangle$ states in the 1D lin$\perp$lin light configuration and illustration of Sisyphus cooling. The field polarisation has an elliptical spatial gradient changing from σ^- at $z = 0$ to linear at $z = \lambda/8$, etc. The light-shifts for the ground state sublevels oscillate in space with period $\lambda/2$ and form the bipotential $U_\pm$. Atoms in the $|g_+\rangle$ (resp. $|g_-\rangle$) sublevel will preferentially jump at the crests of the U_+ (resp. U_-) potential where the transition probability is maximal; jumping between sublevels they will be deposited in the troughs of the U_- (resp. U_+) potential. Experiencing such jumps atoms will on average lose energy of the order of U_0. Atoms undergo a Sisyphus cooling as they climb uphill more than they go downhill.

unbiased fluctuations in the atomic motion. The rate of these transitions is $\Gamma' = \Gamma s_0$ where the saturation parameter s_0 is a function of the laser parameters. By varying Γ' through the laser parameters we can vary the velocity damping the atoms experience. Thus Γ' will be a proxy for the damping coefficient γ of Eq. 2.4. At low saturation, i.e. $s_0 \ll 1$, we may expect the damping γ to be relatively small.

4.1.6 Equations of motion

In this section I establish the equations of motion in the regime of low saturation. I follow the treatment described in Ref. [19] and Ref. [23].

The starting point is the Optical Bloch Equations for the atomic density operator involving only the internal degrees of freedom (the atomic momentum and position are treated classically, as is the light-field) but the dissipative effects are treated in a rigorous way. We have

$$\dot{\rho} = -\frac{i}{\hbar} P_a \left[H, \rho \right] P_b + \left(\dot{\rho}_{ab} \right)_{sp} \tag{4.6}$$

where $a, b = g$ or e. The last term on the rhs models the damping effects due to spontaneous emission and will be described later. The P_g, P_e are projection operators onto the ground and excited state subspaces respectively

$$P_g = \sum_{m_g = -1/2}^{1/2} |g_{m_g}\rangle\langle g_{m_g}| \qquad P_e = \sum_{m_e = -3/2}^{3/2} |e_{m_e}\rangle\langle e_{m_e}| \,. \tag{4.7}$$

The Hamiltonian H is the sum of the atomic Hamiltonian, H_A, and the atom-light interaction Hamiltonian H_{AL}. The atomic Hamiltonian is given by

$$H_A = \frac{p^2}{2m} + \hbar\omega_A \sum_{m_e = -3/2}^{3/2} |e_{m_e}\rangle\langle e_{m_e}| \tag{4.8}$$

which is the sum of the external and internal atomic energies respectively. The Hamiltonian H_{AL} comes from the coupling of the atomic dipole moment d and the light-field

$$H_{AL} = -d \cdot E(z, t) \tag{4.9}$$

which, using the light-field of Eq. 4.1, and the rotating-wave approximation

becomes

$$H_{AL} = \frac{\hbar\Omega_0}{\sqrt{2}} \cos kz \Big(\frac{1}{\sqrt{3}} |e_{-1/2}\rangle\langle g_{+1/2}| + |e_{-3/2}\rangle\langle g_{-1/2}| \Big) e^{-i\omega_L t} + \text{h.c.} \quad + \\ \frac{\hbar\Omega_0}{i\sqrt{2}} \sin kz \Big(|e_{+3/2}\rangle\langle g_{+1/2}| + \frac{1}{\sqrt{3}} |e_{+1/2}\rangle\langle g_{-1/2}| \Big) e^{-i\omega_L t} + \text{h.c.} \quad (4.10)$$

where $\Omega_0 = -DE_0/\hbar$ is the Rabi frequency which is a measure of the strength of the coupling between atom and the light-field , with D being the magnitude of the atomic dipole moment along the light-field direction.

I return now to the last term on the rhs of Eq. 4.6 which describes the damping effects of spontaneous emission. For the excited state populations and coherences and optical coherences we have [18]

$$\left(\dot{\rho}_{ee}\right)_{sp} = -\Gamma\rho_{ee} \quad (4.11)$$

$$\left(\dot{\rho}_{eg}\right)_{sp} = -\frac{\Gamma}{2}\rho_{eg} \quad (4.12)$$

$$\left(\dot{\rho}_{ge}\right)_{sp} = -\frac{\Gamma}{2}\rho_{ge} \ . \quad (4.13)$$

The expressions for the ground state population terms are complicated by the dependency on the polarisation of the spontaneously emitted photon. The general form is [58]

$$\left(\dot{\rho}_{gg}\right)_{sp} = \Gamma' \int_{-k}^{k} dk' \sum_{q=-1}^{1} N_q(k') A_q(z) e^{-ik'z} \rho_{gg} e^{ik'z} A_q^{\dagger}(z) \quad (4.14)$$

where the A_q are atomic lowering operators for a transition with polarisation q i.e.

$$A_1 = |g_{+1/2}\rangle\langle e_{+3/2}| + \frac{1}{\sqrt{3}} |g_{-1/2}\rangle\langle e_{+1/2}| \quad (4.15)$$

$$A_0 = \sqrt{\frac{2}{3}} |g_{+1/2}\rangle\langle e_{+1/2}| + \sqrt{\frac{2}{3}} |g_{-1/2}\rangle\langle e_{-1/2}| \quad (4.16)$$

$$A_{-1} = |g_{-1/2}\rangle\langle e_{-3/2}| + \frac{1}{\sqrt{3}} |g_{1/2}\rangle\langle e_{-1/2}| \ . \quad (4.17)$$

The $N(k')$ describe the associated photon momentum angular distributions [13]

$$N_0(k') = \frac{3}{4k} \left[1 - \left(\frac{k'}{k} \right)^2 \right] \quad (4.18)$$

$$N_{\pm 1}(k') = \frac{3}{8k} \left[1 + \left(\frac{k'}{k} \right)^2 \right] \ . \quad (4.19)$$

The explicit time dependence in the equations of motion for the optical coherences, coming from the $[H_{AL}, \rho]$ terms, can be eliminated by introducing the variables

$$\tilde{\rho}_{ge} := \rho_{ge} e^{-i\omega_L t} \ . \tag{4.20}$$

We then obtain, for example

$$\begin{aligned}\langle g_{+1/2}|\dot{\tilde{\rho}}|e_{+3/2}\rangle = -\left(i\left(\delta + \frac{p^2}{2m\hbar}\right) + \frac{\Gamma}{2}\right)\langle g_{+1/2}|\tilde{\rho}|e_{+3/2}\rangle \quad - \\ i\frac{\Omega_0}{\sqrt{6}}\cos kz\langle e_{-1/2}|\rho|e_{+3/2}\rangle - \frac{\Omega_0}{\sqrt{2}}\sin kz\langle g_{+1/2}|\rho|g_{+1/2}\rangle \quad + \\ \frac{\Omega_0}{\sqrt{2}}\sin kz\langle e_{+3/2}|\rho|e_{+3/2}\rangle \ .\end{aligned} \tag{4.21}$$

Adiabatic elimination of the excited states

The excited states decay at rate of the order Γ whilst the ground states are excited at a rate of the order $s_0\Gamma$. At low field intensities i.e. $s_0 \ll 1$ the ground states evolve much more slowly than the excited states. Thus after a short time of the order of $1/\Gamma$, the ground states 'enslave' the excited state populations and optical coherences, and impose their slow rate of variation on them so that

$$|\dot{\rho}_{ee}| \ll \Gamma\rho_{ee} \qquad\qquad |\dot{\rho}_{eg}| \ll \Gamma|\rho_{eg}| \ . \tag{4.22}$$

Working to the lowest order in the saturation, we can express the excited states and optical coherences in terms of the ground state matrix elements. The contribution from the kinetic energy term is also neglected as the mean kinetic energy is small in comparison to $\hbar\Gamma$ [14]. Applying these approximations Eq. 4.21 becomes

$$\langle g_{+1/2}|\tilde{\rho}|e_{+3/2}\rangle = \frac{i}{\delta - i\Gamma/2}\frac{\Omega_0}{\sqrt{2}}\sin kz\ \langle g_{+1/2}|\rho|g_{+1/2}\rangle \tag{4.23}$$

Substituting such expressions into the equations for the ground states gives a set of closed equations. The general form of these equations is [19]

$$\dot{\rho}_{gg} = -\frac{i}{\hbar}\left[\frac{p^2}{2m} + \hbar\delta'\Lambda(z), \rho_{gg}\right] - \frac{\Gamma'}{2}\left\{\Lambda(z), \rho_{gg}\right\} + \left(\dot{\rho}_{gg}\right)_{sp} \ . \tag{4.24}$$

In this expression $\Lambda(z)$ is the so-called light-shift operator and for this system

we have

$$\Lambda(z) = \frac{1}{3}\Big(2 - \cos 2kz\Big)|g_{+1/2}\rangle\langle g_{+1/2}| + \frac{1}{3}\Big(2 + \cos 2kz\Big)|g_{-1/2}\rangle\langle g_{-1/2}| \ . \quad (4.25)$$

We also have $\delta' = \delta s_0$, $\Gamma' = \Gamma s_0$ with

$$s_0 = 2\Omega_0^2/(4\delta^2 + \Gamma^2) \ . \quad (4.26)$$

It should be noted that this equation of motion is diagonal in the $|g_{\pm 1/2}\rangle$ basis so that there is no coupling between these states.

The second term in the commutator of Eq. 4.24, the $\hbar\delta'\Lambda(z)$ term, forms the bipotential $U_{\pm}(z)$ the atoms experience. That is the optical potential $V(z)$ has the form

$$V(z) = \begin{pmatrix} U_+(z) & 0 \\ 0 & U_-(z) \end{pmatrix} \quad (4.27)$$

with

$$U_{\pm}(z) = \langle g_{\pm 1/2}|\ \hbar\delta'\Lambda(z)\ |g_{\pm 1/2}\rangle \quad (4.28)$$

$$= \frac{U_0}{2}\big(-2 \pm \cos 2kz\big) \quad (4.29)$$

where the characteristic potential depth U_0 is

$$U_0 = -2\hbar\delta'/3 \ . \quad (4.30)$$

The variation terms due to spontaneous-emission, Eq. 4.14, become [58]

$$\big(\dot{\rho}_{gg}\big)_{sp} = \Gamma' \int_{-k}^{k} dk' \sum_{q=-1}^{1} N_q(k') B_q(z) e^{-ik'z}\ \rho_{gg}\ e^{ik'z} B_q^{\dagger}(z) \quad (4.31)$$

where

$$B_1 = \frac{1}{\sqrt{2}}\Big(\sin kz|g_{-1/2}\rangle\langle g_{-1/2}| + 3\sin kz|g_{+1/2}\rangle\langle g_{+1/2}|\Big) \quad (4.32)$$

$$B_0 = \frac{1}{\sqrt{2}}\Big(\cos kz|g_{-1/2}\rangle\langle g_{+1/2}| + \sin kz|g_{+1/2}\rangle\langle g_{-1/2}|\Big) \quad (4.33)$$

$$B_{-1} = \frac{1}{\sqrt{2}}\Big(3\cos kz|g_{-1/2}\rangle\langle g_{-1/2}| + \cos kz|g_{+1/2}\rangle\langle g_{+1/2}|\Big) \quad (4.34)$$

Fokker-Planck equation

The Optical Bloch Equations form the basis of a Fokker-Planck equation of motion for the Wigner distribution. The Wigner distribution is regarded as a "quasi" probability distribution and acts on the internal atomic state space. It is derived from the atomic density operator through the Wigner transform given by the following equivalent expressions

$$W(z,p,t) = \int_{-\infty}^{\infty} dz' \, \langle z + \frac{z'}{2} | \, \rho(t) \, | z - \frac{z'}{2} \rangle e^{-ip\cdot z'/\hbar} \tag{4.35}$$

$$= \int_{-\infty}^{\infty} dp' \, \langle p + \frac{p'}{2} | \, \rho(t) \, | p - \frac{p'}{2} \rangle e^{iz\cdot p'/\hbar} \, . \tag{4.36}$$

We apply the Wigner transform to the equations of motion obtained with the excited states adiabatically eliminated, Eq. 4.24. This equation of motion is diagonal in the $|g_{\pm 1/2}\rangle$ basis so under the Wigner transform we obtain expressions for the components $W_{\pm\pm} = \langle g_{\pm 1/2}|W|g_{\pm 1/2}\rangle$ only; these are the semiclassical 'population's of the $|g_{\pm 1/2}\rangle$ states. We obtain [70] (see Appendix A for details)

$$\Big(\frac{\partial}{\partial t} + \frac{p}{m}\frac{\partial}{\partial z} - \frac{\partial U_{\pm}}{\partial z}\frac{\partial}{\partial p} - \frac{\hbar^2 k^2 \Gamma'}{90}\big(35 \pm 7\cos 2kz\big)\frac{\partial^2}{\partial p^2}\Big) W_{\pm\pm} =$$

$$\mp \frac{\Gamma'}{9}\big(1 + \cos 2kz\big) W_{++} \pm \frac{\Gamma'}{9}\big(1 - \cos 2kz\big) W_{--} \; + \;$$

$$\frac{\hbar^2 k^2 \Gamma'}{90}\big(6 \mp \cos 2kz\big)\frac{\partial^2 W_{\mp\mp}}{\partial p^2} \, . \tag{4.37}$$

These equations can be interpreted as [70], on the left hand side, diffusive motion in the potential U_+ / U_- with the diffusion due to the random jumps in momentum from the emission of π-polarised photons (so that the atom stays in the same ground state) together with, on the right hand side, transitions between states with the associated diffusion due to the emission of $\sigma^{\pm}$-polarised photons.

4.1.7 Monte Carlo simulation

As mentioned in Section 3.1.2, corresponding to a Fokker-Planck equation is an equivalent stochastic differential equation. This stochastic differential equation forms the basis of a Monte Carlo simulation.

Taking the Fokker-Planck equation Eq. 4.37 from the previous section, we determine a one-step stochastic incremental equation for the atom's momentum p. We obtain the following [70]:

- if there's no change in the atoms ground state:

$$\Delta p = -\frac{dU_{\pm}(z)}{dz}\Delta t + \left(2D_{\pm\pm}(z)\Delta t\right)^{1/2} N(0,1) \tag{4.38}$$

- or if there is a change in ground state, an inter-state transition:

$$\Delta p = -\frac{dU_{\pm}(z)}{dz}\Delta t + \left(2D_{\pm\mp}(z)/\gamma_{\pm\mp}(z)\right)^{1/2} N(0,1) \tag{4.39}$$

and in both cases $\Delta z = \frac{p}{m}\Delta t$, and where Δt is a timestep appropriate for the integration. Here $N(0,1)$ represents an independent sampling of a Gaussian distribution with zero mean and unit variance.

It should be noted that, for the purposes of simulating a ratchet, a driving force F can easily be introduced by adding a term directly to the incremental equation for p

$$\Delta p = \cdots + F\Delta t \ . \tag{4.40}$$

I'll show in Section 4.1.8 that this is equivalent to the method used in the experiments of phase-modulating the laser beams.

In the above expressions for Δp

$$D_{\pm\pm}(z) = \frac{\hbar^2 k^2 \Gamma'}{90}(35 \pm 7\cos 2kz) \tag{4.41}$$

$$D_{\pm\mp}(z) = \frac{\hbar^2 k^2 \Gamma'}{90}(6 \mp \cos 2kz) \tag{4.42}$$

and represent the diffusion coefficients for the different state transitions. The quantity γ_{+-} (resp. γ_{-+}) is the rate per unit time for the transition from $|g_{+1/2}\rangle$ to $|g_{-1/2}\rangle$ (resp. $|g_{-1/2}\rangle$ to $|g_{+1/2}\rangle$)

$$\gamma_{+-}(z) = \frac{2}{9}\Gamma' \cos^2 kz \tag{4.43}$$

$$\gamma_{-+}(z) = \frac{2}{9}\Gamma' \sin^2 kz \ . \tag{4.44}$$

One can determine whether a transition between states occurs using the rates $\gamma_{\pm\mp}$. The probability of an inter-state transition in a timestep, $\gamma_{\pm\mp}\Delta t$, is compared with a uniformly distributed random variable u on the interval $[0,1]$; if u is less than this probability then such a transition is deemed to occur at that timestep.

The pertinent laser parameters U_0, Γ', δ' are not independent and by specifying two of the three the third can be determined. In the results I present I generally give the values of U_0 and Γ'.

Amendments to incremental equations

The one-step incremental equations detailed above are consistent with the published literature [70]. However when the Monte Carlo simulation was implemented using these equations a problem arose. Specifically, occasional large jumps in the temperature of the statistical ensemble were observed. This was traced back to large values of Δp occurring in some inter-state transitions. Reviewing Eq. 4.39, and specifically the second term on the rhs, we notice that Δp can be arbitrarily large, albeit that this will occur with a corresponding arbitrarily small probability of $\gamma_{\pm\mp}\Delta t$. These large Δp are rather unphysical. In my simulations I chose to ignore the problematic term $\left(2D_{\pm\mp}(z)/\gamma_{\pm\mp}(z)\right)^{1/2} N(0,1)$ on the rhs of Eq. 4.39. [An alternative approach was taken by the authors of Ref. [8] whereby they exclude atoms with a momentum larger than a threshold that they set.]

I also chose to implement a two-step integration method, attributed to Heun [10], rather than the one-step method highlighted above in order to improve the convergence properties of the integration. The final form of the incremental equations are

$$\Delta p = -\frac{1}{2}\left(\frac{dU_{\pm}(z)}{dz} + \frac{dU_{\pm}(\tilde{z})}{dz}\right)\Delta t + \begin{cases} \left(2D_{\pm\pm}(z)\Delta t\right)^{1/2} N(0,1) & \text{no change in ground state} \\ 0 & \text{change in ground state} \end{cases} \tag{4.45}$$

with

$$\tilde{p} = p - \frac{dU_{\pm}(z)}{dz}\Delta t + \begin{cases} \left(2D_{\pm\pm}(z)\Delta t\right)^{1/2} N(0,1) & \text{no change in ground state} \\ 0 & \text{change in ground state} \end{cases} \tag{4.46}$$

and

$$\tilde{z} = z + \frac{\tilde{p}}{m}\Delta t \ . \tag{4.47}$$

As reported in the next section the results obtained with these equations closely reproduce those in the published literature which allayed any worries over omitting the problematic term in the incremental equations.

Numerical results

This section presents results of Monte Carlo simulations of the system in the absence of any driving. The simulation was implemented using the amended incremental equations given above.

For these calculations the laser parameters are set so that $\delta = -10\Gamma$ in order for comparison with Ref. [70]. In Fig. 4.2 I plot the steady state temperature as a function of the potential depth. This figure closely matches Fig. 2 of Ref. [70], exhibiting the well known *décrochage* at around $U_0 = 100E_r$ with the values for the temperature in very good agreement. This convinces us that the amendments made to the incremental equations have no material detrimental effect.

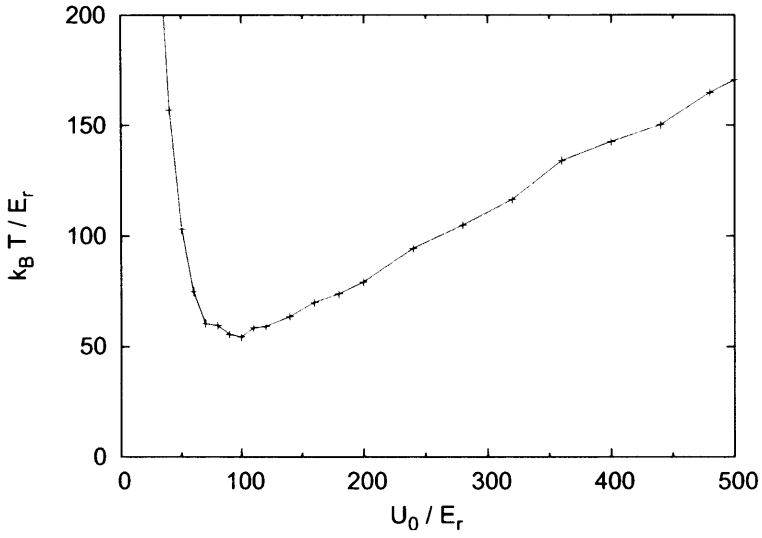

Figure 4.2: Red-Sisyphus system in absence of driving: plot of steady state temperature as a function of the potential depth U_0. The laser detuning is set to $\delta = -10\Gamma$ and this determines all the other relevant free parameters of the system. The points represent the results of Monte Carlo simulations with a sample size of 5000 atoms. The lines are guides for the eye.

Later in this chapter I'll present numerical results for the system in the presence of various drivings. For these simulations the potential depth U_0 is kept constant whilst the damping rate Γ' is varied. From the values of these parameters the laser detuning δ can be implied. For the most part we set $U_0 = 200E_r$; besides wanting to avoid the *décrochage* around $U_0 = 100E_r$ and not wanting too deep a potential the value 200 was arbitrary.

4.1.8 Driving force arising from phase-modulation

By applying a phase-modulation $\alpha(t)$ to one of the two lattice beams we give rise to an instantaneous driving force on the atoms in the lattice. We can see

this as follows: the light-field for a lattice with such a phase-modulation is, for example

$$E(z,t) = \frac{E_0}{2}\Big(\hat{e}_x\big(e^{i(kz-\omega_L t)} + \text{c.c.}\big) + \hat{e}_y\big(e^{i(kz+\omega_L t+\phi+\alpha(t))} + \text{c.c.}\big)\Big) \tag{4.48}$$

$$\equiv E^+(z)e^{-i(\omega_L t+\alpha(t)/2)} + \text{c.c.} \tag{4.49}$$

with

$$E^+(z) = \frac{E_0}{\sqrt{2}}\Big(\hat{e}_-\cos(kz+\alpha(t)/2) - i\hat{e}_+\sin(kz+\alpha(t)/2)\Big) \tag{4.50}$$

for an appropriate choice of ϕ. The field polarisation is now time-dependent and results in the following expression for $\Lambda(z)$

$$\Lambda(z) = \frac{1}{3}\Big(2-\cos(2kz+\alpha(t))\Big)|g_{+1/2}\rangle\langle g_{+1/2}| + \frac{1}{3}\Big(2+\cos(2kz+\alpha(t))\Big)|g_{-1/2}\rangle\langle g_{-1/2}| \tag{4.51}$$

(which can be compared with Eq. 4.25 for the situation without phase-modulation). Working in the laboratory frame z, the phase-modulation results in a moving optical potential

$$V(z,t) \propto \Big(-2 \pm \cos\big(2kz+\alpha(t)\big)\Big)\,. \tag{4.52}$$

In the moving frame $z' = z + \alpha(t)/2k$, the potential is stationary but in this frame there arises an inertial force $F(t)$. This force acts on the atoms and is proportional to the acceleration of the moving frame

$$F(t) = \frac{m}{2k}\ddot{\alpha}(t) \tag{4.53}$$

where m is the mass of the atoms.

Thus the phase-modulation of the lattice is easily modelled through an additional term $F(t)\Delta t$ to the incremental equation for p, as described in Section 4.1.7. We may also derive an alternative equation of motion by working in the laboratory frame; this will be explored in the next section.

Alternative equation of motion

Working in the laboratory frame we can derive new equations of motion using the light-field of Eq. 4.49. Following the steps described in Section 4.1.6 we

obtain the following Fokker-Planck equation

$$\Big(\frac{\partial}{\partial t}+\frac{p}{m}\frac{\partial}{\partial z}-\frac{\partial U_{\pm}^{*}}{\partial z}\frac{\partial}{\partial p}-\frac{\hbar^{2}k^{2}\Gamma^{*}}{90}\big(35\pm 7\cos 2(kz+\alpha/2)\big)\frac{\partial^{2}}{\partial p^{2}}\Big)W_{\pm\pm}=$$
$$\mp\frac{\Gamma^{*}}{9}\big(1+\cos 2(kz+\alpha/2)\big)W_{+\,+}\pm\frac{\Gamma^{*}}{9}\big(1-\cos 2(kz+\alpha/2)\big)W_{--}\quad+$$
$$\frac{\hbar^{2}k^{2}\Gamma^{*}}{90}\Big(6\mp\cos 2(kz+\alpha/2)\Big)\frac{\partial^{2}W_{\mp\mp}}{\partial p^{2}}\qquad(4.54)$$

which can be compared with Eq. 4.37 in the situation without phase-modulation.

The starred quantities are variations of the unstarred ones of Section 4.1.6

$$U_{\pm}^{*}(z)=\frac{U_{0}^{*}}{2}\Big(-2\pm\cos 2\big(kz+\alpha/2\big)\Big)\qquad(4.55)$$
$$U_{0}^{*}=-2\hbar\delta^{*}/3\qquad(4.56)$$
$$\delta^{*}=\frac{\delta+\frac{\dot{\alpha}}{2}}{\big(\delta+\frac{\dot{\alpha}}{2}\big)^{2}+\frac{\Gamma^{2}}{4}}\frac{\Omega_{1}^{2}(z)}{4}\qquad(4.57)$$
$$\Gamma^{*}=\frac{\Gamma}{\big(\delta+\frac{\dot{\alpha}}{2}\big)^{2}+\frac{\Gamma^{2}}{4}}\frac{\Omega_{1}^{2}(z)}{4}\,.\qquad(4.58)$$

This new Fokker-Planck equation is equivalent to a stochastic differential equation for p and as done for the situation in the absence of phase-modulation in Section 4.1.7 we can then derive incremental equations for p and z.

The atomic dynamics resulting from the action of either the inertial force in the moving frame or the moving potential in the laboratory frame is the same and has been confirmed by numerical simulation (see Appendix B for details). We have chosen to use the first method as the computer implementation is simpler.

4.2 Biharmonic driving

To achieve a ratchet with the spatially symmetric bipotential of this 1D lin⊥lin optical lattice with $J_g = 1/2$ to $J_e = 3/2$ atomic transition we need to apply a temporally asymmetric driving. A simple candidate for the driving is one with two harmonics of different parity. This section presents a detailed numerical study of a ratchet with biharmonic driving and was an extension of previous numerical and experimental work [35, 47, 80].

The findings have been published [11]

- M. Brown, and F. Renzoni. Ratchet effect in an optical lattice with biharmonic driving: A numerical analysis. *Physical Review A*, 77(3): 033405, March 2008.

The driving under study has the following form

$$F(t) = F_0\Big(A_d \cos\omega_d t + B_d \cos\left(2\omega_d t + \phi\right)\Big) \,. \tag{4.59}$$

The parameter F_0 scales the overall magnitude of the driving with A and B affecting the relative strengths of each harmonic. The frequency of the driving is $\omega_d = 2\pi/T$, and is normally expressed as a proportion of the vibrational frequency ω_v of the potential wells. The vibrational frequency is calculated by approximating the bottom of the potential well to a harmonic potential. One finds

$$\omega_v = 2\sqrt{\tilde{U}_0}\,\omega_r \tag{4.60}$$

where $\tilde{U}_0 = U_0/E_r$, ω_r is the recoil frequency and $E_r = \hbar\omega_r$ is the recoil energy. The phase-difference ϕ between the two harmonics can be used to induce symmetry breaking as I shall present next.

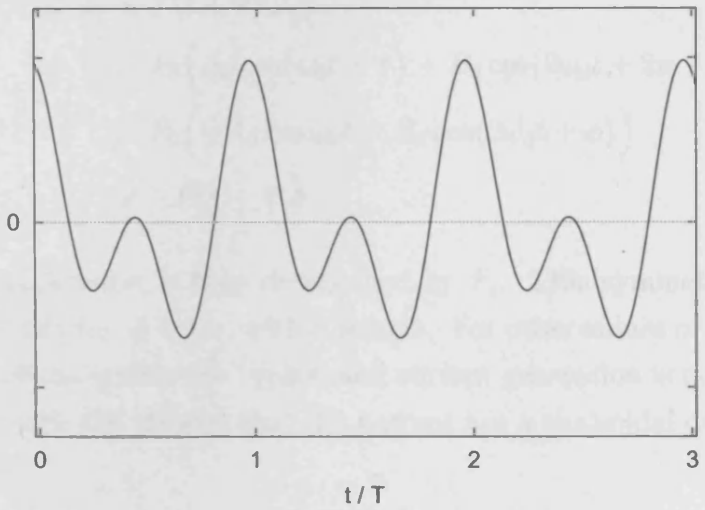

Figure 4.3: An example of biharmonic driving: a plot of $F(t)$ with $\phi = 0.6$ rad.

4.2.1 Symmetry analysis

The biharmonic driving has been well studied and analyses of its symmetries are well understood [80]. I present here a summary of the main results.

With reference to the system symmetries $\hat{S}_a$, $\hat{S}_b$ and $\hat{S}_c$ (Eq. 2.11) it is necessary to determine the symmetries of $f(x) \equiv V'(x)$ and $F(t)$. I restrict the analysis to the lin⊥lin lattice with $J_g = 1/2$ to $J_e = 3/2$ atomic transition so that $V(x) \equiv U_{\pm}(x)$. We then have

$$f(x) = \mp k U_0 \sin 2kx \tag{4.61}$$

which is clearly shift-symmetric in the sense of Section 2.4. One can also easily find an x' such that

$$f(x + x') = f(-x + x') \tag{4.62}$$

and an x'' such that

$$f(x + x'') = -f(-x + x'') \tag{4.63}$$

so that $f(x)$ is also symmetric and anti-symmetric.

With the possible requirements on $f(x)$ satisfied we can turn now to the requirements for $F(t)$. We know that the damping of this system is not so large so that we can assume the symmetry $\hat{S}_c$ can be ignored. We are left with the symmetries $\hat{S}_a$, determined by F_{sh}, and $\hat{S}_b$, determined by F_s for zero dissipation.

The symmetry F_{sh} is broken by the biharmonic form, regardless of ϕ, due to the two harmonics of different parity:

$$\begin{aligned} F(t + T/2) &= F(t + \pi/\omega_d) \\ &= F_0\Big(A_d \cos\big(\omega_d t + \pi\big) + B_d \cos\big(2\omega_d t + 2\pi + \phi\big)\Big) \\ &= F_0\Big(-A_d \cos\omega_d t + B_d \cos\big(2\omega_d t + \phi\big)\Big) \\ &\neq -F(t) \quad \forall\, \phi \end{aligned} \tag{4.64}$$

Current generation is then determined by F_s. This symmetry is realised for $\sin\phi = 0$ only i.e. $\phi = n\pi$, with n integer. For other values of ϕ all relevant symmetries of the system are broken and current generation is not prohibited. Theoretical work [32] showed that the current has a sinusoidal dependence on ϕ

$$I \sim \sin\phi\ . \tag{4.65}$$

These results apply in the absence of dissipation. A small amount of dissipation breaks the symmetry $\hat{S}_b$ even with F_s. Current is now expected for $\phi = n\pi$. In Ref. [86] the authors showed that weak dissipation can be accounted for by a phase-shift ϕ_0 giving

$$I \sim \sin\left(\phi - \phi_0\right)\ . \tag{4.66}$$

This was determined through numerical simulation of the kinetic Boltzmann equation for an ensemble of particles. It was observed that the phase-shift increased with dissipation and vanished in the Hamiltonian limit.

4.2.2 Numerical results

In this work I study the atomic current as a function of the phase-difference ϕ for different scattering rates Γ' and driving amplitudes F_0.

A typical current versus phase-difference *signal* is plotted in Fig. 4.4. Here the scattering rate is varied whilst keeping the driving amplitude constant. For the lowest scattering rate considered the signal is well described by $I \sim \sin\phi$. This is in agreement with the symmetry considerations where the symmetry F_s holds in the Hamiltonian limit and prohibits current for $\phi = n\pi$. For larger scattering rates, the signal displays a phase-shift ϕ_0. Fitting the signal with a function of the form

$$A\sin(\phi - \phi_0) \tag{4.67}$$

we may determine the amplitude of the signal A and the acquired phase-shift ϕ_0.

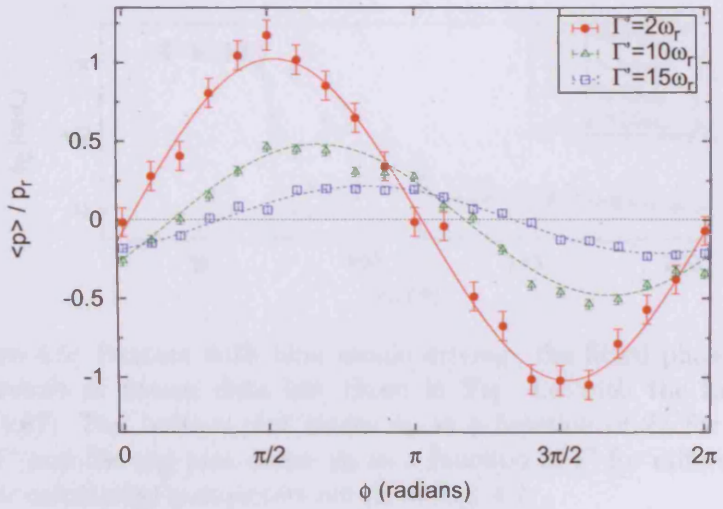

Figure 4.4: Ratchet with biharmonic driving: plot of average current scaled by the momentum recoil p_r versus ϕ for three different Γ'. The curves represent the best fits of the function $p/p_r = A\sin(\phi - \phi_0)$. The other relevant simulation parameters are $U_0 = 200E_r$, $F_0 = 100F_r$, $A_d = 1$, $B_d = 1$, $\omega_d/\omega_v = 1$ with a sample size of 10000; $F_r = \hbar k\omega_r$.

Phase-shift behaviour

I first report the behaviour of the phase-shift as a function of the ratchet parameters. In Fig. 4.5 I present the phase-shift as 1) a function of Γ' for different F_0, and 2) a function of F_0 for different Γ'; all other calculations parameters are the same for the two sets of results.

Looking first at the phase-shift as a function of Γ' we see that the phase-shift

ϕ_0 is essentially zero, mod π, for low Γ'. As Γ' increases from a low value ϕ_0 increases. For these values of Γ' current is generated for $\phi = n\pi$ indicating the breaking of the symmetry F_s. This is to be interpreted as dissipation-induced symmetry breaking [35].

Turning to the plot of phase-shift as a function of F_0 we also see that for very small and very large F_0, ϕ_0 is essentially zero mod π and is substantially non-zero for intermediate values.

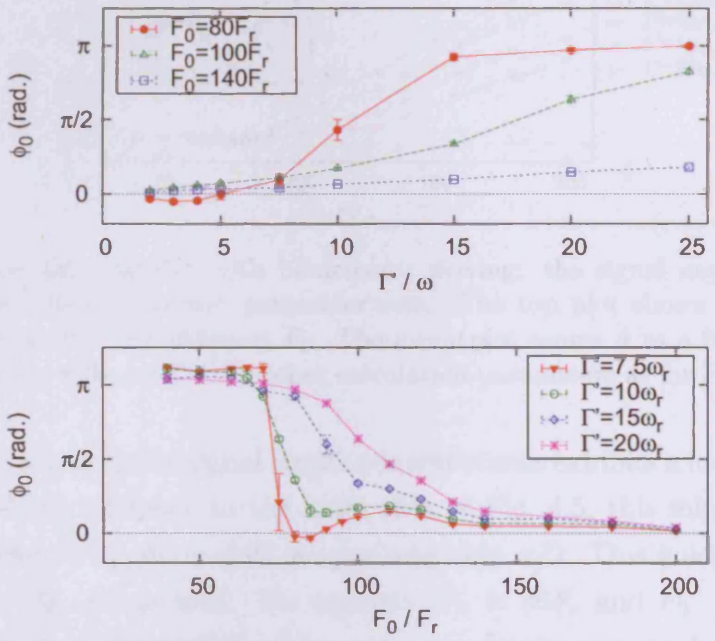

Figure 4.5: Ratchet with biharmonic driving: the fitted phase shift, the result of fitting data like those in Fig. 4.4 with the function Eq. 4.67. The bottom plot shows ϕ_0 as a function of F_0 for different Γ' and the top plot shows ϕ_0 as a function of Γ' for different F_0. Other calculation parameters are as in Fig. 4.4.

Signal amplitude behaviour

The behaviour of the signal amplitude with changes in ratchet parameters is more complicated. Referring to the top plot of Fig. 4.6 which shows the signal amplitude A as a function of Γ' for various driving amplitudes F_0 we see that for large F_0 increasing Γ' reduces the signal amplitude. The noise in this case has a destructive effect on the generation of current. The mechanism of current generation can then be attributed to dynamical harmonic mixing [57]. For smaller F_0 we observe a different behaviour; we see that the signal amplitude initially falls but can then increase with increasing Γ'.

This behaviour is also observed in the bottom plot of Fig. 4.6. For large F_0 the signal amplitude A increases with increasing F_0 as would be expected.

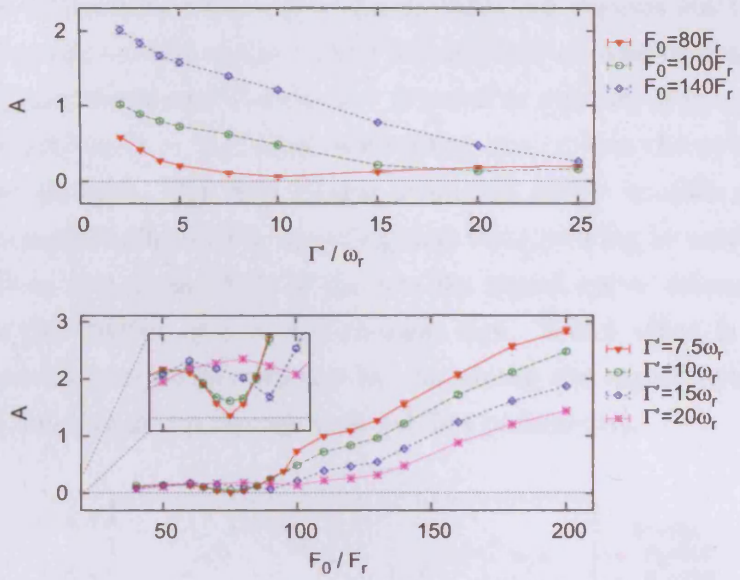

Figure 4.6: Ratchet with biharmonic driving: the signal amplitude A for different ratchet parameter sets. The top plot shows A as a function of Γ' for different F_0. The lower plot shows A as a function of F_0 for different Γ'. All other calculation parameters as for Fig. 4.4.

However for small F_0 the signal amplitude sometimes exhibits a local minimum; see inset. With reference to the lower plot of Fig. 4.5, this minimum occurs for an F_0 where the phase-shift is approximately $\pi/2$. This holds true for the top plot of Fig. 4.6 as well. For example $F_0 = 80F_r$ and $F_0 = 100F_r$ have a minimum at a value of Γ' which, referring to the upper plot of Fig. 4.5, presents a phase-shift of $\pi/2$. This behaviour can be understood as follows. For a phase-shift of $\pi/2$ the maximum in the signal is expected for $\phi = n\pi$. But then F_s holds and so the current is solely produced by dissipation. For phase-shifts other than $\pi/2$, the driving also contributes to the current generation as then the maximum in the signal occurs at a value of ϕ for which F_s does not hold. We thus expect the current to be larger for phase-shifts other than $\pi/2$, as there are now two contributions to the current, and thus to observe a local minimum for a phase-shift of $\pi/2$.

Current reversals

I noted earlier that in all but the simplest of ratchets, the direction of the current has a complicated dependence on the ratchet parameters and that currents may reverse under a change of parameters. Current reversals were observed in the comparable experimental setup [47], however no detailed numerical study was performed; this section reports such a study.

In the experiments the phase-difference ϕ was fixed at $\phi = \pi/2$ and reversals

observed as a function of the driving amplitude for various scattering rates. Here I obtain the sin-like signal curves for different choices of scattering rate and driving amplitude and observe any reversal in current at $\phi = \pi/2$.

The reversal at $\phi = \pi/2$ may arise from one of two distinct effects, or combination thereof. The first results from the whole sin-like signal curve shrinking in amplitude to zero, inverting and then growing in amplitude. The second is from the phase-shift of the sin-like signal curve increasing to the extent that the current at $\phi = \pi/2$ changes sign. Which effect is behind the current reversals can be determined by examining the signal amplitude and phase-shift behaviours for the relevant ratchet parameters.

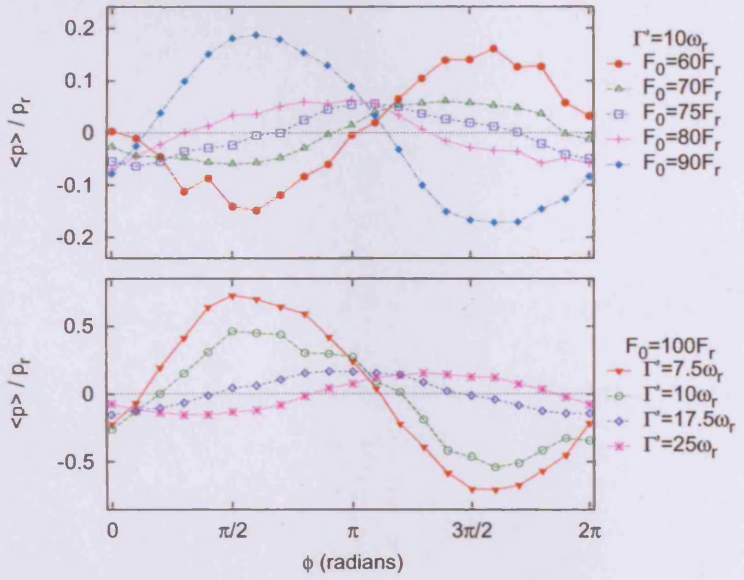

Figure 4.7: Ratchet with biharmonic driving: current reversal at $\phi = \pi/2$ for varying F_0, top plot, and Γ', bottom plot. All other calculation parameters as before. The lines are guides for the eyes.

Figure 4.7 shows the sin-like signal curves for different driving amplitudes, upper plot, and scattering rates, lower plot. Current reversals at $\phi = \pi/2$ are observed in both plots. For the value of F_0 in the lower plot we see from Fig. 4.6 that the signal amplitude is substantially non-zero for our choices of Γ'. At the same time Fig. 4.5 shows that the signal phase-shift varies widely. Thus for the current reversal observed as a function of Γ' it is the second of the two effects described above that is dominant. That is, the reversal in current for an increase in Γ' is due to the large variation in the phase-shift acquired by the signal.

Turning our attention now to the current reversal as a function of F_0 we note that the values of the ratchet parameters in the upper plot of Fig. 4.7 correspond to the inset of Fig. 4.6. In this case the reversal is due to the

combined dependence of the signal amplitude and phase-shift on F_0. Referring to Fig. 4.6 the signal amplitude exhibits a local minimum, which for some parameters can be essentially zero, as a function of F_0. This minimum corresponds to the signal phase-shift acquiring a value of $\pi/2$ as it varies from 0 to π. Thus here the current reversal is a result of the whole signal curve shrinking in amplitude, inverting, and then growing in amplitude as illustrated by the curves $F_0 = 60F_r$ and $F_0 = 90F_r$.

4.3 Multi-frequency driving and route to quasiperiodicity

The previous section described a ratchet with a periodic driving consisting of two harmonics. In this section I study a ratchet with a multi-frequency driving. The study will also explore the route to quasiperiodicity.

The results presented here contributed to the following publication containing both experimental and numerical findings

- R. Gommers, M. Brown, and F. Renzoni. Symmetry and transport in a cold atom ratchet with multifrequency driving. *Physical Review A*, 75 (5):053406, May 2007.

The particular form of driving I study is

$$F(t) = -F_0\Big[\omega_2\cos(\omega_2 t+\delta)\Big(A_d\sin\omega_1 t + B_d\sin 2\omega_1 t\Big)+ \omega_1\sin(\omega_2 t+\delta)\Big(A_d\cos\omega_1 t + 2B_d\cos 2\omega_1 t\Big)\Big] \quad (4.68)$$

This complicated expression derives from the following simplified form for the frequency modulation applied in the experiments

$$c\sin(\omega_2 t+\delta)\Big(a\sin\omega_1 t + b\sin 2\omega_1 t\Big) .$$

The driving is quasiperiodic when ω_2/ω_1 is irrational. Of course in experiments and in simulations this ratio is always rational and can be written as

$$\omega_2/\omega_1 = p/q \quad (4.69)$$

with p, q positive and coprime. However for p and q large, and considering a finite interaction time for our system, we effectively achieve a quasiperiodic driving.

4.3.1 Symmetry analysis

The symmetry analysis for this ratchet has been published [37, 38] and is summarised here.

Consider first the case of periodic driving i.e. ω_2/ω_1 rational. For the symmetry $\hat{S}_a$ (see Section 2.4) to be valid we require f_a and F_{sh}. We know already that the potential satisfies f_a and so we proceed to assess F_{sh}.

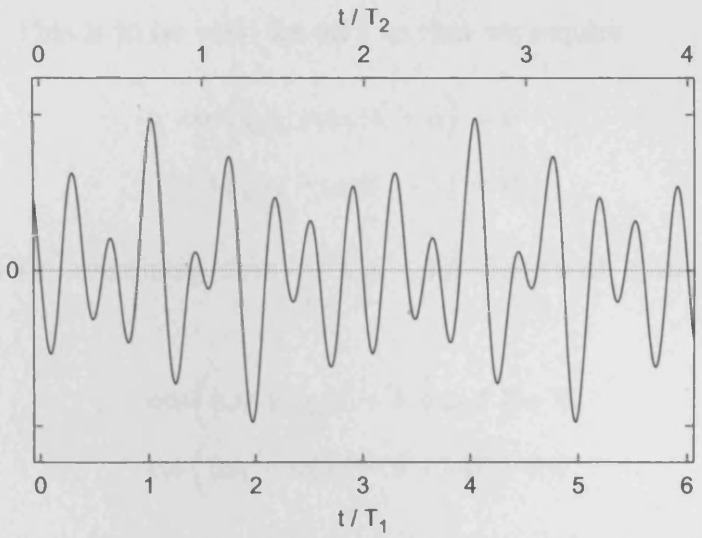

Figure 4.8: An example of multi-frequency driving: a plot of $F(t)$ with $\omega_2/\omega_1 = 2/3$ and $\delta = 0$ and where $T_1 = 2\pi/\omega_1$ and $T_2 = 2\pi/\omega_2$.

The period T of $F(t)$ is $T = qT_1 = pT_2$ with $T_i = 2\pi/\omega_i$, $i = 1, 2$. Under the transformation $t \to t + T/2$ we have

$$\cos(\omega_2 t + \delta) \sin n\omega_1 t \;\to\; \cos(\omega_2 t + \delta) \sin n\omega_1 t \cos p\pi \cos nq\pi \tag{4.70}$$

$$\sin(\omega_2 t + \delta) \cos n\omega_1 t \;\to\; \sin(\omega_2 t + \delta) \cos n\omega_1 t \cos p\pi \cos nq\pi \tag{4.71}$$

where $n = 1$ or 2, so that $F(t+T/2) = -F(t)$ holds for $\cos q\pi = 1$, $\cos p\pi = -1$ i.e. for

$$q \text{ even and } p \text{ odd.}$$

If this condition holds current generation is forbidden.

When this condition doesn't hold, which for p and q coprime is simply when q is odd, current generation is determined by $\hat{S}_b$. In the absence of dissipation this requires F_s i.e. $F(t + t') = F(-t + t')$ for some t'. We will analyse when this is satisfied.

For the $\cos(\omega_2 t + \delta) \sin \omega_1 t$ and $\sin(\omega_2 t + \delta) \cos \omega_1 t$ terms of Eq. 4.68 we find

$$\sin(\omega_1 + \omega_2)t \cos\big((\omega_1 + \omega_2)t' + \delta\big) = -\sin(\omega_1 - \omega_2)t \cos\big((\omega_1 - \omega_2)t' - \delta\big) \tag{4.72}$$

and

$$\sin(\omega_1 + \omega_2)t \cos\big((\omega_1 + \omega_2)t' + \delta\big) = \sin(\omega_1 - \omega_2)t \cos\big((\omega_1 - \omega_2)t' - \delta\big) \tag{4.73}$$

respectively. This is to be valid for all t so that we require

$$\cos\Big((\omega_1+\omega_2)t'+\delta\Big)=0 \tag{4.74}$$

$$\cos\Big((\omega_1-\omega_2)t'-\delta\Big)=0\ . \tag{4.75}$$

Similarly for the remaining terms of Eq. 4.68, those with a $2\omega_1 t$ component, we obtain

$$\cos\Big((\omega_1+\omega_2)t'+\delta+\omega_1 t'\Big)=0 \tag{4.76}$$

$$\cos\Big((\omega_1-\omega_2)t'-\delta+\omega_1 t'\Big)=0 \tag{4.77}$$

which on comparing with the previous conditions we clearly see that $\omega_1 t'$ is a multiple of π. Using the fact that q is odd we obtain the following condition on δ

$$q\delta=(n+1/2)\pi \tag{4.78}$$

with n integer. Thus for these values of δ the symmetry is realised and current is forbidden. For other values of δ, current is to be expected and so we anticipate that

$$I\sim\sin(q\delta-\pi/2)\ . \tag{4.79}$$

Introducing a small amount of dissipation breaks $\hat{S}_b$ even with F_s and current will be generated even for $q\delta=(n+1/2)\pi$. In analogy with the case of biharmonic driving, we anticipate dissipation will have the effect of an additional phase shift δ_0

$$I\sim\sin(q\delta-\pi/2-\delta_0)\ . \tag{4.80}$$

These results were for a periodic driving. Turning now to quasiperiodic driving, theoretical work [31, 68] showed how to generalise the treatment of symmetries in periodic systems to those of quasiperiodic systems.

Applying this treatment to our driving Eq. 4.68 we start by considering $\psi_1\equiv\omega_1 t$ and $\psi_2\equiv\omega_2 t$ as independent variables. Then $F(t)$ is symmetric if

$$F_s(t):\quad F(\psi_1+\chi_1,\psi_2+\chi_2)=F(-\psi_1+\chi_1,-\psi_2+\chi_2)\ , \tag{4.81}$$

asymmetric if

$$F_a(t):\quad F(\psi_1+\chi_1,\psi_2+\chi_2)=-F(-\psi_1+\chi_1,-\psi_2+\chi_2)\ , \tag{4.82}$$

and shift-symmetric if

$$F_{sh}(t): \quad F(\psi_\alpha) = -F(\psi_\alpha + \pi) \ , \tag{4.83}$$

where χ_1 and χ_2 are constants and α is any subset of $\{1, 2\}$.

The symmetries of the system follow as before. One finds the following transformations lead to an invariance in the system and hence forbid the generation of current

$$\hat{S}_a : x \to -x, \quad \psi_\alpha \to \psi_\alpha + \pi \qquad \text{given } F_{sh} \tag{4.84}$$

$$\hat{S}_b : x \to x, \quad \psi_i \to \psi_i + \chi_i \qquad \text{given } F_s \text{ and no dissipation} \tag{4.85}$$

where, as before, I've omitted the explicit requirements on f and omitted $\hat{S}_c$ entirely.

Considering first the transformation $\hat{S}_a$ we require F_{sh}. This is simply satisfied by the transformation

$$\psi_2 \to \psi_2 + \pi \tag{4.86}$$

and hence current generation is forbidden in the quasiperiodic limit, regardless of p and q.

In summary, in the quasiperiodic limit current is forbidden. This is in contrast to the case when the driving was periodic. In that case we expect a current for q odd of the form $I \sim \sin\big(q\delta - \pi/2 - \delta_0\big)$. We can explore the transition to quasiperiodicity by increasing p and q, with q odd, for a constant interaction time. We expect the current to diminish to zero for large enough p, q.

4.3.2 Numerical results

The first results I present are for the range of p, q and interaction time where the driving is periodic. In Fig. 4.9 I plot the dependence of the current on the phase δ for different values of p/q. Also shown is the result of fitting the data with the function

$$v_{max} \sin\big(b\delta - \pi/2 - \delta_0\big) \ . \tag{4.87}$$

We clearly see the effect of the parity of q. For even q the current is negligible regardless of the value of δ. This is due to the symmetry $\hat{S}_a$ being realised for q even; this symmetry forbids current generation as shown in the previous section. For q odd we see the current exhibits a clear sinusoidal

dependence on δ with the period of the signal dependent on q. One finds that the period is $q\pi$, as anticipated from the realisation of the symmetry $\hat{S}_b$.

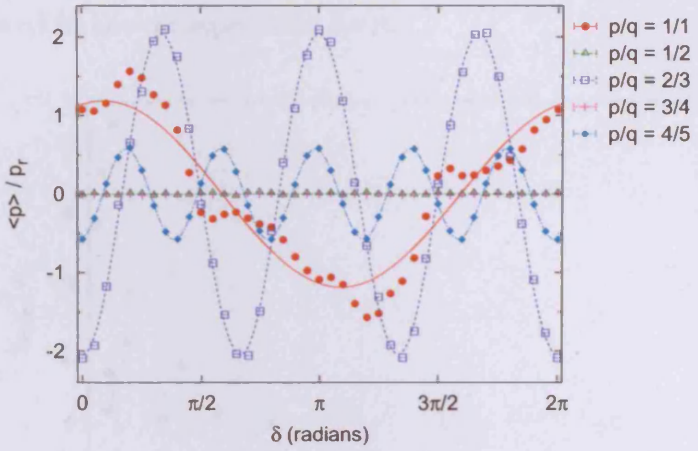

Figure 4.9: Ratchet with multi-frequency driving: plot of current versus phase-difference δ for different values of the ratio p/q. The curves, for q odd, represent the best fits of Eq. 4.87 to the data. The simulations were performed with $U_0 = 200E_r$, $\Gamma' = 10\omega_r$, $F_0 = 20F_r$, $A_d = 1$, $B_d = 0.3$, $\omega_1/\omega_v \approx 0.74$ and the sample size was 10000.

In Fig. 4.10 we plot the amplitude of the signal versus the ratio of the driving frequencies ω_2/ω_1. We see that the current is substantially non-zero for q odd and only then for small values of the product pq.

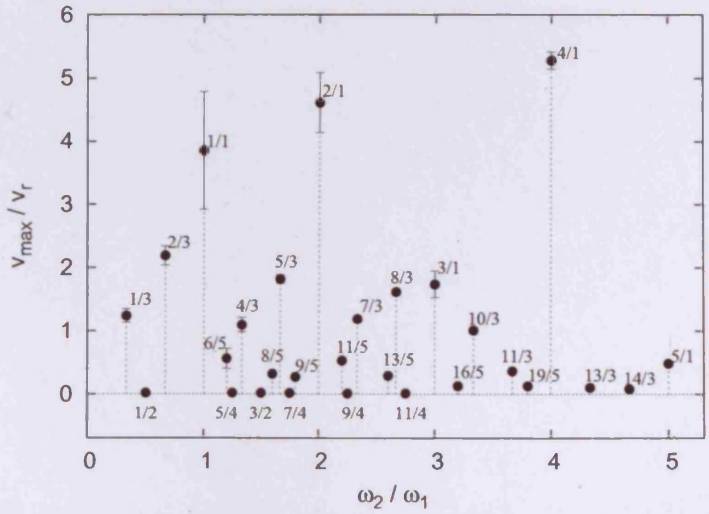

Figure 4.10: Ratchet with multi-frequency driving: signal amplitude versus the ratio of the driving frequencies ω_2/ω_1. The values of $p/q \equiv \omega_2/\omega_1$ label the datapoints. Here $B_d = 1$, the sample size was 5000 with other calculation parameters as in Fig. 4.9.

We now proceed to study the quasiperiodic limit of this driving. As a measure of quasiperiodicity we use the product pq [37]. We increase pq whilst

keeping the interaction time constant. In Fig. 4.11 I plot the current amplitude versus pq for q odd. For increasing pq the amplitude decreases and approaches zero. This in agreement with the symmetry analysis above where we found F_{sh} is restored in the quasiperiodic limit.

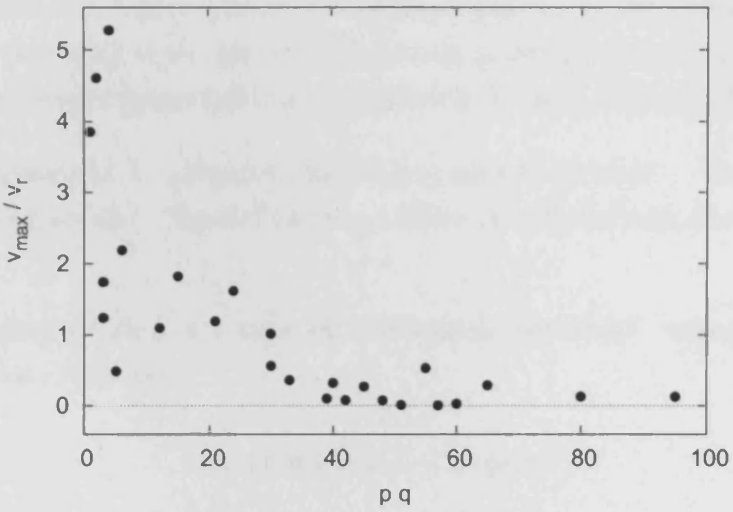

Figure 4.11: Ratchet with quasiperiodic driving: signal amplitude versus pq. The datapoints are derived from those of Fig. 4.10 with q being odd.

4.4 Gating ratchet

The last of the three ratchets I present here is a gating ratchet [79]. This ratchet is characterised by an amplitude modulated spatially symmetric potential together with a zero-mean temporally symmetric driving. Current is generated through a gating effect, the synchronisation of the lowering and raising of the potential with the back and forth motion induced by the driving. Some of the results presented here contributed to the following publication [39]

- R. Gommers, V. Lebedev, M. Brown, and F. Renzoni. Gating ratchet for cold atoms. *Physical Review Letters*, 100(4):040603, February 2008.

The gating ratchet is a type of 'fluctuating potential' ratchet where the potential takes the form

$$V(x,t) \equiv V(x)\big(1 + A\cos\omega_1 t\big) \tag{4.88}$$

and we restrict A to $0 \leq A < 1$. We also apply a single-harmonic driving of the form

$$F(t) = B\cos\big(\omega_2 t + \phi\big)\ . \tag{4.89}$$

In our system the fluctuating potential is realised by modulating the potential depth U_0. In experiments this is achieved by modulating the intensity I of the laser beams whilst keeping the detuning δ constant. We know that

$$U_0 = -2\hbar\delta s_0/3 \ \propto\ I/\delta \tag{4.90}$$

and also

$$\Gamma' = \Gamma s_0 \ \propto\ I/\delta^2\ . \tag{4.91}$$

A consequence of modulating the potential depth U_0 is that we should necessarily modulate the scattering rate Γ' in the same way. We can simulate this ratchet using the same approach as before but for the following minor changes: where before we had just U_0 and Γ' we now have

$$U_0(t) \equiv U_0\Big[1 + A\cos\big(\omega_1 t\big)\Big] \tag{4.92}$$

$$\Gamma'(t) \equiv \Gamma'\Big[1 + A\cos\big(\omega_1 t\big)\Big]\ . \tag{4.93}$$

No new terms are introduced into the incremental equations for p through the new time dependence of these ratchet parameters.

4.4.1 Symmetry analysis

For the previous two ratchets I used the findings of Section 2.4, specifically the requirements on F and f in Eq. 2.11 to determine when the system symmetries $\hat{S}$ hold. However these requirements were derived for $V(x,t) \equiv V(x)$ and $F(x,t) \equiv F(t)$. This is not true for the gating ratchet and we must derive the requirements on the potential modulation and the driving from scratch. To aid the analysis I write here the Langevin equation for the gating ratchet

$$m\ddot{x} = -V'(x)\big(1 + A\cos\omega_1 t\big) + B\cos\big(\omega_2 t + \phi\big) - \gamma\dot{x} + \xi(t) \ . \tag{4.94}$$

As before we are concerned with transformations of x and t that lead to change in sign of p. These are

- $\hat{S}_1 : x \to -x + x', \quad t \to t + t'$
- $\hat{S}_2 : x \to x + x', \quad t \to -t + t'$

with x', t' arbitrary constants.

In performing the symmetry analysis of this gating ratchet we limit ourselves to periodic driving. This is the case when ω_2/ω_1 is rational. As before we write $\omega_2/\omega_1 = p/q$ with p, q positive and coprime. We omit consideration for $\xi(t)$ as it is symmetric.

Consider first the transformations $x \to -x + x', \quad t \to t + t'$. Then Eq. 4.94 transforms to

$$-m\ddot{x} = V'(-x+x')\Big(1 + A\cos\big(\omega_1 t + \omega_1 t'\big)\Big) + B\cos\big(\omega_2 t + \omega_2 t' + \phi\big) + \gamma\dot{x} \tag{4.95}$$

and is unchanged if $\omega_1 t' = 2n\pi$ and $\omega_2 t' = (2m+1)\pi$ with n, m integer, as a suitable x' is readily found. Thus for

$$q \text{ even and } p \text{ odd}$$

Eq. 4.94 is invariant under the transformations $\hat{S}_1$ and no current is generated.

If this condition doesn't hold, i.e. for q odd, current generation is determined by $\hat{S}_2$. To facilitate the analysis we set $\gamma = 0$ and anticipate that reintroducing dissipation will have the effect of a phase-shift as in previous analyses. We find that Eq. 4.94 transforms under $\hat{S}_2$ to

$$m\ddot{x} = -V'(x + x')\Big(1 + A\cos\big(-\omega_1 t + \omega_1 t'\big)\Big) + B\cos\big(-\omega_2 t + \omega_2 t' + \phi\big) \tag{4.96}$$

and is invariant when $\omega_1 t' = 2n\pi$ and $\phi = -\pi(n\omega_2/\omega_1 + m)$. With $\omega_2/\omega_1 = p/q$

the requirement on ϕ simplifies to

$$q\phi = l\pi \tag{4.97}$$

with l integer. We thus expect a current of the form $I \sim \sin q\phi$.

Dissipation is accounted for by a phase shift ϕ_0 so that

$$I \sim \sin(q\phi - \phi_0) \ . \tag{4.98}$$

4.4.2 Numerical results

The numerical results from semiclassical Monte Carlo simulations verify the symmetry analysis. In Fig. 4.12 I plot the signal of current versus phase-difference for different choices of the ratio p/q. The effect of the parity of q can clearly be seen. Non-negligible current is only generated for q odd for which the signal displays a clear sinusoidal dependence. The period of these signals is seen to depend on q. By fitting the data with a function of the form

$$v_{max} \sin(b\phi - \phi_0) \tag{4.99}$$

one can determine the amplitude and period of the signal.

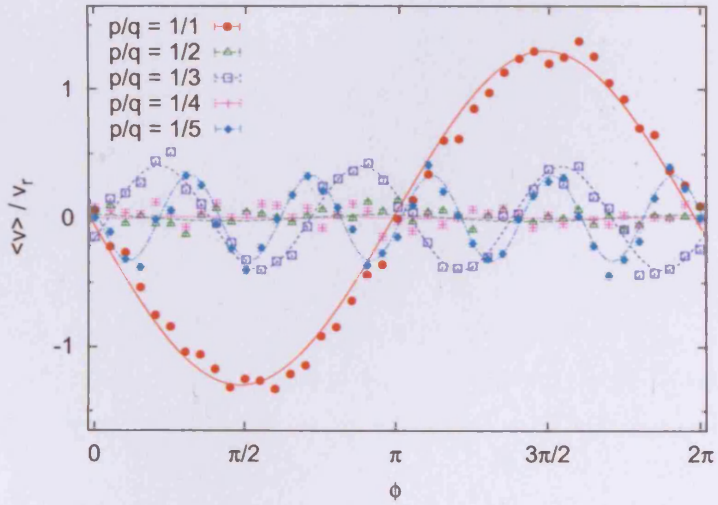

Figure 4.12: Gating ratchet: current versus phase-difference ϕ for different p/q. The curves, plotted only for q odd, represent the best fits of the function $v_{max} \sin(b\phi - \phi_0)$ to the data. The relevant calculation parameters are $U_0 = 200E_r$, $\Gamma' = 10\omega_r$, $A = 0.5$, $B = 40$ and $\omega_1/\omega_v = 0.7$. The sample size is 5000.

One finds that the period of the signal b is equal to q, with an error of less than 1%. This is in agreement with the symmetry analysis.

Figure 4.13 plots the amplitude of the signal v_{max} versus the ratio of the frequencies ω_2/ω_1. The results confirm that a non-zero current is only generated for q odd.

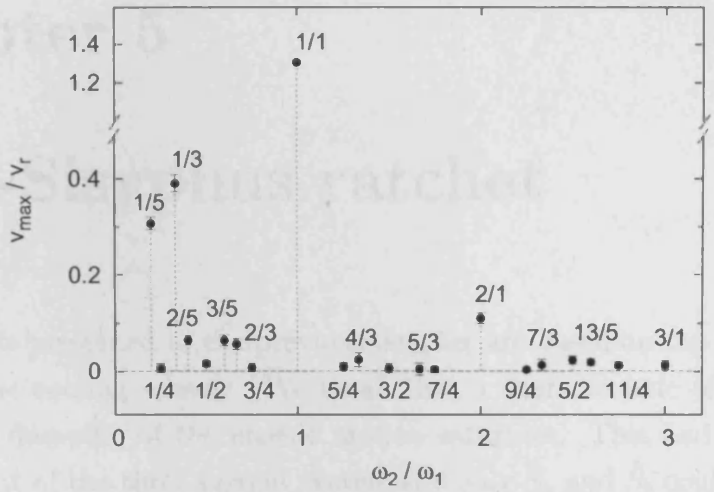

Figure 4.13: Gating ratchet: amplitude of the signal versus ω_2/ω_1. Plotted are the values of the fit parameter v_{max} rescaled by the recoil velocity v_r for different choices of the ratio of the frequencies $\omega_2/\omega_1 = p/q$. The values of p/q label the datapoints. All other calculation parameters as in Fig. 4.12.

Chapter 5

Blue-Sisyphus ratchet

The ratchets presented in the previous chapter are based on the low intensity red-Sisyphus cooling scheme. We recall that a characteristic of this scheme is that the damping of the atomic motion saturates. This had the implication that out of the three system symmetries only $\hat{S}_a$ and $\hat{S}_b$ could be realised in these ratchets, $\hat{S}_c$ only being relevant for overdamped ratchets. This was confirmed by numerical simulation. Our motivation now is to realise an overdamped ratchet with cold atoms. This ratchet is based on the high intensity blue-Sisyphus cooling scheme [3, 21, 24]. In this scheme the damping does not saturate with laser intensity. We rock the atoms with a biharmonic driving. We find that the generation of current is precisely determined by the realisation, or not, of the $\hat{S}_c$ symmetry, consistent with an overdamped ratchet.
The main findings of this study are awaiting publication.

5.1 Blue Sisyphus cooling

I summarise here the main features of the high-intensity blue-Sisyphus cooling scheme as presented in [21]. The essential idea is to obtain eigen-states for the system in the absence of spontaneous emission and then treat spontaneous emission as a perturbation.

5.1.1 Hamiltonian and dressed-states

Consider a one dimensional standing light wave acting on a two-level atom. Excluding spontaneous emission, the Hamiltonian H_S describing this system is the sum of the atomic Hamiltonian H_A, the energy of the light-field H_L and the atom-field interaction H_{AL}

$$H_S = H_A + H_L + H_{AL} \ . \tag{5.1}$$

We have

$$H_A = \frac{p^2}{2m} + \hbar\omega_A b^\dagger b \tag{5.2}$$

the sum of external and internal energies where b is the atomic lowering operator $|g\rangle\langle e|$, and

$$H_L = \hbar\omega_L a^\dagger a \tag{5.3}$$

where a is the annihilation operator of the light-field. In the dipole and rotating wave approximations we have

$$H_{AL}(z) = -d \cdot \left(E(z)b^\dagger a + E^*(z)ba^\dagger\right) \tag{5.4}$$

where

$$E(z) = \hat{e}E_0 \cos kz/\sqrt{n} \tag{5.5}$$

with E_0 the amplitude of each travelling wave and n the number of photons in the mode with polarisation $\hat{e}$.

We proceed by considering the eigen-states of the system at a fixed point z i.e. the $p^2/2m$ kinetic energy term of Eq. 5.2 is dropped. The Hamiltonian we employ is the dressed-atom Hamiltonian

$$H_{DA} = \hbar\omega_A b^\dagger b + \hbar\omega_L a^\dagger a - d \cdot \left(E(z)b^\dagger a + E^*(z)ba^\dagger\right) \tag{5.6}$$

and the basis we use is the set product-states $\{|g; n+1\rangle, |e; n\rangle\}$ where $|g; n+1\rangle$ denotes the product state of ground state atom and $n+1$ photons.

Taking initially $d = 0$ and with $\delta \ll \omega_L, \omega_A$, the eigen-states form into well-separated pairs. A depiction of part of the resulting energy ladder with $\delta > 0$, so that $|g, n+1\rangle$ is above $|e, n\rangle$, is given below.

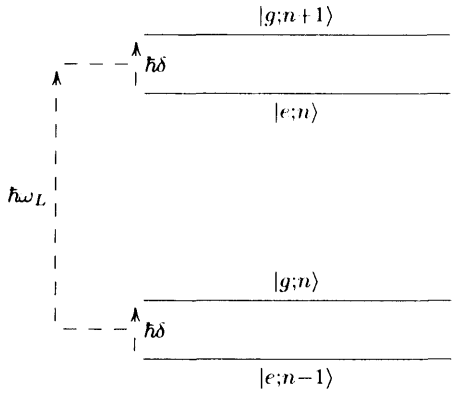

Continuing now with $d \neq 0$, by diagonalising H_{DA} we obtain the dressed-atom eigen-states, the dressed-states

$$|1,n\rangle = \cos\theta|e;n\rangle + \sin\theta|g;n+1\rangle \tag{5.7a}$$

$$|2,n\rangle = -\sin\theta|e;n\rangle + \cos\theta|g;n+1\rangle \ , \tag{5.7b}$$

where the mixing angle θ is given by

$$\cos 2\theta = -\delta/\Omega(z), \quad \sin 2\theta = \Omega_0 \cos kz/\Omega(z) \ . \tag{5.8}$$

The eigen-energies are

$$E_{1n} = \hbar\omega_L(n+1) - \frac{\hbar\delta}{2} + \frac{\hbar\Omega(z)}{2} \tag{5.9}$$

$$E_{2n} = \hbar\omega_L(n+1) - \frac{\hbar\delta}{2} - \frac{\hbar\Omega(z)}{2} \tag{5.10}$$

and form the optical potentials for the dressed-states. The energy splitting between the dressed-states is $\hbar\Omega(z)$ with the generalised Rabi frequency $\Omega(z)$ given by

$$\Omega(z) = (\Omega_0^2 \cos^2 kz + \delta^2)^{1/2} \ . \tag{5.11}$$

The dressed-states are spatially dependent linear combinations of the unperturbed bare product states $|g;n+1\rangle$ and $|e;n\rangle$. They coincide exactly with the bare-states where $\sin\theta = 0$, as portrayed in Fig. 5.1 for a blue detuning $\delta > 0$. At these positions the energy splitting between the two dressed-states reduces from $\hbar\Omega(z)$ to $\hbar\delta$.

5.1.2 Spontaneous emission and Sisyphus cooling

Spontaneous emission induces transitions $|i,n\rangle \rightarrow |j,n-1\rangle$. The rates for these transitions vary in space; the rate is lowest (resp. highest) where the magnitude of the amplitude of the $|g;\bullet\rangle$ (resp. $|e;\bullet\rangle$) component of the dressed-state is lowest (resp. highest).

The damping of atomic motion can be explained as a Sisyphus cooling process. Consider an atom in the $|1,n+1\rangle$ dressed-state moving along its periodic optical potential (see Fig. 5.2). The atom will preferentially decay near the crests of the potential and it can decay to either $|1,n\rangle$ or $|2,n\rangle$, both containing an admixture of atomic ground state. We'll assume the decay is to $|2,n\rangle$ as the other case has no relevant effect. The atom now finds itself in the trough of the periodic potential for $|2,n\rangle$ and starts to climb the potential. It

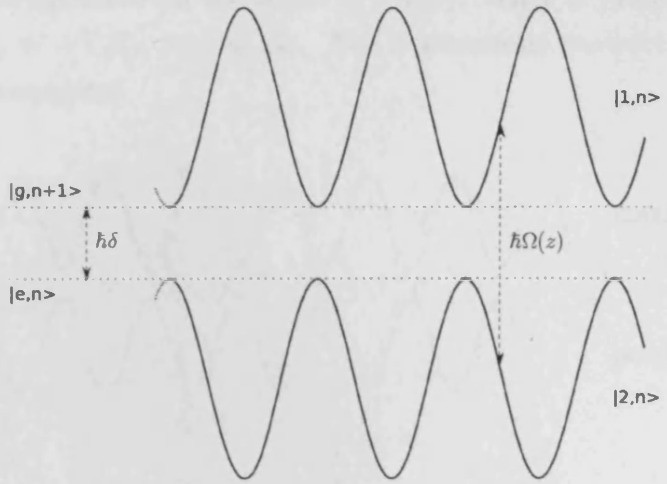

Figure 5.1: The spatial dependence of the dressed-state energies (full lines) in a standing wave for a blue detuning $\delta > 0$. The energy difference between the two dressed-states is $\hbar\Omega(z)$. This reduces to $\hbar\delta$ at nodes where the dressed-states coincide with the unperturbed bare-states (dashed lines).

too will preferentially decay at the crest of the potential and so the process continues. The net effect of repeated transitions is that on average the atom travels uphill more than downhill and hence is slowed and cooled.

The process continues until the atoms energy is of the order of the depth of the potential when the efficiency of the cooling is much reduced. A measure of the potential depth is Ω_0. Thus, equilibrium temperatures scale with Ω_0 and they are some orders of magnitude larger than for the usual laser cooling schemes. For example, equilibrium temperatures for ^{87}Rb are of the order of 10s of mK for this scheme whereas for the low intensity red-Sisyphus scheme considered in the previous chapter they are of the order of 10s of μK.

The effective friction force acting on the atom is determined by the energy loss from transitions. The energy loss per transition is of the order of depth of the optical potential and so scales with Ω_0. The damping of the atomic motion thus also scales with Ω_0 and does not saturate. It is this important characteristic that makes this scheme ideal for realising an overdamped ratchet. For large enough Ω_0 the damping should dominate inertial effects and then the system symmetry $\hat{S}_c$ of Section 2.4 may be realised. Indeed by varying Ω_0 we can 'tune' the damping of the system. For low values of Ω_0 we may even obtain a weakly damped system. Thus we could hope to study both strongly damped and weakly damped ratchets by varying Ω_0.

The random nature of the spontaneous emission events causes the instantaneous forces on the atom to fluctuate. For example, for the atom in the

$|1, n+1\rangle$ state the force on the atom is $-\nabla E_1$. After it jumps to $|2, n\rangle$ the force is $-\nabla E_2 = +\nabla E_1$, and so on. The fluctuations produce a diffusion in the atomic momentum.

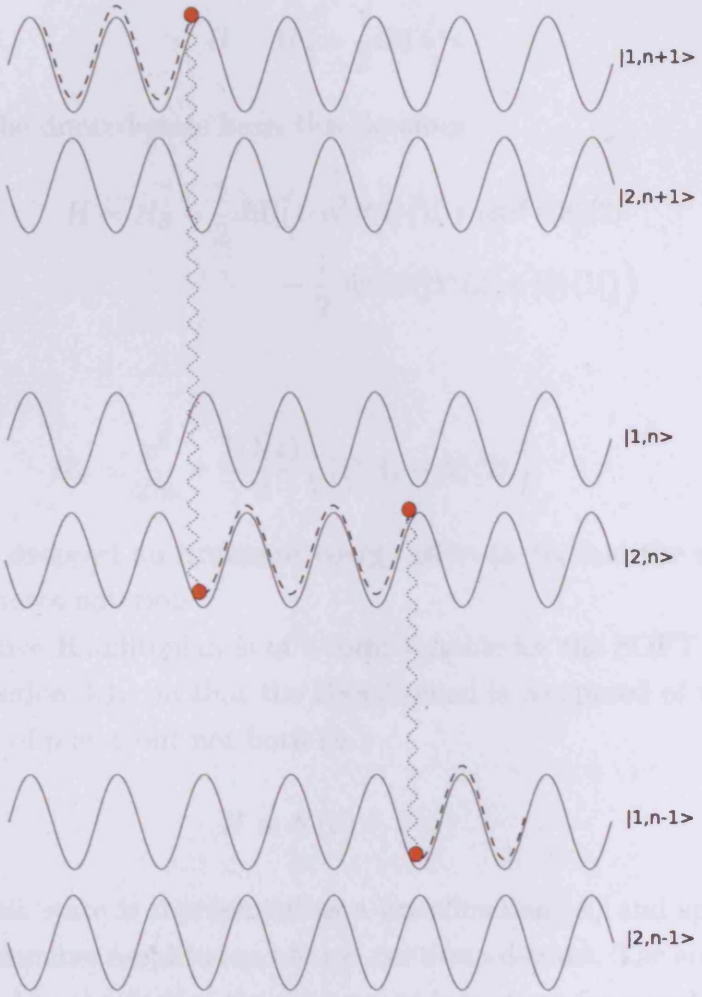

Figure 5.2: Representation of the Sisyphus cooling of an atom for a high intensity blue-detuned standing wave. Sequences of transitions between dressed-states $|1\rangle \rightarrow |2\rangle$ and $|2\rangle \rightarrow |1\rangle$ and so on, have the effect that the atom on average 'travels' uphill more than downhill reducing the atoms energy.

5.2 Numerical simulation treatments

All three numerical simulation treatments discussed in Chapter 3 may be applied to this cooling scheme.

5.2.1 Quantum

Applying the fully quantum approach we form a non-Hermitian effective Hamiltonian for use in the MCWF method [25, 67]

$$H = H_S - \frac{1}{2}i\hbar\Gamma b^\dagger b \,. \tag{5.12}$$

Working in the dressed-state basis this becomes

$$\begin{aligned} H = H_S - \frac{1}{2}i\hbar\Gamma\Big(&\cos^2\theta|1\rangle\langle 1| + \sin^2\theta|2\rangle\langle 2| \\ &- \frac{1}{2}\sin 2\theta\big(|1\rangle\langle 2| + |2\rangle\langle 1|\big)\Big) \end{aligned} \tag{5.13}$$

with

$$H_S = \frac{p^2}{2m} + \frac{\hbar\Omega(z)}{2}\Big(\,|1\rangle\langle 1| - |2\rangle\langle 2|\,\Big) \tag{5.14}$$

where I have dropped an irrelevant energy offset in H_S and the n label from the dressed-states notation.

The effective Hamiltonian is of a form suitable for the SOFT method described in Section 3.1.1 in that the Hamiltonian is composed of terms which are functions of p or z but not both i.e.

$$H \equiv K(p) + V(z) \,. \tag{5.15}$$

The atomic state is represented as a wavefunction $|\psi\rangle$ and specifically as two sets of c-number amplitudes, one set per dressed-state. The entries in each set correspond to the sites of the discrete grids we form for p and z. We work in the spatial representation so at time t

$$|\psi_z(t)\rangle = \sum_{j=1}^{n} \alpha_{z_j}(t)|1, z_j\rangle + \beta_{z_j}(t)|2, z_j\rangle \tag{5.16}$$

where the z_j are the points of the spatial grid, and α_{z_j} and β_{z_j} are the time-dependent amplitudes at the points z_j.

We calculate the SOFT time evolution operators U_V and U_K at each discrete grid point, U_V on the z grid and U_K on the p grid. The operator U_K is diagonal in the dressed-state basis so we can represent it simply as a list of c-numbers. For example at a grid point p_j, the value of U_K for a timestep of size Δt is given as

$$U_K(p_j, \Delta t) = \exp\Big(-\frac{i}{\hbar}\frac{p_j^2}{2m}\Delta t\Big) \,. \tag{5.17}$$

We represent U_V as a list of 2x2 matrices as $V(z)$ is not diagonal in the dressed-state basis. For example, at grid point z_j we have the following 2x2 matrix

$$U_V(z_j, \Delta t) = \exp -\frac{i}{2}\Delta t \begin{pmatrix} \Omega(z_j) - i\Gamma\cos^2\theta(z_j) & i\frac{\Gamma}{2}\sin 2\theta(z_j) \\ i\frac{\Gamma}{2}\sin 2\theta(z_j) & -\Omega(z_j) - i\Gamma\sin^2\theta(z_j) \end{pmatrix} . \tag{5.18}$$

We evolve our wavefunction $|\psi_z(t)\rangle$ with H for a timestep Δt by following Eq. 3.17 and applying the necessary Fourier Transforms to convert between state represenations.

The atomic momentum distribution is rather wide by virtue of the relatively high temperatures realised with this cooling scheme. We need to ensure that our discrete grid representation of the momentum space is large enough to accommodate this distribution. Referring to Section 3.1.1 values for p_{max} of the order of 100 to 1000 were not uncommon, with the space sampled over between 2^{11} to 2^{16} points.

Sample sizes were of the order of 100 to 1000 and limited by the computing resources available.

5.2.2 Semiclassical

In Ref. [21] the authors derive the general equations of motion using a semi-classical approach; this derivation will be described here.

The equations of motion are determined from the master equation for the reduced density matrix ρ of the dressed atom. The effect of spontaneous emission which gives rise to transitions between dressed-states may be simplified in the limit $\Omega(z) \gg \Gamma$. Then, under the secular approximation [18], the diagonal elements of ρ, the populations, are only coupled to themselves and not to the off-diagonal elements, the coherences.

Consider first the atom at a fixed point in space. We obtain the following equations in the secular approximation for the reduced populations

$$\dot{\rho}_{11} = -\Gamma_{21}(z)\,\rho_{11} + \Gamma_{12}(z)\,\rho_{22} \tag{5.19}$$

$$\dot{\rho}_{22} = -\dot{\rho}_{11} \tag{5.20}$$

where $\rho_{ij} = \langle i|\rho|j\rangle$, with $\rho_{11} + \rho_{22} = 1$, and where $\Gamma_{ij}(z)$ are the transition rates from state j to state i

$$\Gamma_{12}(z) = \Gamma\sin^4\theta(z) \tag{5.21}$$

$$\Gamma_{21}(z) = \Gamma\cos^4\theta(z)\ . \tag{5.22}$$

For the coherences we have

$$\dot{\rho}_{12} = \Big(-i\Omega(z) - \Gamma_{coh}(z)\Big)\,\rho_{12} \tag{5.23}$$

$$\dot{\rho}_{21} = \big(\dot{\rho}_{12}\big)^* \tag{5.24}$$

with

$$\Gamma_{coh}(z) = \Gamma\Big(\frac{1}{2} + \cos^2\theta(z)\sin^2\theta(z)\Big)\ . \tag{5.25}$$

For the case of a moving atom we simply take into account the time dependence of the dressed-states so that for example

$$\dot{\rho}_{11} = \langle 1;z|\dot{\rho}|1;z\rangle + \langle \dot{1;z}|\rho|1;z\rangle + \langle 1;z|\rho|\dot{1;z}\rangle \tag{5.26}$$

and where

$$|\dot{1;z}\rangle = v\,\nabla|1;z\rangle\ . \tag{5.27}$$

From the dressed-state expressions Eq. 5.7 we find

$$\nabla|1;z\rangle = \nabla\theta|2;z\rangle \tag{5.28}$$

$$\nabla|2;z\rangle = -\nabla\theta|1;z\rangle \tag{5.29}$$

so that the equations of motion become

$$\dot{\rho}_{11} = -\Gamma_{21}\,\rho_{11} + \Gamma_{12}\,\rho_{22} + v\nabla\theta\big(\rho_{12} + \rho_{21}\big) \tag{5.30a}$$

$$\dot{\rho}_{12} = \Big(-i\Omega(z) - \Gamma_{coh}(z)\Big)\,\rho_{12} + v\nabla\theta\big(\rho_{22} - \rho_{11}\big) \tag{5.30b}$$

with similar expressions for $\dot{\rho}_{22}$ and $\dot{\rho}_{21}$.

[In Ref. [15] the authors give the following simplified equations of motion having neglected the terms arising from spontaneous emission

$$\dot{\rho}_{11} = v\nabla\theta\big(\rho_{12} + \rho_{21}\big) \tag{5.31}$$

$$\dot{\rho}_{12} = -i\Omega(z)\rho_{12} + v\nabla\theta\big(\rho_{22} - \rho_{11}\big)\ . \tag{5.32}$$

In my simulations I use the full expressions Eq. 5.30.]

The force arising from the atom-field interaction determines the external motion. It is given by the spatial gradient of the potential term in Eq. 5.14 averaging over the internal states. A simple calculation yields

$$f(z) = \frac{1}{2}\hbar\nabla\Omega\big(\rho_{22} - \rho_{11}\big) - \hbar\Omega\nabla\theta\big(\rho_{12} + \rho_{21}\big)\ . \tag{5.33}$$

A Monte-Carlo method can be applied to simulate these equations of mo-

tion as is done in Ref. [15]. The atomic state is represented by 4 variables, 2 c-numbers for ρ_{11} and ρ_{12}, and 2 r-numbers for p and z. The state evolves smoothly through time occasionally punctuated by spontaneous emission events. In between these events the evolution is determined by Eqs. 5.30 and 5.33. The probability of a decay event is calculated at each timestep and is compared to a random variable. If a decay is deemed to occur, another random variable is compared to the branching ratio to determine which of the two dressed-states the atom decays to. By performing multiple independent simulations one obtains statistical estimates for the various quantities measured.

5.2.3 Classical

In Ref. [72] the authors adopt a classical approach in deriving the equations of motion. The starting point for their analysis is a Fokker-Planck equation for the Wigner distribution function $W(z,p,t)$ in phase space (z,p)

$$\left(\frac{\partial}{\partial t}+\frac{p}{m}\frac{\partial}{\partial z}\right)W=-\frac{\partial}{\partial p}FW+\frac{\partial}{\partial p^2}DW \tag{5.34}$$

where F is the force on the atom and D the diffusion coefficient. These quantities are well known for a standing wave field [40] and exhibit a strong dependence on z for the case here of intense fields. This gives rise to large spatial gradients in F and D which can cause difficulties in directly simulating the Fokker-Planck equation.

To avoid these difficulties the authors proceed to deal with the Langevin equation equivalent to the Fokker-Planck equation. Using the numerical algorithms of Ref. [56] they obtain stochastic incremental equations for the variables z and p. A Monte Carlo method is applied to obtain ensemble averaged measurements.

5.3 Ratchet

The light-field configuration presented above provides for a system where the damping may be tuned by varying Ω_0. The optical potential the atoms experience is symmetric and therefore we require a driving in order to break system symmetries and generate current. We choose the simplest temporally asymmetric driving, the biharmonic driving seen in Section 4.2

$$F(t)=F_0\Big(A_d\cos\omega_d t+B_d\cos\left(2\omega_d t+\phi\right)\Big)\ . \tag{5.35}$$

The driving frequency ω_d is expressed in units of the vibrational frequency ω_v. A simple calculation yields

$$\omega_v = \sqrt{\omega_r \Omega_0^2/\delta} \ . \tag{5.36}$$

5.3.1 Symmetry analysis

Before discussing the results of numerical simulations I present the symmetry analysis of the system. In assessing the symmetries of a system recall that they are determined by the symmetries of the driving $F(t)$ and of $f(z) \equiv V'(z)$. It should be noted that the optical potential is a simple standing wave and it is easy to show that both f_a and f_{sh} are realised. Therefore we can proceed to analyse the requirements on $F(t)$.

For symmetry $\hat{S}_a$ we require F_{sh}. We found the conditions for F_{sh} for the weakly damped ratchet with biharmonic driving of Chapter 4. Specifically the symmetry F_{sh} is broken, regardless of ϕ, due to the two harmonics of different parity.

There we also found that the system symmetry $\hat{S}_b$ is realised for Hamiltonian ratchets for $\phi = n\pi$ with the current having the form $I \sim \sin\phi$. A small amount of damping is accounted for by a phase-shift giving $I \sim \sin(\phi - \phi_0)$.

For this system we anticipate a stronger damping than previously. In the overdamped limit, where $\hat{S}_c$ is relevant, current generation is determined by F_a. A simple calculation yields that the F_a symmetry is realised for $\cos\phi = 0$ i.e. $\phi = (n + \frac{1}{2})\pi$. For these values of ϕ no current is to be expected. The current in the overdamped limit has been shown [74, 86] to have the form

$$I \sim \cos\phi \tag{5.37}$$

or equivalently that the phase-shift ϕ_0 of $I \sim \sin(\phi - \phi_0)$ is $\pi/2$.

By varying the atomic damping through the quantity Ω_0 we may witness the variation of ϕ_0. For sufficiently large values of Ω_0 we expect $\phi_0 = \pi/2$ consistent with an overdamped ratchet and for sufficiently low values of Ω_0 we might expect $\phi_0 = 0$. For intermediate values of Ω_0 the relationship between Ω_0 and ϕ_0 has no predictable behaviour.

5.3.2 Numerical results

In this section I study the atomic current as a function of the phase-difference ϕ for different dampings represented by the quantity Ω_0. The data are the result of simulations using the quantum approach as described in Section 5.2

above. Typical current versus phase-difference signals are plotted in Fig. 5.3. On the left hand side the data are for a rather large value of Ω_0 and on the left hand side the data are for a rather small value of Ω_0.

For the large value of Ω_0 we see that the current is zero at $\phi = \pi/2, 3\pi/2$ consistent with the F_a symmetry being realised for an overdamped ratchet. Furthermore, for $\phi \neq \pi/2, 3\pi/2$ the current is substantially non-zero. Indeed the current signal is well described by $I \sim \cos\phi$, consistent with the theoretical predictions for an overdamped ratchet.

For the smaller value of Ω_0 we see that the current is non-zero for $\phi = \pi/2$ and $3\pi/2$ indicating that the F_a symmetry is not realised. The current signal retains a regular sinusoidal form but now has acquired a phase-shift $\phi_0 \neq \pi/2$.

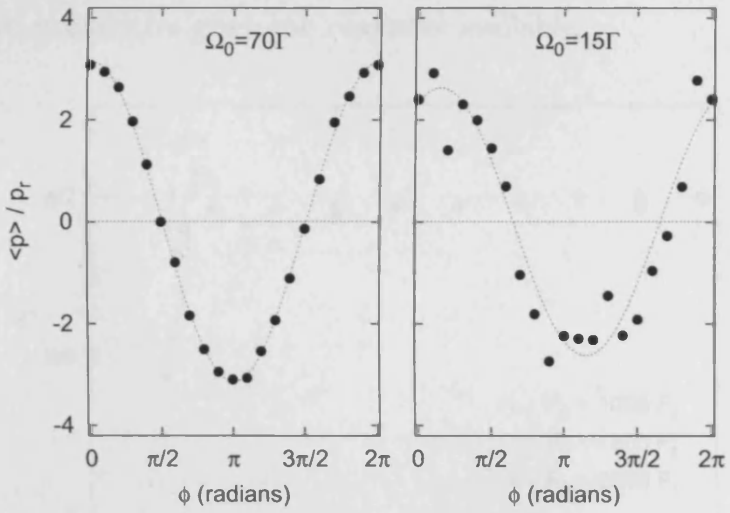

Figure 5.3: Strongly damped ratchet with biharmonic driving: plot of average current scaled by the recoil momentum p_r versus the phase difference ϕ. The data are the result of quantum Monte Carlo Wave Function simulations. The curves represent the best fit to the data of the function Eq. 5.38. On the left hand side the calculations were performed with $\Omega_0 = 70\Gamma$ and on the right hand side with $\Omega_0 = 15\Gamma$. All other calculation parameters were identical, being $\delta = 15\Gamma$, $\omega_d/\omega_v \approx 1$, $F_0 = 2500\hbar k\omega_r$, $A = B = 1$, and with a sample size of 2000.

We fit the signal with the function

$$A\sin(\phi - \phi_0) \tag{5.38}$$

to determine the amplitude and acquired phase-shift. In this study I omit analysis of the behaviour of the amplitude as a function of the ratchet parameters and concentrate on the behaviour of the phase-shift.

In Fig. 5.4 I plot phase-shift ϕ_0 versus Ω_0 for three different driving amplitudes F_0. We see that for large values of Ω_0 i.e. strong damping, the phase-

shift is $\pi/2$. Reducing Ω_0 the phase-shift drifts away from $\pi/2$ and starts to vary somewhat unpredictably. For the lowest values of Ω_0 reported the phase-shift is substantially not equal to $\pi/2$. Furthermore, for this range of values for Ω_0 and for the weakest driving amplitude considered here, $F_0 = 1000F_r$, the phase-shift decreases with Ω_0. This appears to have the characteristic of the transition from a strongly damped to a weakly damped ratchet where we could expect ϕ_0 to vary from $\pi/2$ to 0. To confirm this assertion Ω_0 should be decreased further. However we found for lower values of Ω_0 that the 'current-vs-ϕ' signal became excessively noisy and that reliable values for ϕ_0 could not be obtained. It seems the fluctuations in momentum 'wash' out the directed motion. Increasing the sample size for the simulation would reduce the errors and perhaps give a 'cleaner' signal but the computing time required to do this proved to be prohibitive given the resources available.

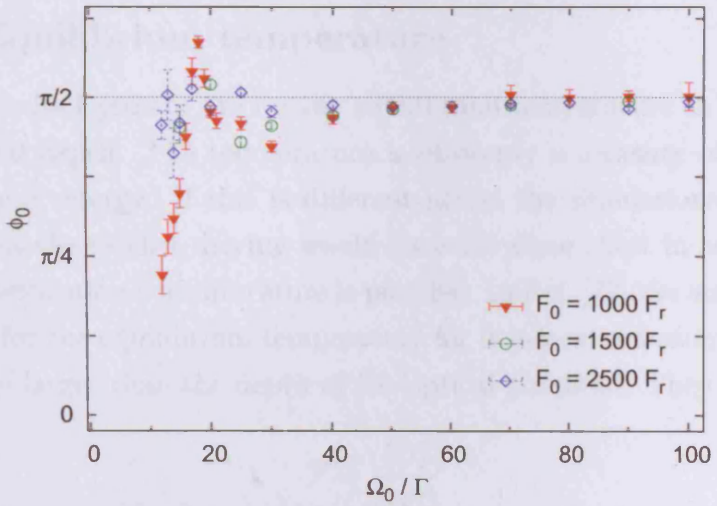

Figure 5.4: Strongly damped ratchet with biharmonic driving: plot of phase-shift ϕ_0 as a function of Ω_0. The phase-shift is determined by fitting data like those of Fig. 5.3 with the function Eq. 5.38. Calculation parameters are as for Fig. 5.3.

5.3.3 A note of caution

The results of the Monte Carlo simulations using the fully quantum treatment are promising. However these results are rather standalone. Simulations using the semiclassical and classical treatments were also performed with unsatisfactory results. The average current versus ϕ signals obtained were very irregular looking. A whole range of simulation parameters were used but no correspondence could be made to the quantum simulation results.

To investigate why the quantum simulation results could not be corrob-

orated a comparative study was embarked upon. The idea was to perform in parallel quantum, semiclassical and classical simulations, taking measurements of key data. By analysing these results and comparing to the literature it is hoped to understand what, if any, differences there may be between the simulations.

5.4 Numerical simulations - a comparative study

In this section I present the results of the study to compare the values of kinetic variables obtained by various numerical simulations. The results are organised by the variable being measured. It should be noted that each simulation was performed in the absence of any ratchet driving. Thus attention is restricted to the treatment of the atomic dynamics.

5.4.1 Equilibrium temperature

The first results I present are for the equilibrium temperature as a function of the potential depth. The temperature is obviously a measure of the average atomic kinetic energy. If this is different across the simulations it would be unlikely that the ratchet driving would have the same effect in each.

Some verification with literature is possible. In Ref. [72] the authors give an expression for the equilibrium temperature for non-localised atoms, i.e. atoms with energy larger than the depth of the optical potential. They give

$$T = \frac{\langle D \rangle}{m\langle \gamma \rangle} \tag{5.39}$$

where $\langle D \rangle$ and $m\langle \gamma \rangle$ are the spatially averaged diffusion coefficient and friction coefficient respectively. This expression should be considered as an upper-bound as we can expect some proportion of atoms to be localised in the potentials. We may compare the results from the classical simulation directly with values calculated using the analytic expression.

In Fig. 5.5 I plot the results of a classical simulation together with the analytic values for two values of the detuning, $\delta = 15\Gamma$ and $\delta = 6\Gamma$. [The value of $\delta = 15\Gamma$ was chosen for comparison to Ref. [15] and $\delta = 6\Gamma$ for comparison to Ref. [72].] The quantity Ω_0 is used as a measure of the potential depth and the average squared momentum $\langle (p/p_r)^2 \rangle$ as a proxy for the temperature.

We see from Fig. 5.5 that there is a clear linear relationship between the temperature and the depth of the potential. This is in agreement with the dressed-state theory discussed above; recall that the cooling mechanism is less

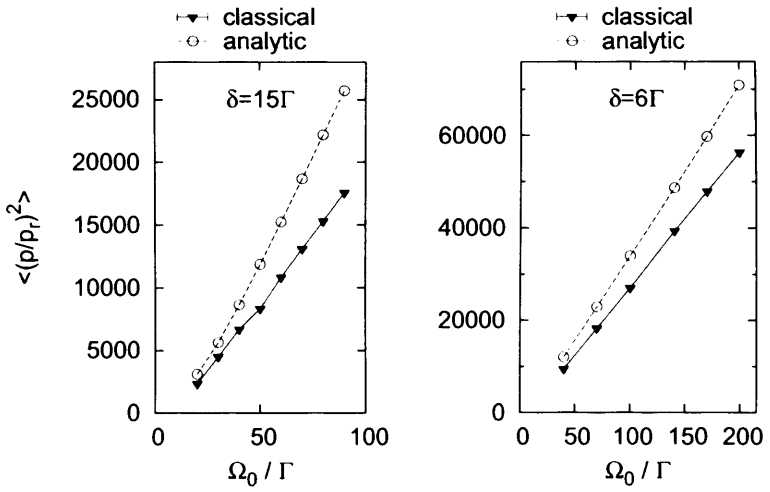

Figure 5.5: Equilibrium 'temperatures' as a function of Ω_0 for the classical simulation of the blue-Sisyphus cooling scheme. Also plotted is the analytic result using the expression Eq. 5.39. On the left hand side we have data for $\delta = 15\Gamma$ and on the right hand side data for $\delta = 6\Gamma$. For the y-axis we have the average squared scaled momentum, scaled by the recoil momentum p_r, and for the x-axis we have Ω_0 scaled by the linewidth Γ. For reference a y-value of 10000 equates to a temperature of approximately 4mK for ^{87}Rb. For these calculations we had a sample size of 5000 atoms. The straight lines are visual guides.

effective when the atoms energy is lower than the potential depth, so that temperatures scale with potential depth. We also see that there is a good agreement between the simulation data and the analytic values, although the analytic values lie above those of the simulations. The difference in values may be attributed to the fact that the analytic expression is derived for non-localised atoms and in the simulations some proportion of the atoms will be localised and thus have lower energies.

I now compare the results from the different simulation approaches. In Fig. 5.6 I plot data from semiclassical and quantum simulations together with the classical data. On the left hand side are the data for $\delta = 15\Gamma$ and on the right hand side data for $\delta = 6\Gamma$; they will be discussed separately.

For $\delta = 15\Gamma$ we see that the semiclassical and quantum data also show a clear linear relationship between temperature and potential depth, and that the results from the three simulation schemes are in good agreement.

For $\delta = 6\Gamma$, however, we cannot draw the same conclusions and some problems were encountered. Firstly, the semiclassical simulation failed to reach an equilibrium temperature for all, but the lowest, values of Ω_0 studied. Thus in Fig. 5.6 and the plot for $\delta = 6\Gamma$ there is only one datapoint for the semiclassical

simulation. A number of simulation parameters were adjusted to help achieve convergence but without success.

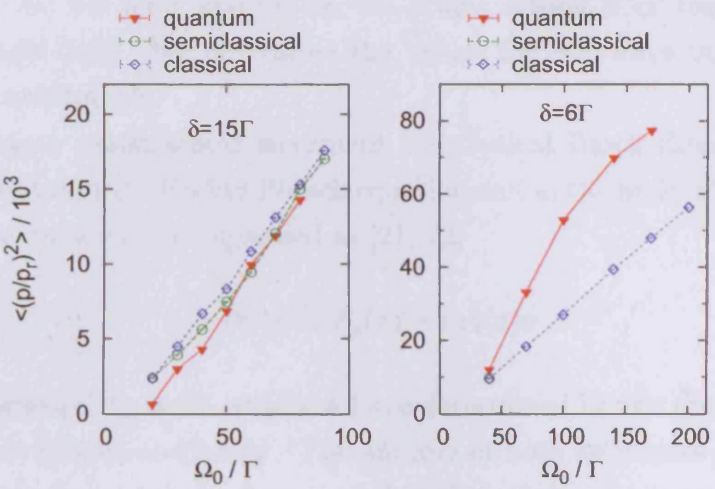

Figure 5.6: A comparison of three simulation approaches for the blue-Sisyphus cooling scheme. Plotted is the average squared scaled momentum, scaled by the recoil momentum p_r, against Ω_0 scaled by the linewidth Γ. On the left hand side we have data for $\delta = 15\Gamma$ and on the right hand side data for $\delta = 6\Gamma$. For $\delta = 6\Gamma$ there is only one datapoint for the semiclassical simulation at $\Omega = 40\Gamma$ - see text for more details. The simulations had the following sample sizes: quantum - 100 atoms, semiclassical - 2000 atoms, classical - 5000 atoms. The straight lines are visual guides.

Turning our attention now to the data for the quantum simulations we see for the lower values of Ω_0 the temperature scales linearly with Ω_0 as expected, before dropping off for the larger values of Ω_0 plotted. This drop-off was found to be due to the momentum grid not being large enough to accommodate the momentum distribution of the atoms. The mean-squared momentum is then artificially lower than it should be. Further simulation runs were made with larger grids but then rounding errors were compounded resulting in nonsensical temperatures. For the lower values of Ω_0 where the relationship between the temperature and Ω_0 is more or less linear, the temperatures differ markedly from those of the classical simulations and the analytic expression. Only for the lowest value of Ω_0 is there good agreement in absolute values.

We content ourselves in the knowledge that the ratchet currents presented in Section 5.3.2 were obtained with $\delta = 15\Gamma$ where there is good agreement for the equilibrium temperature across all three simulation schemes.

5.4.2 Force and diffusion

There are two key factors in determining the dynamics of the atoms. The first of these is the net force exerted on the atoms arising from their interaction with the light-field. We determine the values for this force in the different simulation treatments.

Following a semiclassical treatment the Optical Bloch Equations (OBE) may be reduced into a Fokker-Planck equation and in the limit of low velocities $kv \ll \Gamma$ the force can be expressed as [21, 72]

$$F(z, v) \approx F_g(z) - m\gamma(z)v \ . \tag{5.40}$$

In this expression F_g is the gradient force determined by the optical potential and γ is the friction coefficient. The authors of both references go on to give analytic expressions for the force as a function of the atoms momentum and position; we wish to compare these with values calculated in our simulations.

In our semiclassical simulations we may use Eq. 5.33 to calculate the force on a single atom. However to obtain reasonable statistical averages as a function of z and v would require a vast number of trajectories. We therefore resort to using spatial averages which are feasible to calculate and which we may still compare to the literature.

From Ref. [21] we have

$$m\langle\gamma\rangle \equiv \hbar k^2 \frac{\delta}{\Gamma}\left\{\frac{3}{4}\sqrt{1+s} + \frac{3}{2\sqrt{1+s}} - \frac{1}{4(1+s)^{3/2}} - 2\right\} \tag{5.41}$$

where the '$\langle\cdots\rangle$' denotes the spatial average and where $s = \Omega_0^2/2\delta^2$. In Ref. [72] the authors give

$$m\langle\gamma\rangle = -\hbar k^2 \frac{\Gamma\delta}{4(\delta^2+\Gamma^2/4)} \frac{1}{(1+s)^{3/2}}\left\{s(2+s) - \frac{\delta^2+\Gamma^2/4}{\Gamma^2}\times \frac{8+3s^3+15s^2+20s-8(1+s)^{5/2}}{1+s}\right\} \tag{5.42}$$

with $s = 2\Omega_0^2/(\Gamma^2+4\delta^2)$. For the laser parameters $\Omega_0 = 50\Gamma$ and $\delta = 15\Gamma$ used later, both expressions give the same value to two significant figures.

The above analytic expressions are valid in the limit $kv \ll \Gamma$. In Ref. [65, 66] the authors calculate the spatially averaged force by solving the OBE for an atom moving at constant velocity through the light-field. They employ a continued-fraction method to solve these equations and the values obtained are valid for all atomic velocities. A similar approach is taken in Ref. [9] where

the authors employ a continued-matrix method. Both methods were shown to lead to the same value for the force [9].

Now, we wish to compare the values for the force calculated in the above theoretical treatments with those from our simulations. We may employ two methods to determine the relationship between force and momentum in our simulations.

In the first method we determine the force exerted on the atoms moving with a constant momentum. To do this we start the simulation by launching each atom with a fixed momentum. Then the atomic state is propagated through time according to the equations of motion but keeping the momentum fixed. The force experienced by the atom is calculated at each timestep. After allowing each atom to travel several spatial wavelengths we may determine an ensemble- and spatial- average force for that atomic momentum. The process is repeated for different atomic momenta and we obtain data like those plotted in Fig. 5.7.

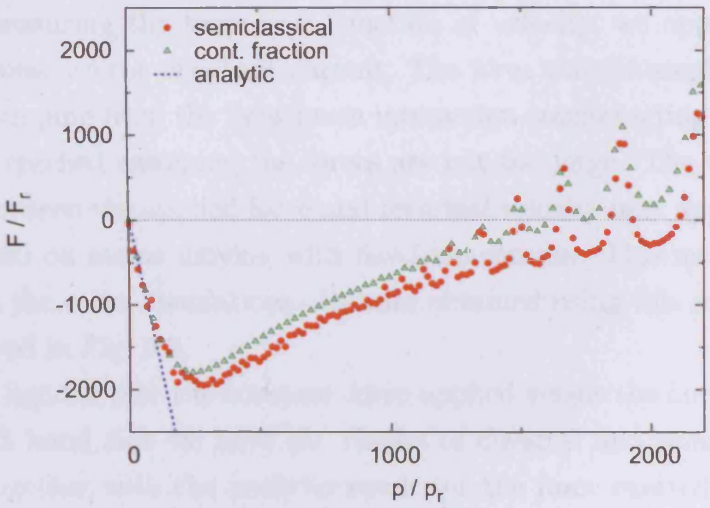

Figure 5.7: Spatially averaged force exerted on atoms as a function of atomic momentum for a blue detuning. Both the force and the atomic momentum are expressed in recoil units. The data points are results from semiclassical simulations and continued-fraction calculations. For atomic momenta smaller than approx. $1500\hbar k$ the force is negative i.e. cooling. Also plotted is the analytic result valid for $kv \ll \Gamma$. The oscillating structure appearing at large momenta is due to doppleron resonances (see text). Laser parameters are $\Omega_0 = 50\Gamma$ and $\delta = 15\Gamma$ with $\Gamma/\omega_r \approx 1550$ for ^{87}Rb.

In this figure we plot the average force as a function of the atomic momentum, both expressed in recoil units. Plotted are the results of semiclassical simulations calculating the force using the method just described, together with those from continued-fraction calculations and the analytic expressions

Eq. 5.41 and Eq. 5.42. The range of validity for these analytic expressions, $kv \ll \Gamma$, is equivalent to $p/p_r \ll 775$ in this plot. The semiclassical simulation data shows reasonable agreement to the continued-fraction calculations across the whole range of momentum considered, but especially so for low values where the analytic expressions are valid. This disparity at higher momentum is also exhibited in Ref. [15] for the same simulations and parameters. The resonance structures appearing at large atomic momenta are due to velocity-tuned multi-photon processes and are known as "Dopplerons" [88].

In the quantum simulations we are unable to use this first method to determine the relationship between force and momentum. Recall that in the quantum simulations we form a discrete basis set for the conjugate momentum and position, and that the atomic state is represented as a vector of amplitudes on this vector space. As such, there is no apparent way to propagate the atom through space whilst keeping the observed value of the momentum operator constant.

As a result we employ a second method for the quantum simulations. Instead of measuring the force as a function of velocity, we apply a constant force and measure the resultant current. The force will set atoms into motion with the damping from the light-atom interaction counteracting it; a terminal velocity is reached assuming the forces are not too large. The resulting relationship between the applied force and terminal velocity may approximate the force exerted on atoms moving with fixed momentum. This method can also be used in the other simulations. Results obtained using this second method are displayed in Fig. 5.8.

In this figure I plot the constant force applied versus the current attained. On the left hand side we have the results of classical and semiclassical simulations together with the analytic result for the force exerted on a moving atom. On the right hand side we have the results of quantum simulations. We see that the classical and semiclassical simulations are in reasonably close agreement with the analytic results. This suggests that this second method is also suitable for determining the force on a moving atom.

However the results from the quantum simulations are very different. Noting the different axes scales, it appears a force an order of magnitude larger is required to produce the same sized current. Thus the effective damping experienced by the atoms in the quantum simulations is much greater than that in the other simulations. There is no obvious explanation for this difference. Also, this difference does not explain why, for the semiclassical and classical simulations of the ratchet of Section 5.3, we don't obtain a regular signal. If the damping is the only difference between the simulations then one could

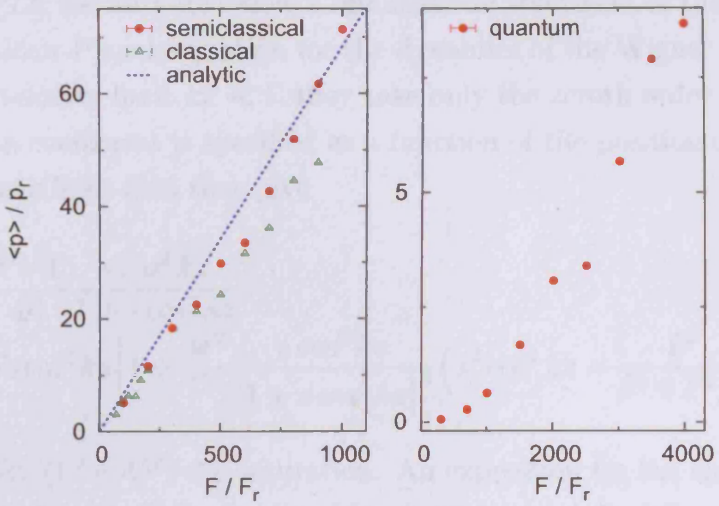

Figure 5.8: Results of measuring the current resulting from applying a constant force in the blue-Sisyphus cooling scheme. On the left hand side we have results from classical and semiclassical simulations together with the analytic result for the force exerted on an atom moving with constant velocity. On the right hand side we have the results of quantum simulations; note the different axes scales for the two plots. Simulation parameters as for Fig. 5.7.

expect the signal from the semiclassical and classical versions to be regular but with a phase-shift appropriate for a ratchet with lower damping. This is not the case so other effects must be at play. One possible explanation is that the diffusion in momentum in the semiclassical and classical simulations is 'washing-out' any rectification effect; we proceed now to examine the diffusion.

The second key factor in determining the atomic dynamics is the diffusion in momentum. As for the case of the damping force, we would like to compare the values of the diffusion across the different simulation schemes. The references cited in the previous discussion for the damping force are suitable for these purposes. However in each of these works the diffusion is determined as a function of either the velocity or the position only. No reference could be found to indicate how to calculate the diffusion as a function of both.

Working in the dressed-state picture Dalibard and Cohen-Tannoudji [21] determined the diffusion due to the fluctuations in the gradient force between the two values $\pm\nabla E_1$. This gives

$$D_{fluct}(z) = \frac{\hbar^2 k^2}{2\Gamma}\left(\frac{\Omega_0^2\cos^2 kz}{\Omega_0^2\cos^2 kz + 2\delta^2}\right)^3 \Omega_0^2 \sin^2 kz \ . \tag{5.43}$$

This expression of course does not include the diffusion due to spontaneous emission events but this is very small in comparison.

In Ref. [72] the authors follow a semiclassical treatment of the OBE. They obtain a Fokker-Planck equation for the dynamics of the Wigner distribution. In the low velocity limit $kv \ll \Gamma$ they take only the zeroth order term so that the diffusion coefficient is specified as a function of the position only. For our standing wave light-field they give

$$D(z) = \frac{\hbar^2 k^2 \Gamma}{10} \frac{s \cos^2 kz}{1 + s \cos^2 kz} + \frac{\hbar^2 k^2 \Gamma}{4} s \sin^2 kz \left[1 + \frac{4\delta^2}{\Gamma^2} \frac{s \cos^2 kz}{\left[1 + s \cos^2 kz\right]^3} \left(s^2 \cos^4 kz - \frac{\Gamma^2}{\delta^2 + \Gamma^2/4} \right) \right] \quad (5.44)$$

with $s = 2\Omega_0^2/(\Gamma^2 + 4\delta^2)$ the saturation. An expression for the spatial average is also given. In general Eq. 5.43 and Eq. 5.44 give slightly different values but for intense fields they are in very good agreement.

In a follow-up to Ref. [65] in Ref. [64] the authors determine the diffusion coefficient by solving the OBE by a continued-fraction method. The premise of this method is that the coefficients in the OBE are periodic in position so that a Fourier series expansion may be applied. The results are valid for all velocities but for strong fields only. The diffusion coefficient they obtain is a function of the position only.

The strong field approximation of Ref. [64] is overcome in Ref. [9] in which the authors employ a continued-matrix method. The premise for this method is the same as that for the continued-fraction method. However the approximation introduced by Minogin [64] is overcome. The diffusion coefficient calculated by this method is also a spatially averaged value as a function of momentum. For the case of zero momentum, the equations they address are much simplified and the authors give an expression for the diffusion as a function of position; the values obtained with this expression coincide with those obtained from Ref. [72] using the expression Eq. 5.44.

We plot values for the momentum diffusion coefficient using these methods in Fig. 5.9. On the lhs of the figure we plot the spatial dependence of the velocity independent diffusion coefficient given by the analytic expression Eq. 5.44. The diffusion shows a strong spatial dependence with the minima located at the nodes of the standing wave. The value for the spatial average is indicated.

On the rhs the results of continued-fraction and continued-matrix calculations are plotted. These calculations give the spatially averaged diffusion coefficient as a function of atomic velocity. We see that for large kv/Γ the two calculation methods give approximately the same values for the diffusion. However, at low velocities the values differ markedly. Berg-Sørensen et al.

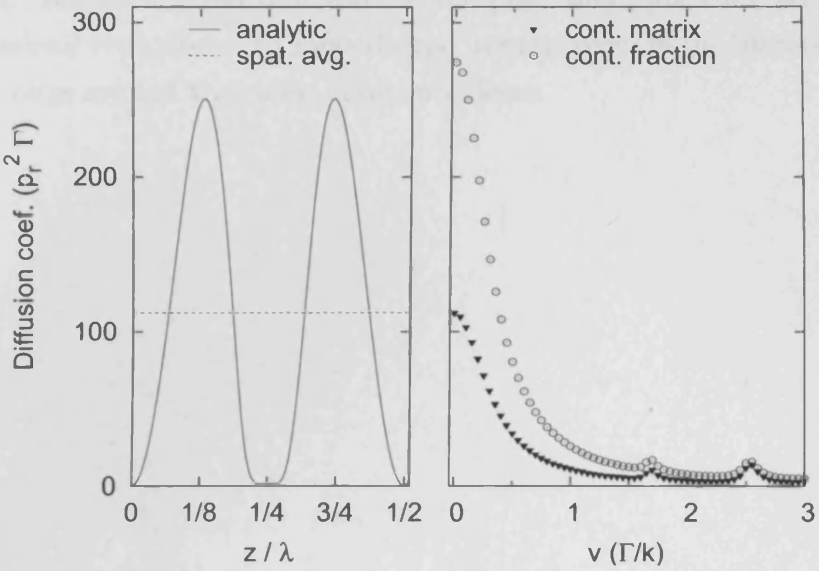

Figure 5.9: Momentum diffusion coefficient for the blue-Sisyphus cooling scheme. On the lhs is plotted the diffusion coefficient as a function of the position z using the analytic expression Eq. 5.44. The spatial average is indicated. On the rhs is plotted the diffusion as a function of the velocity v. These values have been calculated using the continued-fraction and continued-matrix methods (see text). Calculation parameters are as before.

[9] attribute the differences at low velocities to the approximation made in Ref. [64]. We note that the value of the diffusion at zero velocity calculated using the continued-matrix method, matches the velocity independent spatial average calculated using the analytic expression. This would suggest the continued-matrix method is more accurate.

We also see clearly from Fig. 5.9 that the diffusion displays a strong velocity dependence. The global maximum occurs at zero velocity and then sharply falls away with atomic velocity. Local maxima are exhibited but the trend is otherwise decreasing.

This strong velocity dependence perhaps hints at a possible explanation for our problem. In the classical simulations the velocity dependence is not modelled and so the diffusion used is an overestimate for the 'true' values. As suggested earlier, this may 'wash-out' any rectification effect when the ratchet driving is applied. In the semiclassical simulations the diffusion is realised through the fluctuations in the gradient force, as is effectively the case in the quantum simulations. It's not obvious that we can apply this same explanation to the semiclassical simulations. Thus the non-generation of a ratchet signal with the semiclassical simulations remains an open issue.

The possibility of software 'bugs' in the computer implementation is a very

real one. However, given that each of the programs (quantum, semiclassical and classical) reproduces, to some degree, results given in the literature would suggest bugs are not the cause of our problems.

Chapter 6

Conclusion

I started off by introducing the notion of Brownian motors and ratchets. I showed how their various features are fulfilled by a system based on cold atoms. In these systems the atoms move in an optical potential whilst subject to fluctuating forces resulting from photon absorption/emission events. Considering such systems we found that no currents can be generated when the system is symmetric and at equilibrium. I concluded that there are two fundamental requirements for the generation of currents; the system must be driven out of equilibrium and the symmetries of the system, that would otherwise inhibit current generation, must be broken.

In our cold atom ratchets both requirements are generally fulfilled by applying an asymmetric driving. In experiments this is realised by phase-modulating the lattice beams. I showed how this is equivalent to a driving force exerted directly on the atoms. The parameters of the phase-modulation/driving, and the lattice itself, are used to control the breaking of the symmetries of the system.

I derived a simple dynamical model by considering a classical particle moving in a potential subject to unbiased random noise. This led to a stochastic Langevin equation of motion. Such an equation resulted from the semiclassical treatment of the lin⊥lin $J_g = 1/2$ to $J_e = 3/2$ system. The first ratchets I studied were based on this configuration.

The lin⊥lin configuration gives rise to a symmetric optical bipotential. The atoms experience a damping of their motion through a Sisyphus cooling mechanism. This damping is easily tuned by the laser parameters. Optical pumping processes introduce fluctuations in the atomic motion. Due to the inherent symmetry of the optical bipotential we require an asymmetric driving to break the system symmetries.

We first considered a driving of biharmonic form, two harmonics with phase difference ϕ. From symmetry considerations in the Hamiltonian limit we de-

termined a sinusoidal relationship between the current and this phase difference. Away from the Hamiltonian limit we surmised that a phase shift would be found. This was confirmed by Monte-Carlo simulations of the stochastic Langevin equations of motion. We explored the dependence of the current amplitude and phase shift on the ratchets parameters and found largely nonlinear behaviour. We found current reversals for fixed ϕ in two situations: as a function of the driving amplitude with fixed damping rate and as a function of the damping rate with fixed driving amplitude.

For the next ratchet under consideration we applied multi-frequency driving. We studied the symmetries for this ratchet when the driving was periodic and then in the quasiperiodic limit. We found certain symmetries were restored in the quasiperiodic limit and that these symmetries inhibit the generation of currents. This was confirmed by numerical simulation and by experiment.

The last ratchet for this light configuration was a gating ratchet, realised by modulation of the light potential amplitude and application of a single harmonic driving force. In a gating ratchet, the current is generated by a synchronisation effect between the driving and the potential amplitude modulation.

The damping of atomic motion in the lin⊥lin system saturates with light intensity. This prevents us from discovering behaviour of the ratchet in the overdamped limit. However, an intense standing wave with blue detuning gives rise to a Sisyphus cooling mechanism where the damping scales with light intensity and so does not saturate. Results from Monte-Carlo simulations using a fully quantum treatment of the atomic dynamics agree with symmetry analyses and would suggest an overdamped ratchet is indeed realised with this light configuration. However these results cannot be corroborated with semiclassical or classical simulations. The effective forces and momentum diffusion experienced by the atoms were calculated by the different methods available. The values from the semiclassical simulation are in good agreement with Refs. [9, 21, 64]. This is not entirely surprising given that they follow a similar treatment of the equations of motion. The values for the effective damping calculated in the quantum simulations, however, are much larger and this discrepancy cannot be explained at this time and remains an open issue. This casts some doubt on the quantum simulations although the results are nonetheless persuasive.

Looking to the future there are two areas of immediate interest. Firstly, we would like to realise a quantum ratchet [26, 41, 76] with cold atoms. The ratchets studied so far have featured essentially classical dynamics. A quantum ratchet is one where quantum mechanical effects play a significant role in the generation of current. A preliminary investigation has been performed on such

a ratchet with promising results.

The second area for further research is the study of ratchets in two or three dimensions. The ratchets reported here have all been in one dimension. Extending the system to more than one dimension allows for the possibility of not only non-zero average translational currents but also non-zero average vortex currents. Optical potentials in two or three dimensions are readily realised and recent theoretical work [27] showed that the generation of translational and vortex currents can be controlled through the form of the optical potentials and choice of drivings.

Appendices

Appendix A

Fokker-Planck equation derivation

Derivation of the Fokker-Planck equation Eq. 4.37 .

We apply the Wigner transform Eq. 4.35 to each term of Eq. 4.24 taking $|g_{\pm 1/2}\rangle$ components where appropriate. We denote $W_{\pm\pm} = \langle g_{\pm 1/2}|W|g_{\pm 1/2}\rangle$. We assume the spatial extent of the atom is small, since we're treating the external degrees of freedom classically, so that we may take z' to be small and can expand in powers of z' where necessary.

$$\int_{-\infty}^{\infty} dz' \langle z + \frac{z'}{2}| \frac{\partial \rho}{\partial t} |z - \frac{z'}{2}\rangle e^{-ip\cdot z'/\hbar} = \frac{\partial}{\partial t} W(z,p,t) \tag{A.1}$$

$$\begin{aligned}\int_{-\infty}^{\infty} dp' \langle p + \frac{p'}{2}| -\frac{i}{\hbar}\left[\frac{p^2}{2m}, \rho\right] |p - \frac{p'}{2}\rangle e^{iz\cdot p'/\hbar} = \\ -\frac{p}{m}\frac{\partial}{\partial z}\int_{-\infty}^{\infty} dp' \langle p + \frac{p'}{2}| \rho |p - \frac{p'}{2}\rangle e^{iz\cdot p'/\hbar} = \\ -\frac{p}{m}\frac{\partial W(z,p,t)}{\partial z}\end{aligned} \tag{A.2}$$

$$\int_{-\infty}^{\infty} dz' \,\langle z+\frac{z'}{2}|\, -\frac{i}{\hbar}\Big[\hbar\delta'\Lambda(z),\rho\Big]\,|z-\frac{z'}{2}\rangle e^{-ip\cdot z'/\hbar} =$$
$$-i\delta'\int_{-\infty}^{\infty} dz'\Big(\Lambda(z+\frac{z'}{2})\langle z+\frac{z'}{2}|\,\rho\,|z-\frac{z'}{2}\rangle - \langle z+\frac{z'}{2}|\,\rho\,|z-\frac{z'}{2}\rangle\Lambda(z-\frac{z'}{2})\Big)e^{-ip\cdot z'/\hbar} \tag{A.3}$$

Expanding in powers of small z'

$$\Lambda(z+\frac{z'}{2}) \approx \Lambda(z) + \frac{z'}{2}\frac{\partial\Lambda(z)}{\partial z} + \frac{1}{2}\Big(\frac{z'}{2}\Big)^2\frac{\partial^2\Lambda(z)}{\partial z^2} \tag{A.4}$$

and using

$$z'e^{-ip\cdot z'/\hbar} = i\hbar\frac{\partial}{\partial p}e^{-ip\cdot z'/\hbar} \tag{A.5}$$

we get

$$-i\delta'\int_{-\infty}^{\infty} dz'\Big(\Lambda(z+\frac{z'}{2})\langle z+\frac{z'}{2}|\,\rho\,|z-\frac{z'}{2}\rangle - \langle z+\frac{z'}{2}|\,\rho\,|z-\frac{z'}{2}\rangle\Lambda(z-\frac{z'}{2})\Big)e^{-ip\cdot z'/\hbar} \approx$$
$$-i\delta'\int_{-\infty}^{\infty} dz'\,\Big(\Big(\Lambda(z)+\frac{\partial\Lambda(z)}{\partial z}\frac{i\hbar}{2}\frac{\partial}{\partial p}+\frac{1}{2}\frac{\partial^2\Lambda(z)}{\partial z^2}\Big(\frac{i\hbar}{2}\Big)^2\frac{\partial^2}{\partial p^2}\Big)\langle z+\frac{z'}{2}|\,\rho\,|z-\frac{z'}{2}\rangle -$$
$$\langle z+\frac{z'}{2}|\,\rho\,|z-\frac{z'}{2}\rangle\Big(\Lambda(z)-\frac{\partial\Lambda(z)}{\partial z}\frac{i\hbar}{2}\frac{\partial}{\partial p}+\frac{1}{2}\frac{\partial^2\Lambda(z)}{\partial z^2}\Big(\frac{i\hbar}{2}\Big)^2\frac{\partial}{\partial p^2}\Big)\Big)e^{-ip\cdot z'/\hbar} =$$
$$\hbar\delta'\int_{-\infty}^{\infty} dz'\,\frac{\partial\Lambda(z)}{\partial z}\frac{\partial}{\partial p}\,\langle z+\frac{z'}{2}|\,\rho\,|z-\frac{z'}{2}\rangle e^{-ip\cdot z'/\hbar} \equiv$$
$$\frac{\partial U_+}{\partial z}\frac{\partial W_{++}}{\partial p}+\frac{\partial U_-}{\partial z}\frac{\partial W_{--}}{\partial p}\,. \tag{A.6}$$

Similarly

$$\int_{-\infty}^{\infty} dz' \,\langle z+\frac{z'}{2}|\, -\frac{\Gamma'}{2}\Big\{\Lambda(z),\rho\Big\}\,|z-\frac{z'}{2}\rangle e^{-ip\cdot z'/\hbar} =$$
$$-\frac{\Gamma'}{2}\int_{-\infty}^{\infty} dz'\Big(\Lambda(z+\frac{z'}{2})\langle z+\frac{z'}{2}|\,\rho\,|z-\frac{z'}{2}\rangle + \langle z+\frac{z'}{2}|\,\rho\,|z-\frac{z'}{2}\rangle\Lambda(z-\frac{z'}{2})\Big)e^{-ip\cdot z'/\hbar} \approx$$
$$-\frac{\Gamma'}{2}\int_{-\infty}^{\infty} dz'\,\Big(\Lambda(z)\langle z+\frac{z'}{2}|\,\rho\,|z-\frac{z'}{2}\rangle + \langle z+\frac{z'}{2}|\,\rho\,|z-\frac{z'}{2}\rangle\Lambda(z)+$$
$$\frac{1}{2}\Big(\frac{i\hbar}{2}\Big)^2\Big(\frac{\partial^2\Lambda(z)}{\partial z^2}\frac{\partial^2}{\partial p^2}\langle z+\frac{z'}{2}|\,\rho\,|z-\frac{z'}{2}\rangle+\frac{\partial^2}{\partial p^2}\langle z+\frac{z'}{2}|\,\rho\,|z-\frac{z'}{2}\rangle\frac{\partial^2\Lambda(z)}{\partial z^2}\Big)\Big)e^{-ip\cdot z'/\hbar} =$$
$$-\Gamma'\Big(\Lambda_{++}W_{++}+\Lambda_{--}W_{--}\Big)+\frac{\hbar^2\Gamma'}{8}\Big(\frac{\partial^2\Lambda_{++}}{\partial z^2}\frac{\partial^2 W_{++}}{\partial p^2}+\frac{\partial^2\Lambda_{--}}{\partial z^2}\frac{\partial^2 W_{--}}{\partial p^2}\Big) =$$
$$-\frac{\Gamma'}{3}\Big((2-\cos 2kz)W_{++}+(2+\cos 2kz)W_{--}\Big)+$$
$$\frac{\hbar^2k^2\Gamma'}{6}\cos 2kz\Big(\frac{\partial^2 W_{++}}{\partial p^2}-\frac{\partial^2 W_{--}}{\partial p^2}\Big)\,. \tag{A.7}$$

$$\int_{-\infty}^{\infty} dz' \langle z+\frac{z'}{2}| \Gamma' \int_{-k}^{k} dk' \sum_{q=-1}^{1} N_q(k') B_q^\dagger(z) e^{-ik'z/\hbar} \rho\, e^{ik'z/\hbar} B_q(z)\, |z-\frac{z'}{2}\rangle e^{-ip\cdot z'/\hbar} =$$

$$\Gamma' \int_{-\infty}^{\infty} dz' \int_{-k}^{k} dk' \sum_{q=-1}^{1} N_q(k') e^{-ik'z'} B_q^\dagger(z+\frac{z'}{2}) \langle z+\frac{z'}{2}|\, \rho\, |z-\frac{z'}{2}\rangle B_q(z-\frac{z'}{2}) e^{-ip\cdot z'/\hbar} \tag{A.8}$$

Expanding for small z' one finds

$$\int_{-k}^{k} dk' N_{\pm 1}(k') e^{-ik'z'} \approx 1 - \frac{k^2 z'^2}{5} \tag{A.9}$$

$$\int_{-k}^{k} dk' N_0(k') e^{-ik'z'} \approx 1 - \frac{k^2 z'^2}{10} \tag{A.10}$$

$$B_1^\dagger(z+\frac{z'}{2}) \langle z+\frac{z'}{2}|\, \rho\, |z-\frac{z'}{2}\rangle B_1(z-\frac{z'}{2}) \approx$$
$$\left(\sin^2 kz - \left(\frac{kz'}{2}\right)^2\right)\left(\rho_{++}|+\rangle\langle+| + \frac{1}{9}\rho_{--}|-\rangle\langle-|\right) \tag{A.11}$$

$$B_{-1}^\dagger(z+\frac{z'}{2}) \langle z+\frac{z'}{2}|\, \rho\, |z-\frac{z'}{2}\rangle B_{-1}(z-\frac{z'}{2}) \approx$$
$$\left(\cos^2 kz - \left(\frac{kz'}{2}\right)^2\right)\left(\frac{1}{9}\rho_{++}|+\rangle\langle+| + \rho_{--}|-\rangle\langle-|\right) \tag{A.12}$$

$$B_0^\dagger(z+\frac{z'}{2}) \langle z+\frac{z'}{2}|\, \rho\, |z-\frac{z'}{2}\rangle B_0(z-\frac{z'}{2}) \approx$$
$$\frac{2}{9}\left[\rho_{++}|-\rangle\langle-|\left(\cos^2 kz - \left(\frac{kz'}{2}\right)^2\right) + \rho_{--}|+\rangle\langle+|\left(\sin^2 kz - \left(\frac{kz'}{2}\right)^2\right)\right] \tag{A.13}$$

so that

$$\Gamma' \int_{-\infty}^{\infty} dz' \int_{-k}^{k} dk' \sum_{q=-1}^{1} N_q(k') e^{-ik'z'} B_q^\dagger(z+\frac{z'}{2}) \langle z+\frac{z'}{2}|\rho|z-\frac{z'}{2}\rangle B_q(z-\frac{z'}{2}) e^{-ip\cdot z'/\hbar} \approx$$

$$\begin{aligned}
\Gamma' \int_{-\infty}^{\infty} dz'\, e^{-ip\cdot z'/\hbar} \quad & \rho_{++}\left[\left(1-\frac{k^2z'^2}{5}\right)\left(\sin^2 kz-\left(\frac{kz'}{2}\right)^2+\frac{1}{9}\cos^2 kz-\frac{1}{9}\left(\frac{kz'}{2}\right)^2\right)\right]|+\rangle\langle+| \quad + \\
& \rho_{++}\left[\left(1-\frac{k^2z'^2}{10}\right)\left(\frac{2}{9}\cos^2 kz-\frac{2}{9}\left(\frac{kz'}{2}\right)^2\right)\right]|-\rangle\langle-| \quad + \\
& \rho_{--}\left[\left(1-\frac{k^2z'^2}{5}\right)\left(\frac{1}{9}\sin^2 kz-\frac{1}{9}\left(\frac{kz'}{2}\right)^2+\cos^2 kz-\left(\frac{kz'}{2}\right)^2\right)\right]|-\rangle\langle-| \quad + \\
& \rho_{--}\left[\left(1-\frac{k^2z'^2}{10}\right)\left(\frac{2}{9}\sin^2 kz-\frac{2}{9}\left(\frac{kz'}{2}\right)^2\right)\right]|+\rangle\langle+| \qquad \text{(A.14)}
\end{aligned}$$

$$\begin{aligned}
\approx \Gamma' \Bigg(& \left[\frac{1}{9}\left(5-4\cos 2kz\right)+\frac{1}{90}\left(35-8\cos 2kz\right)\hbar^2k^2\frac{\partial}{\partial p^2}\right]W_{++}|+\rangle\langle+| \quad + \\
& \left[\frac{2}{9}\cos^2 kz+\frac{1}{90}\left(6+\cos 2kz\right)\hbar^2k^2\frac{\partial}{\partial p^2}\right]W_{++}|-\rangle\langle-| \quad + \\
& \left[\frac{1}{9}\left(5+4\cos 2kz\right)+\frac{1}{90}\left(35+8\cos 2kz\right)\hbar^2k^2\frac{\partial}{\partial p^2}\right]W_{--}|-\rangle\langle-| \quad + \\
& \left[\frac{2}{9}\sin^2 kz+\frac{1}{90}\left(6-\cos 2kz\right)\hbar^2k^2\frac{\partial}{\partial p^2}\right]W_{--}|+\rangle\langle+| \Bigg) \qquad \text{(A.15)}
\end{aligned}$$

where I've used

$$z'^2 e^{-ip\cdot z'/\hbar} = -\hbar^2 \frac{\partial}{\partial p^2} e^{-ip\cdot z'/\hbar} \qquad \text{(A.16)}$$

Putting all these terms together and taking $\langle g_{\pm 1/2}| \cdots |g_{\pm 1/2}\rangle$ components we obtain

$$\begin{aligned}
\left(\frac{\partial}{\partial t}+\frac{p}{m}\frac{\partial}{\partial z}-\frac{\partial U_+}{\partial z}\frac{\partial}{\partial p}\right)W_{++} = & -\frac{\Gamma'}{9}\left(1+\cos 2kz\right)W_{++}+\frac{\Gamma'}{9}\left(1-\cos 2kz\right)W_{--} \quad + \\
& \frac{\Gamma'}{90}\left(35+7\cos 2kz\right)\hbar^2k^2\frac{\partial^2 W_{++}}{\partial p^2}+\frac{\Gamma'}{90}\left(6-\cos 2kz\right)\hbar^2k^2\frac{\partial^2 W_{--}}{\partial p^2} \qquad \text{(A.17)}
\end{aligned}$$

and

$$\Big(\frac{\partial}{\partial t}+\frac{p}{m}\frac{\partial}{\partial z}-\frac{\partial U_-}{\partial z}\frac{\partial}{\partial p}\Big)W_{--} = -\frac{\Gamma'}{9}\big(1-\cos 2kz\big)W_{--}+\frac{\Gamma'}{9}\big(1+\cos 2kz\big)W_{++} \quad + \\ \frac{\Gamma'}{90}\Big(35-7\cos 2kz\Big)\hbar^2k^2\frac{\partial^2 W_{--}}{\partial p^2}+\frac{\Gamma'}{90}\Big(6+\cos 2kz\Big)\hbar^2k^2\frac{\partial^2 W_{++}}{\partial p^2} \quad \text{(A.18)}$$

Appendix B

Phase-modulation study

Referring to Section 4.1.8 we saw that the phase-modulation of the optical lattice resulted in an inertial force when working in the moving frame and a moving potential when working in the stationary laboratory frame. The atomic dynamics for both cases is identical and is confirmed by numerical simulation as presented here.

We performed two sets of simulations; one set using the re-derived equations of motion in the stationary frame the other set by the inclusion of a force term in the original equations of motion. For this study we chose a phase-modulation $\alpha(t)$ of biharmonic form

$$\alpha(t) = \alpha_0\Big(A_d \cos\omega_d t + \frac{1}{4}B_d \cos\big(2\omega_d t + \phi\big)\Big) \tag{B.1}$$

which results in an inertial force $F(t)$

$$F(t) = F_0\Big(A_d \cos\omega_d t + B_d \cos\big(2\omega_d t + \phi\big)\Big) \tag{B.2}$$

where

$$F_0 = -\frac{m}{2k}\,\omega_d^2\,\alpha_0\ . \tag{B.3}$$

Using $\omega_v = 2\sqrt{\tilde{U}_0}\,\omega_r$ from Section 4.2 we have

$$F_0 = \Big(\frac{\omega_d}{\omega_v}\Big)^2 \hbar U_0 \alpha_0\ . \tag{B.4}$$

We set $U_0 = 200E_r$ and $\omega_d/\omega_v = 1$ to simply give

$$F_0 = 200\alpha_0 F_r \tag{B.5}$$

with $F_r = \hbar k \omega_r$.

We determined the average atomic current as a function of the phase dif-

ference ϕ for three different values of α_0 and their equivalent F_0; the results are presented in Fig. B.1. We see that for equivalent amplitudes of α_0 and F_0 the data-points from the two methods are in very good agreement confirming that either method may be used in the simulation of a cold atom ratchet.

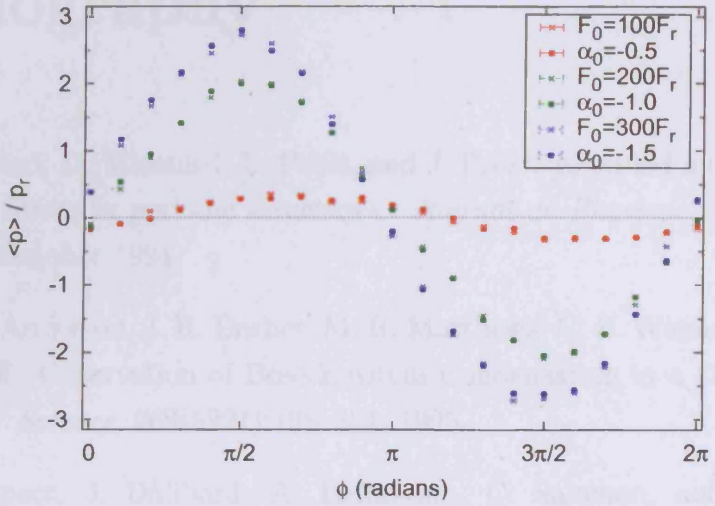

Figure B.1: Comparison of methods for modelling the phase-modulation of the optical lattice: the case of biharmonic driving. Plotted is the average current scaled by the recoil momentum versus ϕ for three equivalent driving amplitudes. The data labelled with a value for α_0 were generated using the re-derived equations of motion in the stationary frame; those data labelled with a value for F_0 were generated by applying the equivalent inertial force in the moving frame. For these calculations $U_0 = 200E_r$, $\Gamma' = 10\omega_r$, $A_d = 1$, $B_d = 1$, $\omega_d/\omega_v = 1$ with a sample size of 1000.

Bibliography

[1] A. Ajdari, D. Mukamel, L. Peliti, and J. Prost. Rectified motion-induced by ac forces in periodic structures. *Journal de Physique I*, 4(10):1551–1561, October 1994.

[2] M. H. Anderson, J. R. Ensher, M. R. Matthews, C. E. Wieman, and E. A. Cornell. Observation of Bose-Einstein Condensation in a Dilute Atomic Vapor. *Science*, 269(5221):198–201, 1995.

[3] A. Aspect, J. Dalibard, A. Heidmann, C. Salomon, and C. Cohen-Tannoudji. Cooling atoms with stimulated emission. *Physical Review Letters*, 57(14):1688–1691, October 1986.

[4] R. Dean Astumian and Martin Bier. Fluctuation driven ratchets: Molecular motors. *Physical Review Letters*, 72(11):1766–1769, Mar 1994.

[5] R. Bartussek, P. Hanggi, and J. G. Kissner. Periodically rocked thermal ratchets. *Europhysics Letters*, 28(7):459–464, December 1994.

[6] J. Baudon, R. Mathevet, and J. Robert. Atomic interferometry. *Journal of Physics B: Atomic, Molecular and Optical Physics*, 32:R173–R195, Aug 1999.

[7] M. Beck, E. Goldobin, M. Neuhaus, M. Siegel, R. Kleiner, and D. Koelle. High-efficiency deterministic josephson vortex ratchet. *Physical Review Letters*, 95:090603, Aug 2005.

[8] K Berg-Sørensen. PhD thesis, Aarhus University, Denmark, 1993.

[9] K. Berg-Sørensen, Y. Castin, E. Bonderup, and K. Mølmer. Momentum diffusion of atoms moving in laser fields. *Journal of Physics B: Atomic, Molecular and Optical Physics*, 25(20):4195–4215, October 1992.

[10] Heinz-Peter Breuer and Francesco Petruccione. *The Theory of Open Quantum Systems*. Oxford University Press, 2002.

[11] M. Brown and F. Renzoni. Ratchet effect in an optical lattice with biharmonic driving: A numerical analysis. *Physical Review A*, 77(3):033405, March 2008.

[12] R. Brown. *Philos. Mag. N. S.*, 4:161, 1828.

[13] Y. Castin, H. Wallis, and J. Dalibard. Limit of doppler cooling. *Journal of the Optical Society of America B-Optical Physics*, 6(11):2046–2057, November 1989.

[14] Y. Castin, K. Berg-Sørensen, J. Dalibard, and K. Mølmer. Two-dimensional sisyphus cooling. *Physical Review A*, 50(6):5092–5115, December 1994.

[15] J. Chen, J. G. Story, and R. G. Hulet. Evolution of atomic motion in an intense standing wave. *Physical Review A*, 47(3):2128–2138, March 1993.

[16] Steven Chu. Nobel lecture: The manipulation of neutral particles. *Reviews of Modern Physics*, 70(3):685–706, Jul 1998.

[17] Steven Chu and Carl E. Wieman. Laser cooling and trapping of atoms: Introduction. *J. Opt. Soc. Am. B*, 6(11):2020, 1989.

[18] C. Cohen-Tannoudji. Atoms in strong resonant fields. In *Frontiers in Laser Spectroscopy*. North-Holland, Amsterdam, 1977.

[19] C. Cohen-Tannoudji. Atomic motion in laser light. In *Frontiers in Laser Spectroscopy*. Elsevier, New York, 1991.

[20] P. Curie. Sur la symetrie dans les phenomenes physiques, symetrie d'un champ electrique et d'un champ magnetique. *Journal de Physique*, 3: 393–415, 1894.

[21] J. Dalibard and C. Cohen-Tannoudji. Dressed-atom approach to atomic motion in laser light: The dipole force revisited. *Journal of the Optical Society of America B-Optical Physics*, 2(11):1707–1720, 1985.

[22] J. Dalibard and C. Cohen-Tannoudji. Atomic motion in laser light: connection between semiclassical and quantum descriptions. *Journal of Physics B: Atomic, Molecular and Optical Physics*, 18(8):1661–1683, 1985.

[23] J. Dalibard and C. Cohen-Tannoudji. Laser cooling below the doppler limit by polarization gradients - simple theoretical-models. *Journal of the Optical Society of America B-Optical Physics*, 6(11):2023–2045, November 1989.

[24] J. Dalibard, C. Salomon, A. Aspect, H. Metcalf, Heidmann A., and C. Cohen-Tannoudji. Atomic motion in a laser standing wave. In W. Persson and S. Svanberg, editors, *Proceedings of the Eighth International Conference on Laser Spectroscopy, Are, Sweden*, pages 81–86, 1987.

[25] J. Dalibard, Y. Castin, and K. Mølmer. Wave-function approach to dissipative processes in quantum optics. *Physical Review Letters*, 68(5):580–583, February 1992.

[26] S. Denisov, L. Morales-Molina, S. Flach, and P. Hanggi. Periodically driven quantum ratchets: Symmetries and resonances. *Physical Review A*, 75(6):063424, June 2007.

[27] S. Denisov, Y. Zolotaryuk, S. Flach, and O. Yevtushenko. Vortex and translational currents due to broken time-space symmetries. *Physical Review Letters*, 100:224102, 2008.

[28] Ivan H. Deutsch and Poul S. Jessen. Quantum-state control in optical lattices. *Physical Review A*, 57(3):1972–1986, Mar 1998.

[29] C. R. Doering, W. Horsthemke, and J. Riordan. Nonequilibrium fluctuation-induced transport. *Physical Review Letters*, 72(19):2984–2987, May 1994.

[30] F. P. Feynman, R. B. Leighton, and M Sands. *The Feynman Lectures on Physics*, volume 1. Addison Wesley, 1963.

[31] S. Flach and S. Denisov. Symmetries and transport with quasiperiodic driving. *Acta Physica Polonica B*, 35(4):1437–1445, April 2004.

[32] S. Flach, O. Yevtushenko, and Y. Zolotaryuk. Directed current due to broken time-space symmetry. *Physical Review Letters*, 84(11):2358–2361, March 2000.

[33] D. T. Gillespie. The mathematics of brownian motion and johnson noise. *American Journal of Physics*, 64(3):225–240, March 1996.

[34] R Gommers. PhD thesis, University College London, 2007.

[35] R. Gommers, S. Bergamini, and F. Renzoni. Dissipation-induced symmetry breaking in a driven optical lattice. *Physical Review Letters*, 95(7): 073003, August 2005.

[36] R. Gommers, P. Douglas, S. Bergamini, M. Goonasekera, P. H. Jones, and F. Renzoni. Resonant activation in a nonadiabatically driven optical lattice. *Physical Review Letters*, 94(14):143001, April 2005.

[37] R. Gommers, S. Denisov, and F. Renzoni. Quasiperiodically driven ratchets for cold atoms. *Physical Review Letters*, 96(24):240604, June 2006.

[38] R. Gommers, M. Brown, and F. Renzoni. Symmetry and transport in a cold atom ratchet with multifrequency driving. *Physical Review A*, 75(5): 053406, May 2007.

[39] R. Gommers, V. Lebedev, M. Brown, and F. Renzoni. Gating ratchet for cold atoms. *Physical Review Letters*, 100(4):040603, February 2008.

[40] J.P. Gordon and A. Ashkin. Motion of atoms in a radiation trap. *Physical Review A*, 21(5):1606–1617, 1980.

[41] M. Grifoni, M. S. Ferreira, J. Peguiron, and J. B. Majer. Quantum ratchets with few bands below the barrier. *Physical Review Letters*, 89(14): 146801, Sep 2002.

[42] G. Grynberg and J. Y. Courtois. Proposal for a magneto-optical lattice for trapping atoms in nearly-dark states. *Europhysics Letters*, 27(1):41–46, July 1994.

[43] G. Grynberg and C. Robilliard. Cold atoms in dissipative optical lattices. *Physics Reports-Review Section of Physics Letters*, 355:335–451, December 2001.

[44] P. Hänggi, F. Marchesoni, and F. Nori. Brownian motors. *ANNALEN DER PHYSIK*, 14(1-3):51–70, 2005.

[45] T. W. Hänsch and A. L. Schawlow. Cooling of gases by laser radiation. *Optics Communications*, 13(6):68–69, 1975.

[46] Dale Henderson. Essen and the national physical laboratory's atomic clock. *Metrologia*, 42(3):S4–S9, 2005.

[47] P. H. Jones, M. Goonasekera, and F. Renzoni. Rectifying fluctuations in an optical lattice. *Physical Review Letters*, 93(7):073904, August 2004.

[48] F. Julicher, A. Ajdari, and J. Prost. Modeling molecular motors. *Reviews of Modern Physics*, 69:1269–1281, 1997.

[49] R. Kosloff. Time-dependent quantum-mechanical methods for molecular-dynamics. *Journal of Physical Chemistry*, 92(8):2087–2100, April 1988.

[50] H. Linke, W. Sheng, A. Löfgren, Hongqi Xu, P. Omling, and P. E. Lindelof. A quantum dot ratchet: Experiment and theory. *EPL (Europhysics Letters)*, 44(3):341–347, 1998.

[51] H. Linke, T. E. Humphrey, A. Löfgren, A. O. Sushkov, R. Newbury, R. P. Taylor, and P. Omling. Experimental Tunneling Ratchets. *Science*, 286 (5448):2314–2317, 1999.

[52] H. Linke, W. Sheng, A. Löfgren, Hongqi Xu, P. Omling, and P. E. Lindelof. A quantum dot ratchet: Experiment and theory. *EPL (Europhysics Letters)*, 45(3):406–406, 1999.

[53] M. O. Magnasco. Forced thermal ratchets. *Physical Review Letters*, 71 (10):1477–1481, September 1993.

[54] Marcelo O. Magnasco. Molecular combustion motors. *Physical Review Letters*, 72(16):2656–2659, Apr 1994.

[55] MO Magnasco and G Stolovitzky. Feynman's ratchet and pawl. *Journal of Statistical Physics*, 93:615–632, 1998.

[56] R. Mannella. Numerical integration of stochastic differential equations.

[57] F. Marchesoni. Harmonic mixing signal - doubly dithered ring laser gyroscope. *Physics Letters A*, 119(5):221–224, December 1986.

[58] P. Marte, R. Dum, R. Taieb, and P. Zoller. Resonance fluorescence from quantized one-dimensional molasses. *Physical Review A*, 47(2):1378–1390, February 1993.

[59] C. Mennerat-Robilliard, D. Lucas, S. Guibal, J. Tabosa, C. Jurczak, J. Y. Courtois, and G. Grynberg. Ratchet for cold rubidium atoms: The asymmetric optical lattice. *Physical Review Letters*, 82(4):851–854, January 1999.

[60] D. Meschede and H. Metcalf. Atomic nanofabrication: atomic deposition and lithography by laser and magnetic forces. *Journal of Physics D: Applied Physics*, 36(3):R17–R38, 2003.

[61] H. Metcalf and P. van der Straten. *Laser Cooling and Trapping*. Springer, 1999.

[62] H. J. Metcalf and P. van der Straten. Laser cooling and trapping of atoms. *Journal of the Optical Society of America B-Optical Physics*, 20 (5):887–908, May 2003.

[63] Mark M. Millonas and Dante R. Chialvo. Nonequilibrium fluctuation-induced phenomena in josephson junctions. *Physical Review E*, 53(3): 2239–2242, Mar 1996.

[64] V. G. Minogin. Atomic scattering by a resonant standing light wave. *Optics Communications*, 37(6):442–446, 1981.

[65] V. G. Minogin and O.T. Serimaa. Resonant light pressure forces in a strong standing laser wave. *Optics Communications*, 30:373–379, 1979.

[66] V.G. Minogin and V.S. Letokhov. *Laser light pressure on atoms*. Gordon and Breach Science Publishers, 1987.

[67] K. Mølmer, Y. Castin, and J. Dalibard. Monte-carlo wave-function method in quantum optics. *Journal of the Optical Society of America B-Optical Physics*, 10(3):524–538, March 1993.

[68] E. Neumann and A. Pikovsky. Quasiperiodically driven josephson junctions: strange nonchaotic attractors, symmetries and transport. *European Physical Journal B*, 26(2):219–228, March 2002.

[69] S. Ooi, S. Savel'ev, M.B. Gaifullin, T. Mochiku, K. Hirata, and F. Nori. Nonlinear nanodevices using magnetic flux quanta. *Physical Review Letters*, 99:207003, Nov 2007.

[70] K. I. Petsas, G. Grynberg, and J. Y. Courtois. Semiclassical monte carlo approaches for realistic atoms in optical lattices. *European Physical Journal D*, 6(1):29–47, April 1999.

[71] M. B. Plenio and P. L. Knight. The quantum-jump approach to dissipative dynamics in quantum optics. *Reviews of Modern Physics*, 70(1):101–144, January 1998.

[72] O. N. Prudnikov and E. Arimondo. Quasiclassical laser cooling in an intense standing wave. *Journal of Optics B-Quantum and Semiclassical Optics*, 6(7):336–344, July 2004.

[73] J. Qiang and S. Habib. Second-order stochastic leapfrog algorithm for multiplicative noise brownian motion. *Physical Review E*, 62(5):7430–7437, November 2000.

[74] P. Reimann. Supersymmetric ratchets. *Physical Review Letters*, 86(22): 4992–4995, May 2001.

[75] P. Reimann. Brownian motors: noisy transport far from equilibrium. *Physics Reports-Review Section of Physics Letters*, 361(2-4):57–265, April 2002.

[76] Peter Reimann, Milena Grifoni, and Peter Hänggi. Quantum ratchets. *Physical Review Letters*, 79(1):10–13, Jul 1997.

[77] Hannes Risken. *The Fokker-Planck Equation*. Springer-Verlag, 1984.

[78] J. Rousselet, L. Salome, A. Ajdari, and J. Prost. Directional motion of brownian particles induced by a periodic asymmetric potential. *Nature*, 370:446–448, 1994.

[79] S. Savel'ev, F. Marchesoni, P. Hänggi, and F. Nori. Nonlinear signal mixing in a ratchet device. *Europhysics Letters*, 67(2):179–185, July 2004.

[80] M. Schiavoni, L. Sanchez-Palencia, F. Renzoni, and G. Grynberg. Phase control of directed diffusion in a symmetric optical lattice. *Physical Review Letters*, 90(9):094101, March 2003.

[81] S. Stenholm. Quantum dynamics of simple systems. In *Proceedings of the 44th SUSSP*, 1994.

[82] M. von Smoluchowski. *Physik. Zeitschr.*, 13:1069, 1912.

[83] H. Wallis. Quantum-theory of atomic motion in laser-light. *Physics Reports-Review Section of Physics Letters*, 255(4):204–287, April 1995.

[84] E. Wigner. On the quantum correction for thermodynamic equilibrium. *Phys. Rev.*, 40(5):749–759, Jun 1932.

[85] D. Wineland and H. Dehmelt. Proposed 1014 delta upsilon lt upsilon laser fluorescence spectroscopy on t1+ mono-ion oscillator iii. *Bulletin of the American Physical Society*, 20(4):637–637, 1975.

[86] O. Yevtushenko, S. Flach, Y. Zolotaryuk, and A. A. Ovchinnikov. Rectification of current in ac-driven nonlinear systems and symmetry properties of the boltzmann equation. *Europhysics Letters*, 54(2):141–147, April 2001.

[87] I. Zapata, R. Bartussek, F. Sols, and P. Hänggi. Voltage rectification by a squid ratchet. *Physical Review Letters*, 77(11):2292–2295, Sep 1996.

[88] Erkki Kyröla and Stig Stenholm. Velocity tuned resonances as multi-doppleron processes. *Optics Communications*, 22(2):123–126, 1977/8.

Index

Nomenclature

δ	Laser detuning; $\delta := \omega_L - \omega_A$
F_a, F_s, F_{sh}	antisymmetric, symmetric, shift-symmetric; see Section 2.4
Γ'	Optical pumping rate in the red-Sisyphus cooling system
Γ	Linewidth of the atomic excited state
I	Ratchet current calculated in the simulations; see Eq. 3.25
ω_L, ω_A	Frequency of laser and atomic transition respectively
ω_v	Vibrational frequency of potential wells
Ω_0	Rabi frequency associated with a light-field of amplitude E_0
p_r, ω_r, E_r, F_r	Recoil units for momentum, frequency, energy and force respectively; $p_r = \hbar k, \omega_r = \hbar k^2/2m, E_r = \hbar\omega_r, F_r = \hbar k\omega_r$
$\hat{S}$	Symmetries of system; see Section 2.4
s_0	Saturation parameter; see Eq. 4.26
U_0	Depth of the potentials in the red-Sisyphus cooling system
$U_\pm$	Bipotential in the red-Sisyphus cooling system